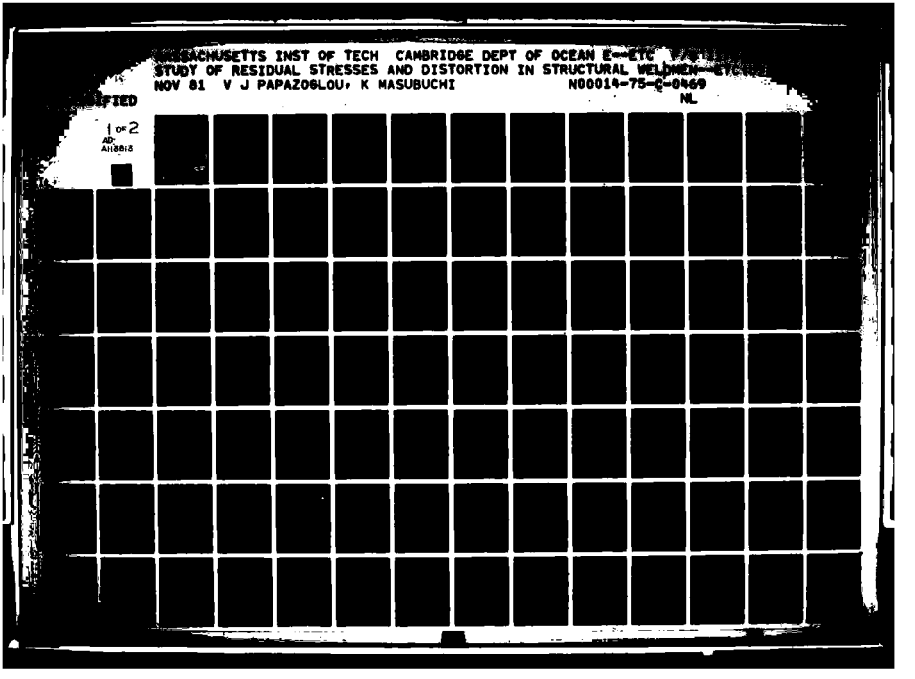
SACHUSETTS INST OF TECH CAMBRIDGE DEPT OF OCEAN E--ETC
STUDY OF RESIDUAL STRESSES AND DISTORTION IN STRUCTURAL WELDMEN--
NOV 81 V J PAPAZOGLOU, K MASUBUCHI N00014-75-C-0469
NL
FIED
1 OF 2
AD
A138818

THIRD
TECHNICAL PROGRESS REPORT

of

CONTRACT N00014-75-C-0408
(M.I.T. DSR 76300)

STUDY OF RESIDUAL STRESSES AND DISTORTION IN STRUCTURAL WELDMENTS IN HIGH-STRENGTH STEELS

by

VASSILIOS J. PAPAZOGLOU
AND
KOICHI MASUBUCHI

to

OFFICE OF NAVAL RESEARCH

NOVEMBER 1981

MASSACHUSETTS INSTITUTE OF TECHNOLOGY
DEPARTMENT OF OCEAN ENGINEERING
CAMBRIDGE, MASS. 02139

THIRD

TECHNICAL PROGRESS REPORT

of

Contract N00014-75-C-0469

(M.I.T. OSP #82558)

STUDY OF RESIDUAL STRESSES AND DISTORTION IN STRUCTURAL WELDMENTS IN HIGH-STRENGTH STEELS

to

Office of Naval Research

November 30, 1981

by

Vassilios J. Papazoglou
and
Koichi Masubuchi

UNCLASSIFIED

SECURITY CLASSIFICATION OF THIS PAGE (When Data Entered)

REPORT DOCUMENTATION PAGE		READ INSTRUCTIONS BEFORE COMPLETING FORM
1. REPORT NUMBER Third Technical Progress Report	2. GOVT ACCESSION NO.	3. RECIPIENT'S CATALOG NUMBER
4. TITLE (and Subtitle) STUDY OF RESIDUAL STRESSES AND DISTORTION IN STRUCTURAL WELDMENTS IN HIGH-STRENGTH STEEL		5. TYPE OF REPORT & PERIOD COVERED Interim. December 1, 1980 to November 30, 1981 6. PERFORMING ORG. REPORT NUMBER
7. AUTHOR(s) Vassilios J. Papazoglou and Koichi Masubuchi		8. CONTRACT OR GRANT NUMBER(s) Contract N00014-75-0469 (M.I.T. OSP # 82558)
9. PERFORMING ORGANIZATION NAME AND ADDRESS Massachusetts Institute of Technology 77 Massachusetts Ave. Cambridge, Mass. 02139		10. PROGRAM ELEMENT, PROJECT, TASK AREA & WORK UNIT NUMBERS
11. CONTROLLING OFFICE NAME AND ADDRESS Department of the Navy Office of Naval Research Arlington, Virginia 22217		12. REPORT DATE November 30, 1981 13. NUMBER OF PAGES 134 + 7
14. MONITORING AGENCY NAME & ADDRESS(if different from Controlling Office)		15. SECURITY CLASS. (of this report) Unclassified 15a. DECLASSIFICATION/DOWNGRADING SCHEDULE

16. DISTRIBUTION STATEMENT (of this Report)

This document has been approved for public release and sale; its distribution is unlimited. Reproduction in whole or in part is permitted by the U.S. Government.

17. DISTRIBUTION STATEMENT (of the abstract entered in Block 20, if different from Report)

18. SUPPLEMENTARY NOTES

19. KEY WORDS (Continue on reverse side if necessary and identify by block number)

Welding	Numerical Analysis
Residual Stresses	Fracture Analysis
Distortion	Stress Relief Treatment
High Strength Steels	Nickel-Bronze Alloys

20. ABSTRACT (Continue on reverse side if necessary and identify by block number)

Numerical analyses based on the finite element method for the prediction of temperatures, thermal strains, and residual stresses due to welding and of the fracture characteristics of weldments are detailed. The obtained results are compared with experimentally obtained data from butt welding 1 in thick HY-130 steel plates using the gas metal arc process.

Experimental results on the effects various welding parameters have on the welding distortion of Nickel-Aluminum bronze thin weldments are also

DD FORM 1 JAN 73 1473 EDITION OF 1 NOV 68 IS OBSOLETE
S/N 0102-LF-014-6601

UNCLASSIFIED

SECURITY CLASSIFICATION OF THIS PAGE (When Data Entered)

included. Optimum welding procedures are then proposed.

Finally, initial efforts towards studying the thermal stress relieving operation are outlined. They include a simple mathematical model for the description of the phenomena involved and a series of experiments.

B

EXECUTIVE SUMMARY

This report presents the progress made during the fourth year of the O.N.R. sponsored research program entitled "Study of Residual Stresses and Distortion in Structural Weldments in High Strength Steels". Details on the progress made on all five tasks are included.

Regarding Task 1 which deals with butt welds in thick HY-130 plates all the proposed subtasks have been completed. Since most of the experimental part of this task has been completed during the first three years, emphasis for the fourth year was placed on analysis. Heat transfer analyses were performed using both a newly developed analytical solution based on a moving finite heat source model and the multipurpose nonlinear heat transfer finite element computer program ADINAT which was modified to take into account latent heat effects.

Calculations of the thermal strain, transient stress, and residual stress distributions developed during the multipass GMA welding of thick plates were also performed using the thermal-elastic-plastic constitutive model of the multipurpose finite element program ADINA. The program was enhanced by incorporating the phase transformation strains developed during the steel allotropic phase changes.

A hybrid crack element was also developed aimed at facilitating an inexpensive evaluation of the fracture characteristics of weldments in the presence of a residual stress field. Using this element linear elastic finite element analyses of the fracture experiments were performed. Both the crack opening displacement and the strain energy released during the propagation of a crack in a residual stress field were calculated.

Finally, results from all the aforementioned analyses were compared with data obtained from experimental measurements. Good correlation was generally observed.

With respect to Task 2, which deals with girth welds in cylindrical shells, all proposed subtasks have been completed by the end of the third

year of this research project. Therefore, the only work performed during the fourth year pertained to a general assessment of the already obtained results.

Task 3, aimed at developing information on weldments in bronze, was carried in its entirety during the fourth year. A literature survey was first conducted to obtain material properties on nickel-aluminum bronze. Experimental studies consisting of bead-on-plate and edge welds on one quarter inch thick plates were then performed to determine the resulting temperature, strain, and displacement changes. The experimental results were finally compared with baseline data to study the effects of restraint, block welding, preheating, postheating, and grinding on the final distortion.

Efforts to study the thermal stress relieving of weldments were initiated under Task 4. After a literature survey covering thermal and mechanical stress relieving treatments was completed, an initial analysis of the thermal treatment was performed based on the M.I.T. one-dimensional computer program, properly modified for this purpose. Plans for the experimental verification of the obtained results are currently under way. It is expected that this task will have been completed by the end of the research program.

Under Task 5 a series of manuals have been or are currently being developed for the computer programs related to welding that have been developed or improved during the course of the present research program. This task will be completed by the end of the program.

All in all, therefore, the proposed program of research was carried out as originally proposed but with a delay of approximately six months. A final report is expected to be issued at the conclusion of the four-and-a-half-year study.

TABLE OF CONTENTS

1. INTRODUCTION

The objective of this research program, which started on December 1, 1977, is to experimentally and analytically study temperatures, thermal strains, residual stresses and distortion in structural weldments in high-strength steel.

This program includes (1) generation of experimental data and (2) development of analytical systems. HY-130 is the primary material to be investigated; a limited number of experiments are, however, to be conducted using low-carbon steel specimens. Experiments are to be made using the multipass gas metal arc (GMA) and electron beam (EB) one-pass welding processes.

More specifically,

Materials: HY-130 steel (with some control specimens in low-carbon steel)

Thickness: 1 inch (with some specimens 1/2" thick)

Welding processes: Electron beam (EB) and multipass gas metal arc (GMA) processes

Specimen geometries: The following types of specimens are considered

a. Butt welds in thick plates

   (1) Unrestrained butt welds
   (2) Simple restrained butt welds
   (3) Restrained welds simulating practical weldments

b. Girth welds of cylindrical shells

   (4) Girth welding along the groove of a cylindrical shell
   (5) Girth welding between unstiffened cylindrical shells

The work to be performed has been divided into two main tasks:

Task 1: Research on butt welds in thick plates

Task 2: Research on girth welds in cylindrical shells

The program was initially proposed to cover a three-year period. Table 1.1 illustrates the tasks and phases of this study. The planned progress for each task appears in the original proposal, dated July 1977, where also a more detailed description of each task can be found.

Towards the end of the initial three-year period a proposal, dated November 1980, was sent to O.N.R. requesting a one-year extension of the research program to November 30, 1981. Under this proposal, which was accepted, work on three additional tasks would be done as follows:

Task 3: Development of information on weldments in bronze

Task 4: Research on thermal stress relieving of weldments

Task 5: Development of improved computer programs

For the most part the program has been carried out as originally proposed. The few changes made as well as work in the final stages of completion will be dealt with in the appropriate places.

Three progress reports, dated October 10, 1978, August 31, 1979, and July 15, 1980 and two technical progress reports, dated November 30, 1979 (covering work performed during the first two years) and November 30, 1980 (covering the work performed during the third year) have already been issued. This third technical progress report covers the efforts carried out during the fourth year of the research program and should be considered as a companion to the first two technical reports.

Note that no final report of the program is issued at this time as preplanned because of a request for a six-month extension of the program to May 31, 1982 as per a formal proposal dated October 1981. It is expected that a final report covering all five tasks previously mentioned will be issued at the end of the program extension.

TABLE 1.1

TASKS AND PHASES OF THE PROGRAM

	Task 1: Thick Plate	Task 2: Cylindrical Shell
First Year	1.1 Develop details of research plan	2.1 Develop details of research plan
	1.2 Experiments on unrestrained butt welds	2.2 Experiment on girth welding along groove of a cylindrical shell
	1.3 Analysis of data obtained in 1.2	2.3 Analysis of data obtained in 2.2
Second Year	1.4 Develop details of research plan	2.4 Develop details of research plan
	1.5 Measurement of residual stresses in specimens made in 1.2	2.5 Measurement of residual stresses in specimens made in 2.2
	1.6 Experiment on simple restrained butt welds	2.6 Experiment on butt welds between unstiffened cylindrical shells
	1.7 Analysis of data obtained in 1.5 and 1.6	2.7 Analysis of data obtained in in 2.5 and 2.6
Third Year	1.8 Develop details of research plan	2.8 Develop details of research plan
	1.9 Experiment on restrained cracking test specimens	2.9 ---
	1.10 Measurement of strain energy release on specimens made in 1.6 and 1.9	2.10 Measurement of residual stresses in specimens made in 2.6
	1.11 Analysis of data obtained in 1.9 and 1.10	2.11 Analysis of data obtained in 2.10
	Preparation of the Final Report	

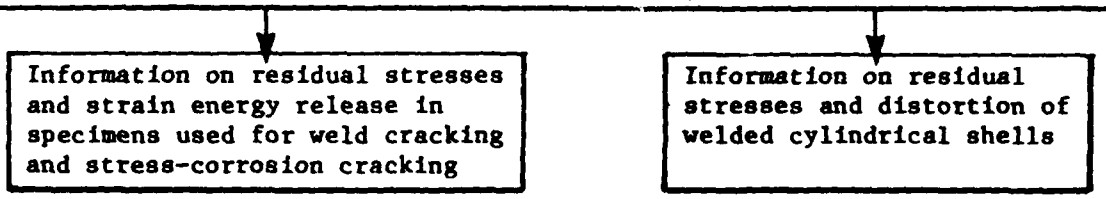

2. PROGRESS OF TASK 1 - THICK PLATES (DECEMBER 1, 1980 to NOVEMBER 30, 1981)

2.1 General Status

The objective of Task 1 of this research program is to experimentally and analytically study temperatures, thermal strains, residual stresses and distortion in thick butt welded high strength steel (specifically HY-130) plates. All eleven steps (see Table 1.1) of this task have been completed successfully as originally planned.

Most of the experimental work has already been completed during the first three years of the research program. Details of this work can be found in the first two technical progress reports to O.N.R. Measurements of the strain energy release on the simple restrained specimens (Step 1.10) was performed during the first part of the fourth year. Section 2.2 describes in some detail these measurements, after a brief summary of the first three-year experimental program is provided.

The analysis of the experimental results is outlined in the subsequent sections, where some details of the computer programs developed as well as numerical results are provided.

2.2 Experimental Program

A summary of the experimental work carried out during the first three years of this research program is given in the first subsection. This summary will help the reader gain a perspective of the program, while serving at the same time as a bridge between this and the first two technical progress reports.

The next subsection deals with details of the fracture experiments performed on the simple restrained specimens to determine the strain energy release rate.

2.2.1 Summary of Experiments Performed During the First Three Years

The following number of experiments, classified according to type of measurements taken, specimen configuration and welding process used, were performed during the first three years of this research project (December 1, 1977 to November 30, 1980):

A. Measurement of temperature and thermal strain distributions during welding.

A.1 Unrestrained specimens

A.1.1 Gas Metal Arc Welding

(a) One 24" x 24" x 1" SAE 1020 specimen

(b) Two 24" x 24" x 1" HY-130 specimen

A.1.2 Electron Beam Welding

(a) Two 24" x 24" x 1" SAE 1020 specimens

(b) Two 24" x 24" x 1" HY-130 specimens

(c) One 24 5/16" x 26" x 1" HY-130 specimen

A.2 Clamped specimens

A.2.1 Laser Beam Welding

(a) Two 11" x 14 3/4" x 1" HY-130 specimens

A.3 Simple restrained specimens[1]

A.3.1 Gas Metal Arc Welding

(a) Two 30" x 30" x 1/2" SAE 1020 specimens

(b) Two 30" x 30" x 1" SAE 1020 specimens

(c) Two 30" x 30" x 2" SAE 1020 specimens

(d) Two 30" x 30" x 7/8" HY-130 specimens

(e) One 30" x 30" x 2" HY-130 specimen

[1]These specimens had H-type slits of different dimensions to simulate various degrees of restraint (see Figure 2.1). The degree of restraint was calculated numerically (see Section 2.7.1 of Second Technical Progress Report to O.N.R., November 30, 1980).

A.4 Restrained cracking (window) test specimen

A.4.1 Gas Metal Arc Welding

(a) One 15" x 24" x 2" HY-130 specimen on a 30" x 30" x 3" SAE 1020 base plate

B. Measurement of triaxial distribution of residual stresses[2]

B.1 Electron Beam welded specimens

(a) One 24" x 24" x 1" SAE 1020 specimen (see number A.1.2a)

(b) One 24 5/6" x 26" x 1" HY-130 specimen (see number A.1.2c)

B.2 Gas Metal Arc welded specimens

(a) One 18" x 32" x 7/8" HY-130 specimen

(b) One 18" x 32" x 1" HY-130 specimen

Details of the experimental procedures used and recorded results are provided in the first two technical progress reports to the Office of Naval Research.

2.2.2 Fracture Experiments

This section deals with experiments performed during the first part of the fourth year of this research project on the simple restrained specimens aimed at determining the energy release during crack propagation. Details of the work can be found in the following completed thesis: Gonçalves, E., "Fracture Analysis of Welded Structures", Ph.D. Thesis, M.I.T., May 1981.

[2]These measurements were performed using the Rosenthal-Norton sectioning technique (see Section 2.6 of First Technical Progress Report to O.N.R., November 30, 1979 for a detailed description of the method).

General Discussion. The purpose of measuring the strain energy release rate during crack propagation is that such a measurement will be the stepping stone based on which the stress intensity factor can be calculated. Alternatively, this intermediate step can be bypassed if measurements of the crack opening displacement (COD) can be made. This latter approach was followed in this research program.

COD measurements were made on the simply restrained welded specimens prepared in an earlier part of the program.[3] Eight specimens were used for this purpose having the general geometric configuration shown in Fig. 2.1. Some details of the specimens' parameters as well as the numerically calculated degree of restraint, K_s, for each specimen are provided in Table 2.1.

Notch Characteristics. The COD was recorded while a notch, inserted in a direction parallel to the weld (x-direction) and located on the weld centerline, was continuously propagating in the specimen's thickness direction. No external stresses were applied during this process; the only stresses present were the residual stresses due to welding. Under such conditions the crack would propagate through zones of relatively constant fracture toughness (that of the weld metal) under the influence of high values of transverse residual stresses, σ_y, which can be considered to be independent of x in the central portion of the specimen.

Notches were made with 1/32 in (0.8 mm) thick, 6 in (15.24 cm) in diameter circular blade saws. The saw tips were ground to a 90° angle so that a sharp notch tip could be obtained.

Figure 2.2 presents the geometry and position of the notches. It can easily be seen that the following geometric relation is valid

$$c = \sqrt{a\ (6-a)} \qquad (2.2.1)$$

where c = notch half length at specimen surface, in

a = notch depth, in.

[3] See Section 2.4 of the Second Technical Progress Report to O.N.R., November 30, 1980.

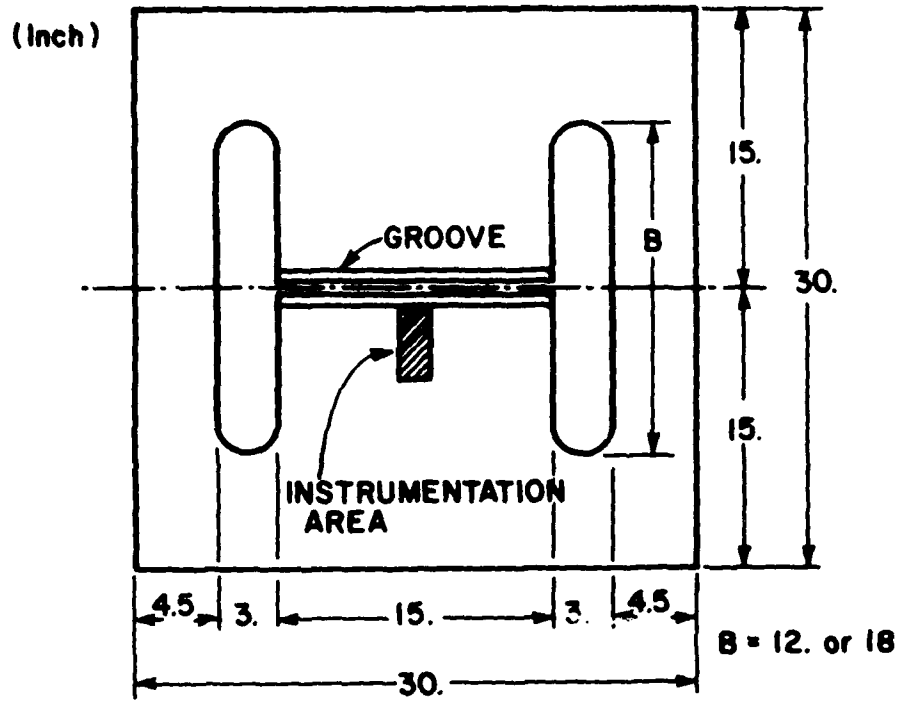

GROOVE DETAILS

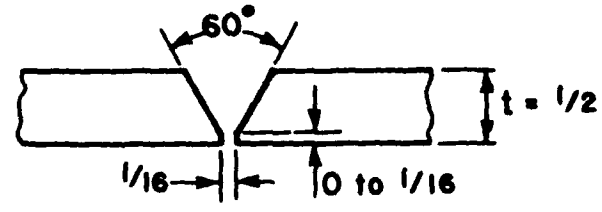

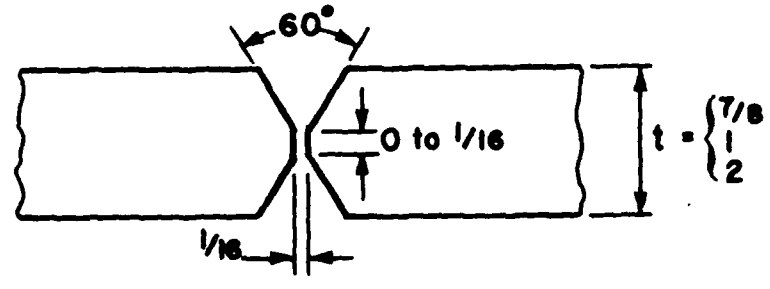

FIGURE 2.1 Configuration of simple restrained specimens. (Dimensions are in inches)

TABLE 2.1

PARAMETERS OF SPECIMENS FOR FRACTURE EXPERIMENTS

Specimen Number	Type of Steel	Thickness (in)	B (in)	K_g (ksi/in)
1	SAE 1020	1/2	12	119.9
2	SAE 1020	1	18	125.3
3	SAE 1020	1	12	239.8
4	SAE 1020	2	18	250.6
5	SAE 1020	2	12	479.6
6	HY-130	7/8	18	109.6
7	HY-130	7/8	12	209.8
8	HY-130	2	12	479.6

NOTES:
1. The degree of restraint, K_g, of each specimen is a function of the plate's thickness, t, and of the height of the H-slit, B.
2. Both steels have the same degree of restraint for the same geometry, since the Young's modulus, E, is assumed to be the same for both.

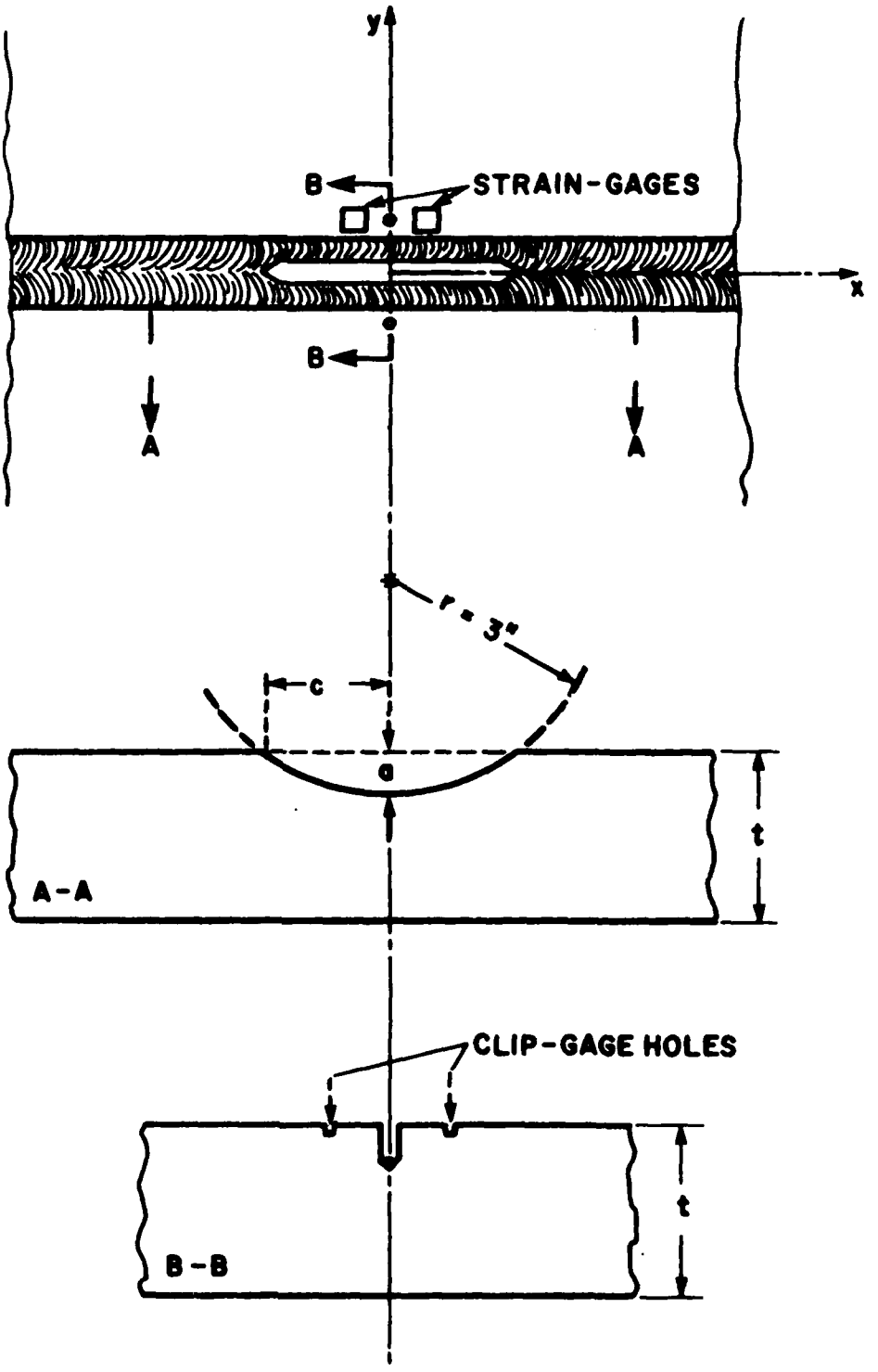

FIGURE 2.2 Notch characteristics and positioning of strain gages and clip-gage holes for fracture experiment

Specimen Preparation and Instrumentation. The weld reinforcement was first removed from the specimens by grinding. Electric resistance strain gages (type FAE-D6-12-S6) were then bonded to continuously measure the strain relaxation during the crack propagation. Two reference holes were also drilled close to the weld centerline to facilitate COD measurements (see Fig. 2.2).

The Crack Opening Displacement was measured using the clip-gage especially designed for these experiments and shown in Figure 2.3. Four type SP-133-20-35 semiconductor strain gages were bonded on the spring steel clip-gage arms. To improve accuracy and sensitivity of measurements, all four strain gages were active in the Wheatstone Bridge arrangement.

Both strains and displacements (COD) were recorded simultaneously and continuously by a Visicorder recorder.

After the specimens were prepared, they were positioned in a horizontal milling machine which drove the circular blade saw. Care has been taken so that no undesirable plate bending stresses or vibrations of the clip-gage during cutting took place.

Results. Curves of COD versus notch depth were obtained for all specimens tested. The relevant curves for the HY-130 specimens (numbers 6 through 8 in Table 2.1) are reproduced here in Figures 2.4 and 2.5. Note that Fig. 2.5 does not present results up to the plate's full thickness; this is due to the fact that the saw's blades became dull before the plate's opposite surface was reached.

It is interesting to mention that the relatively high values of COD shown were obtained with no applied external stresses. Furthermore, the non-linear character of the curves signifies the presence of a complex through thickness stress distribution.

Results of the strain measurements are not presented since they are not of significant interest. The main reason for recording strains was to double-check the COD measurements.

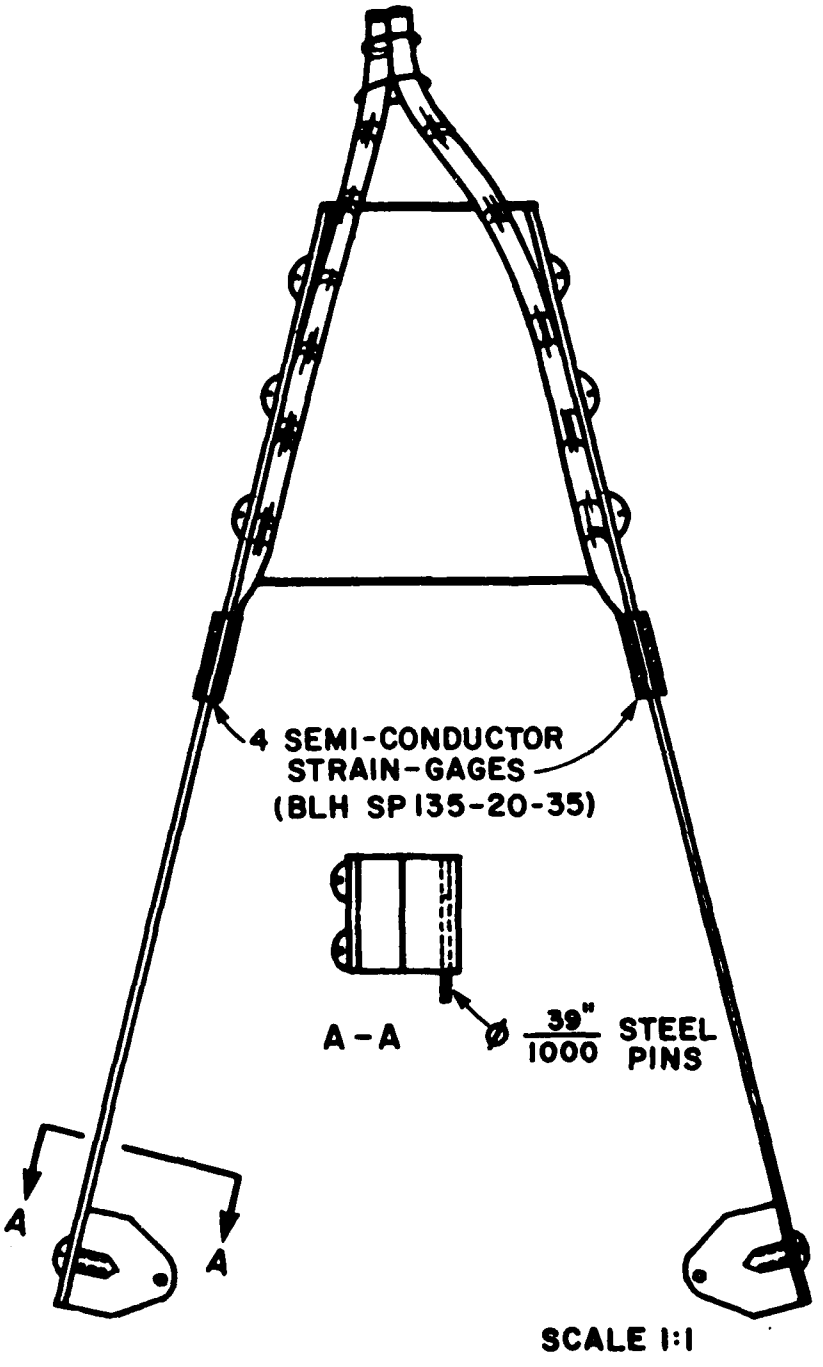

FIGURE 2.3 Schematic representation of the clip gage used to measure C O D

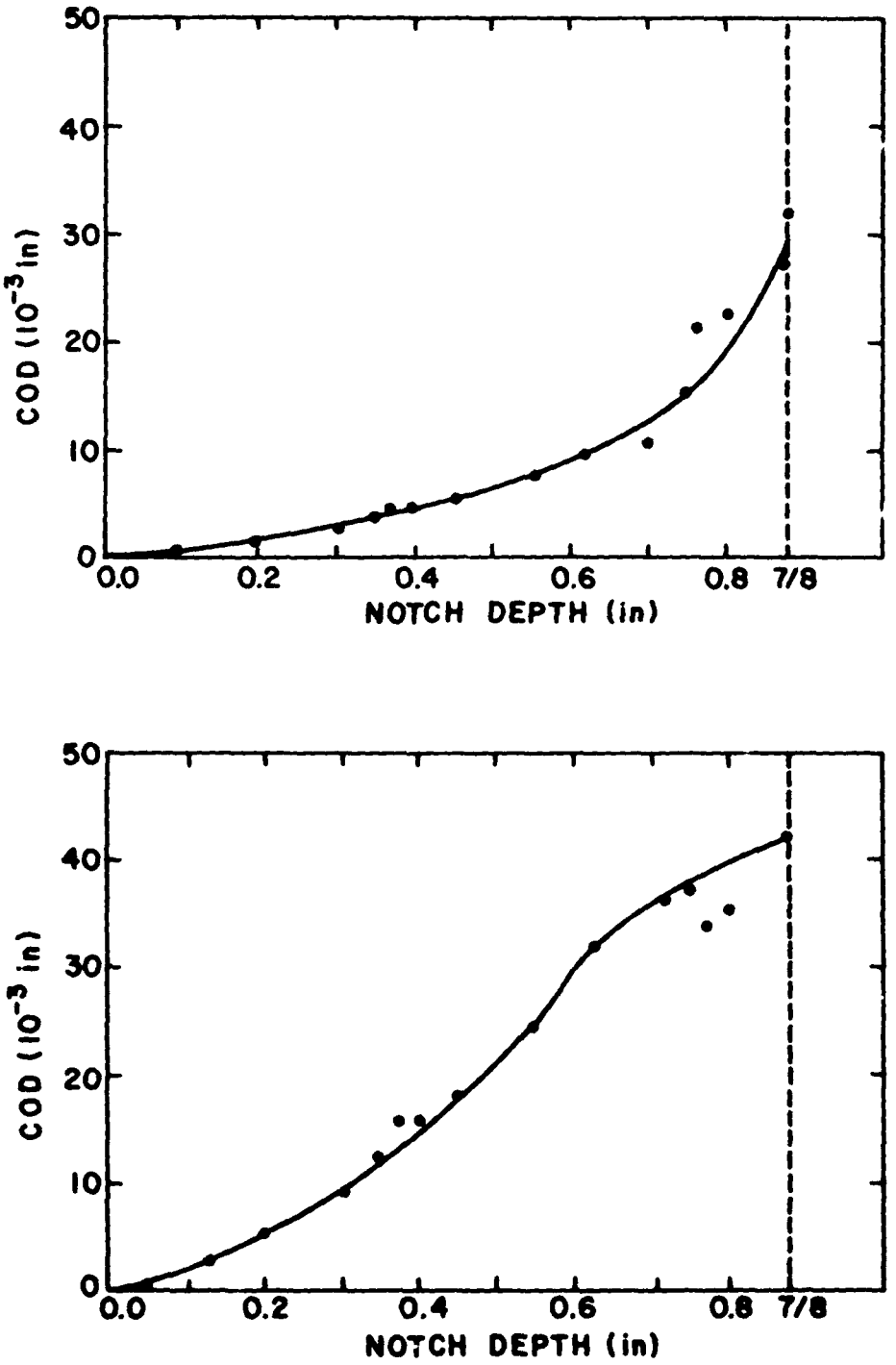

FIGURE 2.4 Crack opening displacement vs. notch depth for specimens 6 and 7 (7/8 in thick HY-130 plates)

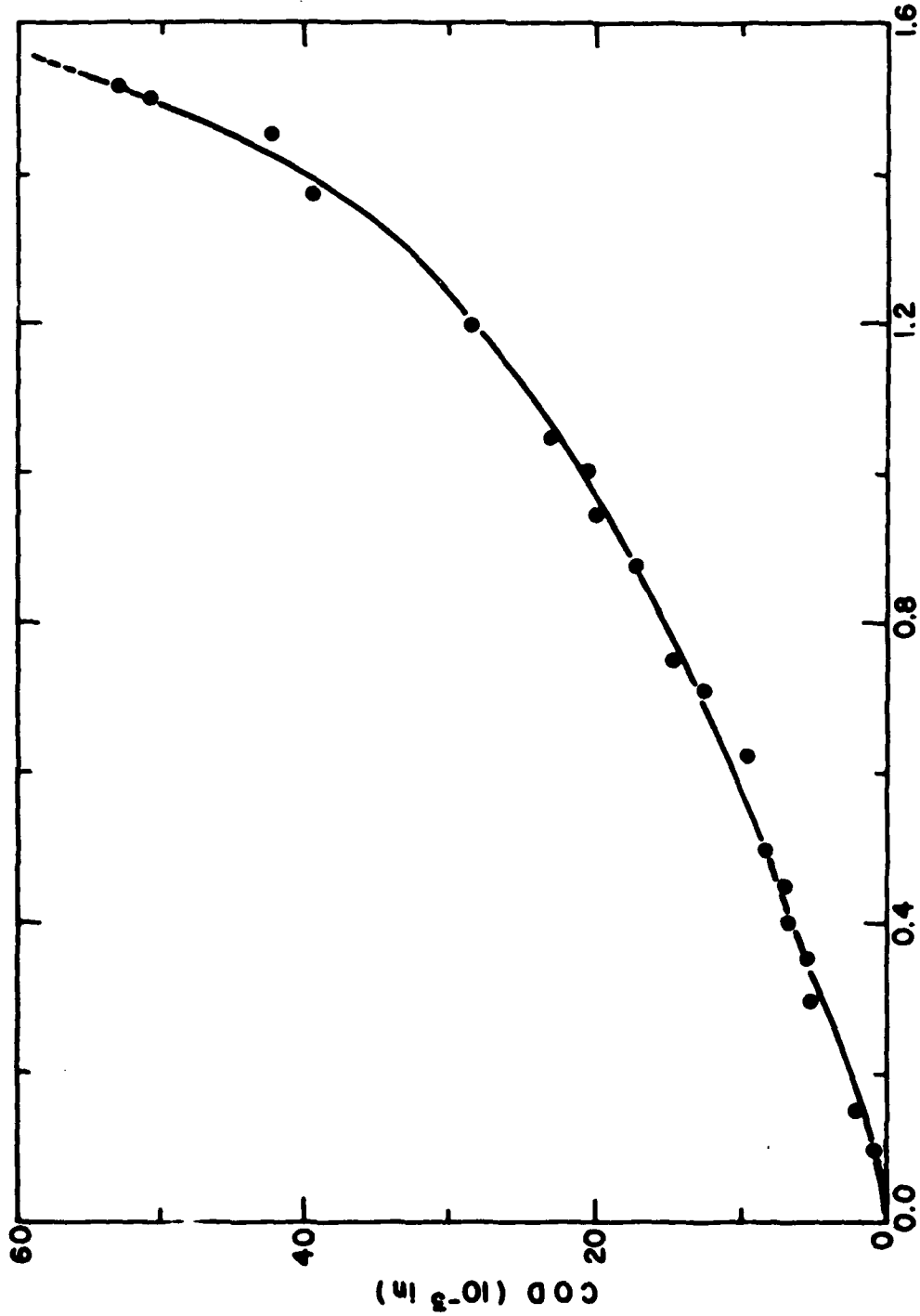

FIGURE 2.5 Crack opening displacement vs. notch depth for Specimen 8 (2 in thick HY-130 plate)

2.3 Heat Transfer Analysis

Efforts to improve the prediction capabilities of both analytical and numerical solutions of the heat transfer problem during welding were successfully completed during the first half of the fourth year of this research project. This section provides a summary of these efforts and the obtained results. For more details one is referred to the following thesis:

Papazoglou, V.J., "Analytical Techniques for Determining Temperatures, Thermal Strains, and Residual Stresses During Welding", Ph.D. Thesis, M.I.T., May 1981.

2.3.1 Closed-Form Solutions

Closed-form analytical solutions of the problem of heat transfer during welding, though not as accurate as the numerical ones, are very useful. They provide for the establishment of the general laws that govern the phenomenon, thus facilitating a better understanding of it. Moreover, given the fact that the computer programs implementing such solutions are very inexpensive to run, they allow for a series of parametric analyses that help one understand the relative importance of the various parameters.

Based on these considerations, efforts were undertaken during the course of this investigation towards devising new or improving already existing analytical solutions with the aim of obtaining more accurate predictions.

3D Finite Heat Source Model. A three-dimensional finite heat source model for solving the governing partial differential equation of heat transfer was developed under the following assumptions:

(1) Quasi-stationary state, i.e., steady state conditions with respect to a coordinate system moving with the heat source.

(2) The heat input is provided by a moving three-dimensional skewed normally distributed heat source moving on the surface of the plate and given by

$$q(r,\xi) = q_o \cdot \exp(-Cr^2 - \lambda v\xi) \qquad (2.3.1)$$

where q_o is the maximum heat flux at the center of the heat spot, C the heat flux concentration coefficient, r the radial distance from the center of the heat spot, $1/2\lambda$ the thermal diffusivity, v the welding speed, and ξ the moving coordinate in the welding direction (x-vt).

(3) The thermal conductivity of the material, k, is assumed to be a linear function of temperature, θ, given by

$$k(\theta) = k_o \cdot [1 + \gamma(\theta-\theta_o)] \qquad (2.3.2)$$

where k_o is the value of the thermal conductivity at the initial plate temperature θ_o and γ the proportionality coefficient.

(4) The thermal diffusivity of the material, κ, is assumed to be constant.

(5) Convective and radiation boundary heat losses from the plate's surface are taken into account through a constant average "effective" heat transfer coefficient, h, which can be different for the top and bottom surfaces of the plate.

(6) The initial temperature of the plate, θ_o, can be different from the environmental (ambient) temperature, θ_e, to allow for preheating.

(7) Phase transformation and Joule heating effects can be neglected.

Based on these assumptions the governing P.D.E. was solved using the method of separation of variables, the appropriate boundary conditions and by dividing the plate into two regions, inside and outside the heat input circle of radius r_h.

The obtained solution can be written as

$$\theta = \theta_o + \frac{1}{\gamma} \cdot \left(\sqrt{1+2\gamma \cdot e^{-\lambda v\xi} \cdot \phi(r,z)} - 1\right) \qquad (2.3.3)$$

where

$$\phi(r,z) = \phi^i(r,z) \cdot [u_{-1}(r)-u_{-1}(r-r_h] + \phi^o(r,z) \cdot u_{-1}(r-r_h)$$

with $u_{-1}(r-a)$ being the unit step function and

$$\phi^{o}(r,z) = \sum_{n=1}^{\infty} C_n \cdot K_o(\zeta_n r) \cdot \left[\frac{h_2}{k_o \cdot \omega_n} \cdot \sin(\omega_n z) + \cos(\omega_n z) \right]$$

$$\phi^{i}(r,z) = \sum_{n=1}^{\infty} \left[\frac{2 \cdot q_o \cdot K_n \cdot J_o(\delta_n r) \cdot [h_2 \cdot \sinh(\chi_n z) + k_o \cdot \chi_n \cdot \cosh(\chi_n z)]}{J_1^2(\delta_n r_h) \cdot [k_o \chi_n (h_1+h_2) \cdot \cosh(\chi_n H) + (k_o^2 \chi_n^2 + h_1 h_2) \cdot \sinh(\chi_n H)} \right.$$

$$\left. + C_n \cdot K_o(\zeta_n r_h) \cdot \frac{I_o(\zeta_n r)}{I_o(\zeta_n r_h)} \cdot \left[\frac{h_2}{\omega_n \cdot k_o} \cdot \sin(\omega_n z) + \cos(\omega_n z) \right] \right]$$

$$C_n = \frac{1}{a_n} \cdot \sum_{m=1}^{\infty} \frac{2 \cdot q_o \cdot K_m \cdot \delta_m \cdot [r_{mn} \cdot \tanh(\chi_m H) + s_{mn}]}{(\chi_m^2 + \omega_n^2) \cdot (J_1(\delta_m r_h) \cdot [d_m + e_m \cdot \tanh(\chi_m H)]}, \quad n = 1,2,3,\ldots$$

$$a_n = b_n \cdot c_n$$

$$b_n = \zeta_n \cdot \left[K_1(\zeta_n r_h) + K_o(\zeta_n r_h) \cdot \frac{I_1(\zeta_n r_h)}{I_o(\zeta_n r_h)} \right]$$

$$c_n = \frac{H}{2} \cdot \left(1 + \frac{h_2^2}{\omega_n^2 \cdot k_o^2} \right) + \frac{1}{4\omega_n} \cdot \left(1 - \frac{h_2}{\omega_n^2 \cdot k_o^2} \right) \cdot \sin(2\omega_n H) + \frac{h_2}{\omega_n^2 \cdot k_o} \cdot \sin^2(\omega_n H)$$

$$d_m = k_o \cdot \chi_m \cdot (h_1 + h_2)$$

$$e_m = k_o^2 \cdot \chi_m^2 + h_1 \cdot h_2$$

$$r_{mn} = h_2 \cdot \left(\omega_n + \frac{\chi_m^2}{\omega_n} \right) \cdot \sin(\omega_n H) + \left(k_o \chi_m^2 - \frac{h_2^2}{k_o} \right) \cdot \cos(\omega_n H)$$

$$s_{mn} = \chi_m \cdot \left(k_o \cdot \omega_n + \frac{h_2^2}{k_o \cdot \omega_n} \right) \cdot \sin(\omega_n H)$$

$$\zeta_n^2 = \omega_n^2 + (\lambda v)^2$$

$$(k_o^2 \cdot \omega_n^2 - h_1 \cdot h_2) \cdot \tan(\omega_n H) = k_o \cdot \omega_n \cdot (h_1 + h_2)$$

$$J_o(\delta_n \cdot r_h) = 0, \quad n=1,2,3,..$$

$$\delta_n^2 = \chi_n^2 - (\lambda v)^2$$

$$K_n = \int_o^1 x \cdot e^{-C \cdot r_h^2 \cdot x^2} \cdot J_o(\delta_n \cdot r_h \cdot x) \cdot dx$$

h_1 and h_2 the heat transfer coefficients at the top and bottom surfaces of the plate respectively, H the plate thickness, $J_o(x)$ and $J_1(x)$ the Bessel functions of first kind and of zero and first order respectively, $I_o(x)$ and $I_1(x)$ the modified Bessel functions of first kind and of zero and first order respectively, and $K_o(x)$ and $K_1(x)$ the modified Bessel functions of second kind and of zero and first order respectively. All other variables have been previously defined.

A computer program has been written in the FORTRAN IV language to perform the necessary calculations.

This computer program was used to perform a parametric investigation in an effort to study the effects the arc efficiency, η_a, the concentration coefficient, C, and the average heat loss coefficient, $h(=h_1=h_2)$, have on the predicted temperature distribution.

As a case study, the laying of a bead on the top surface of a 1 in (25.4 mm) thick HY-130 plate using the GMA welding process was chosen. The plate measured 24 in x 24 in (610 mm x 610 mm) so that the quasi-stationary state could be assumed to hold in its mid-length region. Two arc efficiencies, 0.50 and 0.60, were assumed. For the concentration

coefficient C the values of 39.5 and 8.2 in^{-2} (6.12 and 1.28 cm^{-2}) were investigated corresponding to a heat spot radius r_h of 0.275 and 0.600 in (7.0 and 15.2 mm) respectively.[4] The average heat loss coefficient for both surfaces ranged from 0 to 0.0006 Btu/sec in^2 °F corresponding to adiabatic boundary conditions and heat losses at relatively high temperatures. Finally, the cases of constant thermal conductivity (γ=0) and of linearly varying thermal conductivity (γ=0.0001) were examined, the latter value being computed from data for the HY-130 steel using least squares approximation.

Figures 2.6 and 2.7 show two examples of the results obtained for a location 0.5 in (12.7 mm) away from the weld centerline. Based on these figures and on similar ones the following conclusions can be drawn:

(1) Larger arc efficiencies, i.e., larger heat inputs, result in higher temperatures.

(2) The smaller the concentration coefficient, i.e., the larger the heat spot radius, the higher the temperatures. This effect is more pronounced at the high temperature range.

(3) The inclusion of linearly varying thermal conductivity does not alter by much the temperature distribution predicted using a constant thermal conductivity. Only in high temperature regions (e.g., inside the HAZ) is the effect pronounced, resulting in lower temperatures.

(4) The average heat loss coefficient (from convection and radiation) has the largest impact on the temperature distribution, with the adiabatic boundary conditions resulting in unreasonably high temperatures.

Finally, an analysis of experimental results using the finite heat source solution was attempted. At first the multipass GMA welding tests described in Section 2.3.1 of the first technical progress report

---

[4] See Rykalin, N.N., and Nikolaev, A.V., "Welding Arc Heat Flow", Welding in the World, 9 (3/4), 1971, pp. 112-132.

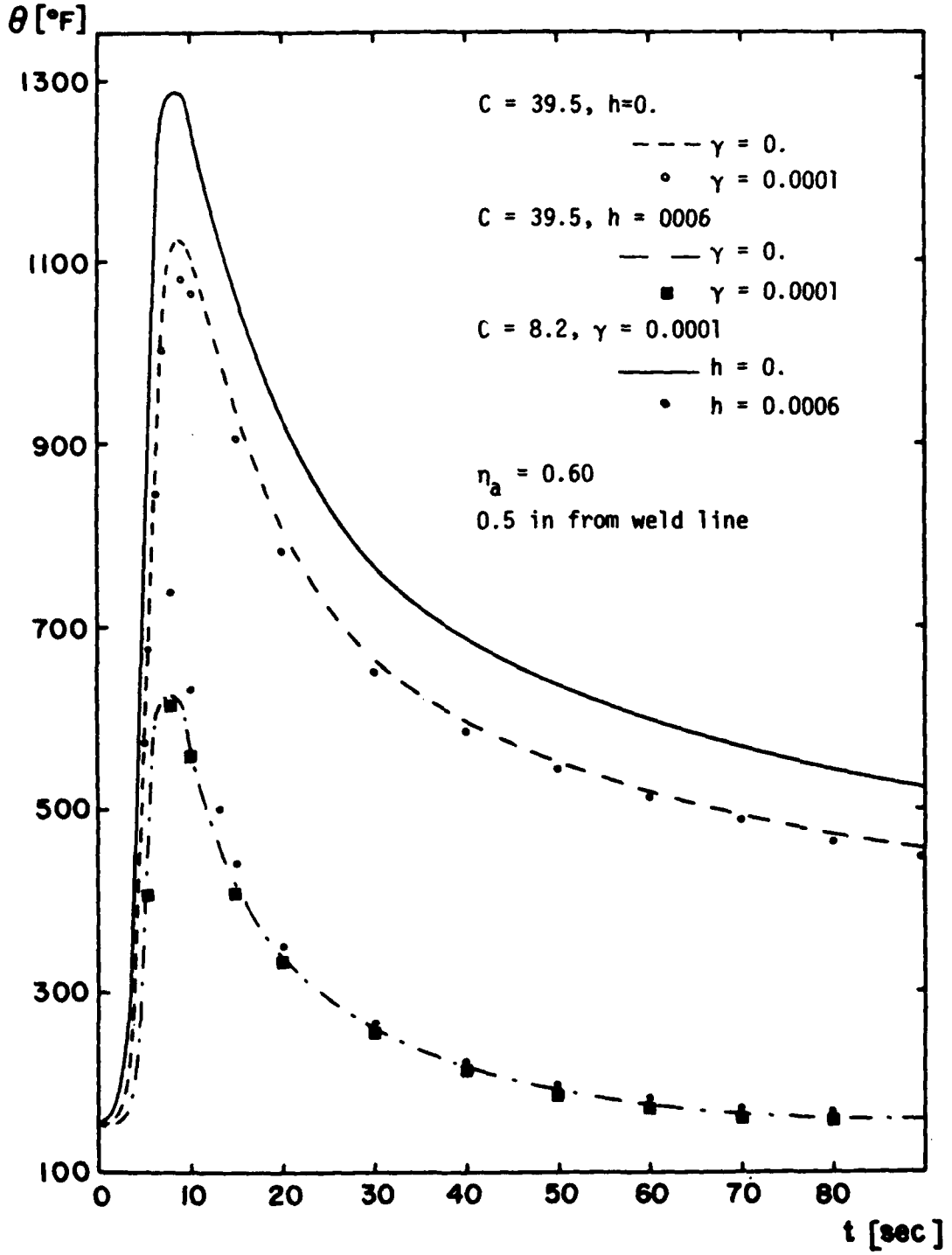

FIGURE 2.6 Parametric investigation of finite heat source solution (at 0.5 in away from the weld centerline)

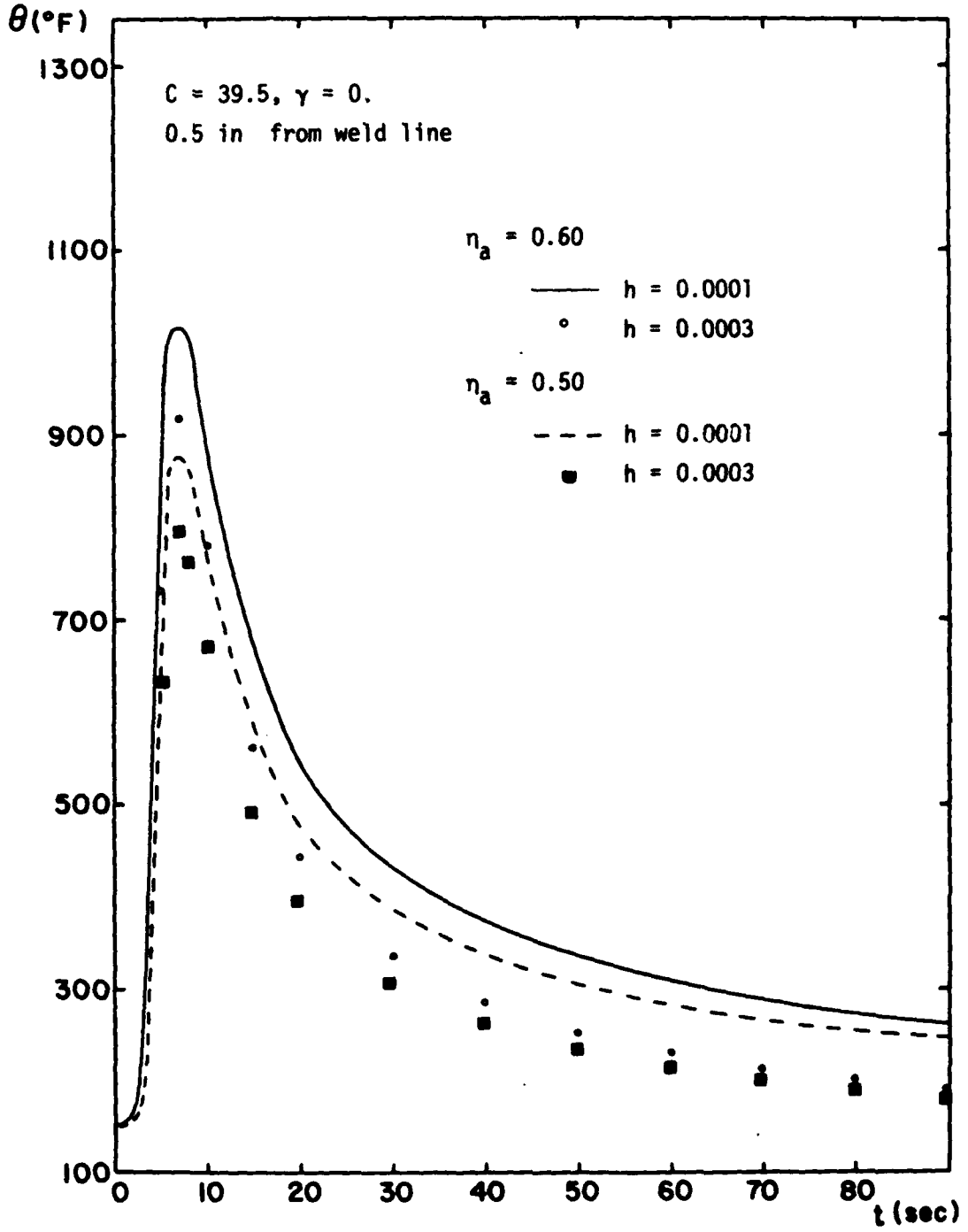

FIGURE 2.7 Effect of heat input and heat losses on finite heat source solution (at 0.5 in away from the weld centerline)

(dated November 30, 1979) were analyzed. No good correlation was obtained, however, owing to the assumptions inherrent in the model. These assumpions make its use more appropriate in the case of thin plates.

To test this proposition, experimental results previously obtained[5] when welding a 0.125 in (3.2 mm) thick low carbon steel plate were analyzed. The welding speed was 9 ipm and the arc power 5000 J/sec. Figure 2.8 shows the comparison between experiments and analysis at two points located 0.4 and 0.7 in (10.2 and 17.8 mm) away from the weld centerline. As postulated, the finite heat source model gives good results in this thin plate test case.

Modified Point Heat Source Model. The conventional point heat source closed form solution[6] fails to give good results in the case of multipass welding. This is due to the fact that the solution is based on the point source being located at the top surface of the plates being welded.

To accommodate the multipass welding case, a modification of the solution was made enabling one to locate the point source at any point through the plate's thickness. It thus becomes possible to simulate each welding pass by positioning the point source at the center of the pass.

The basic assumptions of the conventional solution were kept the same. Furthermore, the adiabatic boundary conditions on the top and bottom surfaces of the plate were satisfied by using the method of images. The obtained solution can then be expressed by the following equation

$$\theta = \theta_o + \frac{Q}{4\pi k} \cdot e^{-\lambda v \xi} \cdot \left\{ \frac{e^{-\lambda v R}}{R} + \sum_{n=1}^{\infty} \left[\frac{e^{-\lambda v R_n}}{R_n} + \frac{e^{-\lambda v R_{n'}}}{R_{n'}} \right] \right\} \quad (2.3.4)$$

---

[5] Tsai, C. L., "Parametric Study on Cooling Phenomena in Underwater Welding", Ph.D. Thesis, M.I.T., Sept. 1977.

[6] Rosenthal, D., "Mathematical Theory of Heat Distribution During Welding and Cutting", Welding Journal, 20 (5), 1941, pp. 220s-234s

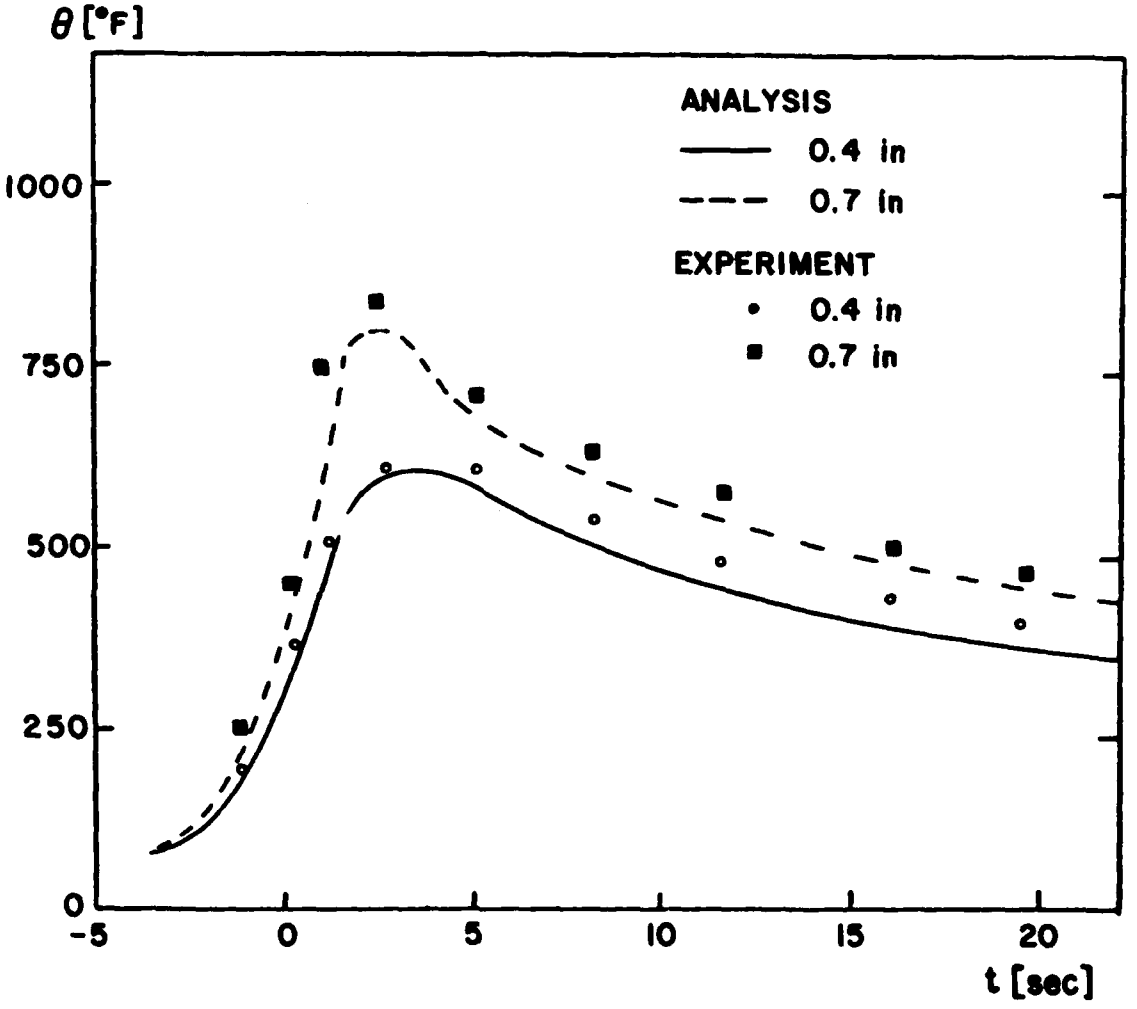

FIGURE 2.8 Comparison of finite heat source solution with experimental data for a 0.125 in thick welded plate

where

$$R_n = \sqrt{\xi^2 + y^2 + (OT_n+z)^2}$$

$$R_{n'} = \sqrt{\xi^2 + y^2 + (OB_n-z)^2}$$

$$OT_n = \sqrt{OB_{n-1} + 2.F}$$

$$OB_n = \sqrt{OT_{n-1} + 2.G}$$

with F and G being the distances of the point heat source from the top and bottom surfaces of the plate respectively, and OT_n and OB_n the distances of the point heat source from the nth imaginary ones with respect to the top and bottom surfaces respectively. All other quantities have been previously defined.

A computer program has been written in FORTRAN IV language to implement the above solution. In addition to the above, the program can take into account the temperature variation of the material properties through an iterative procedure, as well as the effect of each welding pass on the weld joint shape.[7]

Figure 2.9 presents a comparison of the various point heat source solutions as applied to the same case as the one for the finite heat source model discussed earlier. Shown are the cases of constant material properties with the point heat source on the top surface of the plate and at a distance 0.4375 in (11.1 mm) from the top (simulating the first pass of an actual welding experiment) and the case of variable properties.

The results show clearly the overestimation of temperatures if the conventional point heat source is applied even if the temperature variation of material properties is considered. This overestimation is

[7] Nishida, M., "Analytical Prediction of Distortion in Welded Structures," S.M. Thesis, M.I.T., May 1976.

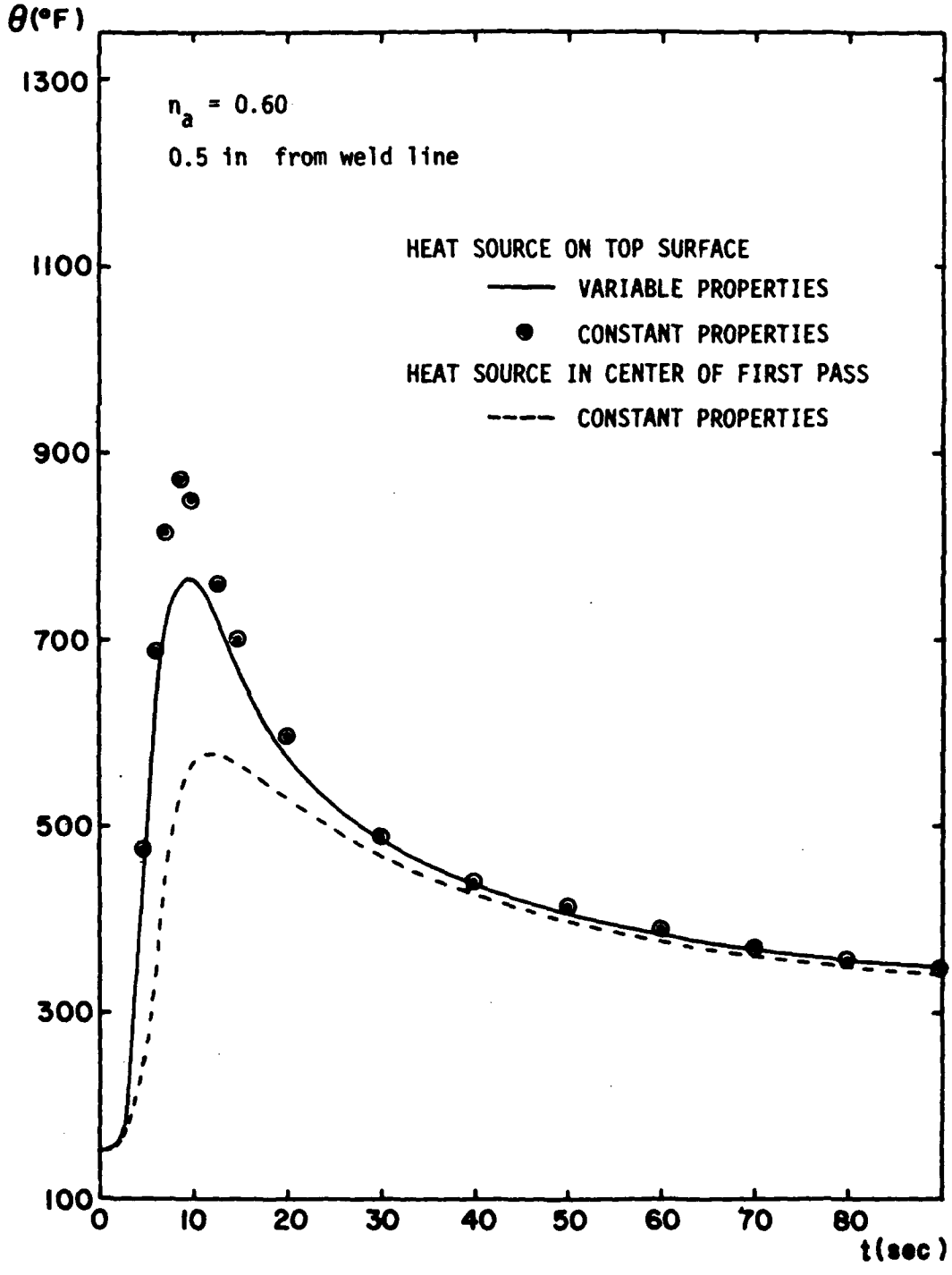

FIGURE 2.9 Investigation of point heat source solutions (0.5 in from weld line)

even more pronounced in the high temperature region close to the weld centerline. At the same time experimental results previously obtained[8] seem to have a good correlation with the ones obtained using the modified approach.

Furthermore, a comparison of the modified point heat source solution results with the ones obtained using the finite heat source model reveals that the latter predicts too high cooling rates if the maximum temperatures reached are matched for the two solutions.

Conclusion. The new finite heat source model developed for predicting temperature distributions during welding can be applied when welding thin plates, preferably made of materials exhibiting a linear temperature dependence of the thermal conductivity (e.g., aluminum). In these cases good correlations can be obtained with experimental data in the regions outside the fusion zone.

When analyzing multipass welding the modifications made in the conventional point heat source solution allow it to better predict the temperature distributions outside the fusion zone.

2.3.2 Numerical Solution

Since the advent of the electronic digital computer several serious efforts have been made to numerically solve the heat transfer problem. The finite difference method had initially the edge in these numerical calculations; today, however, the advantages of the finite element method, especially if coupled with thermal stress analyses, are more and more recognized.

In this section efforts at performing the heat transfer analysis during welding using the finite element method will be described. This analysis is based on the multipurpose finite element program ADINAT

[8] See Section 2.3.1 of First Technical Progress Report to O.N.R., November 30, 1979.

(Automatic Dynamic Incremental Nonlinear Analysis of Temperatures) developed by Bathe and coworkers[9] at the Department of Mechanical Engineering, M.I.T.

Governing Equation. The governing incremental isoparametric finite element equations for the nonlinear heat transfer problem can be written in matrix form as follows:

$$({}^{t}\underline{K}^{k} + {}^{t}\underline{K}^{c} + {}^{t}\underline{K}^{r})\,\Delta\underline{\theta}^{(i)} = {}^{t+\alpha\Delta t}\underline{Q} + {}^{t+\alpha\Delta t}\underline{Q}^{c(i-1)} + {}^{t+\alpha\Delta t}\underline{Q}^{r(i-1)} - {}^{t+\alpha\Delta t}\underline{Q}^{k(i-1)} \tag{2.3.5}$$

or

$${}^{t}\hat{\underline{K}}\,\Delta\underline{\theta}^{(i)} = {}^{t+\alpha\Delta t}\hat{\underline{Q}}^{(i-1)} \tag{2.3.5a}$$

where ${}^{t}\hat{\underline{K}}$ is the effective conductivity matrix at time t consisting of the conductivity, nonlinear convection, and radiation matrices; ${}^{t+\alpha\Delta t}\underline{Q}$ is the heat flow vector including the effects of surface heat flow inputs, internal heat generation and temperature-dependent heat capacity; ${}^{t+\alpha\Delta t}\hat{\underline{Q}}^{(i-1)}$ is the effective heat flow vector; and $\Delta\underline{\theta}^{(i)}$ is the increment in nodal-point temperatures in iteration i,

$${}^{t+\alpha\Delta t}\underline{\theta}^{(i)} = {}^{t+\alpha\Delta t}\underline{\theta}^{(i-1)} + \Delta\underline{\theta}^{(i)} \tag{2.3.6}$$

Equation (2.3.5) represents the heat flow equilibrium at time $t+\alpha\cdot\Delta t$, where $0\leq\alpha\leq1$ and α is chosen to obtain optimum stability and accuracy in the solution. Furthermore, the solution using these equations corresponds to the modified Newton-Raphson iteration scheme.

---

[9] Bathe, K.J., "ADINAT-A Finite Element Program for Automatic Dynamic Incremental Nonlinear Analysis of Temperature," AVL Report 82448-5, Mech. Eng. Dept., M.I.T., May 1977 (revised December 1978).

Boundary conditions. Convection and radiation boundary conditions are taken into account by including the matrices ${}^{t}\underline{K}^{c}$ and ${}^{t}\underline{K}^{r}$ and the vectors ${}^{t+\alpha\Delta t}\underline{Q}^{c}$ and ${}^{t+\alpha\Delta t}\underline{Q}^{r}$ in Eqn. (2.3.5). Additional external heat flow input on the boundary is specified in ${}^{t+\alpha\Delta t}\underline{Q}$ as surface heat flow input. Prescribed temperature conditions can also be specified.

With respect to the welding problem these boundary conditions can be stated in more detail as follows:

(1) Convection heat losses from the plates' surfaces can be modelled according to Newton's linear law

$$q^{s} = h \cdot (\theta_{e} - \theta^{s}) \tag{2.3.7}$$

where h is the temperature dependent convection coefficient, θ_{e} the environmental temperature, and θ^{s} the surface temperature at the point under consideration. There is some difficulty in estimating the temperature dependence of h. Although most previous investigators considered h to be constant, efforts were made in this study to rationally estimate it on the basis of past semi-empirical studies. Table 2.2 provides the three different sets of values tested. Discussion of the obtained results will be made later.

(2) Radiation heat losses are very significant in the vicinity of the weld metal because of the large difference between the surface and environmental temperatures. These losses are modelled according to the quartic Stefan-Boltzman law

$$q^{s} = \sigma\varepsilon A(\theta_{r}^{4} - \theta^{s4}) \tag{2.3.8}$$

where σ = Stefan-Boltzman constant
ε = emissivity of the surface
A = shape factor
θ_{r} = sink temperature
θ^{s} = surface temperature

TABLE 2.2

TEMPERATURE DEPENDENCE OF HEAT CONVECTION COEFFICIENT

$\theta^s - \theta_e$ [°R]	h [Btu/sec in^2°R]		
	Case 1	Case 2	Case 3
0	0	0	0
100	$.2 \times 10^{-5}$	$.2 \times 10^{-5}$	$.1 \times 10^{-4}$
500	$.5 \times 10^{-5}$	$.1 \times 10^{-4}$	$.6 \times 10^{-4}$
1000	$.1 \times 10^{-4}$	$.2 \times 10^{-4}$	$.1 \times 10^{-3}$
5000	$.58 \times 10^{-3}$	$.58 \times 10^{-4}$	$.6 \times 10^{-3}$
50000	$.12 \times 10^{-2}$	$.12 \times 10^{-2}$	$.12 \times 10^{-2}$

Note: θ^s = surface temperature
θ_e = environmental temperature

In this study the shape factor was taken to be unity and the emissivity coefficient 0.8.

(3) Temperatures can be prescribed at any point and/or surface of a weldment. Such a case, however, seldom arises in welding analyses.

(4) The heat input during welding is modelled using the concept of arc efficiency. For the space distribution of the heat input, a consistent formulation was adopted assuming a uniform distribution over the top of each weld bead. Finally, the time distribution of the heat input was modelled in such a way that the passing of the arc over the cross section examined could be simulated (a linear increase as the arc approaches, uniform as the arc travels over the cross section, followed by a linear decrease).

Time integration schemes. A family of one-step methods[10] is considered for the time integration using the parameter α. The scheme was found to be unconditionally stable for $\alpha \geq 1/2$ and to generally give better solution accuracy when $\alpha = 1$ (Euler backward method). Finally the modified Newton iteration is guaranteed to converge provided the time step Δt is small enough.

Material Properties. The temperature dependence of the thermal conductivity, k, the specific heat, c, and the density, ρ, are taken into account in the analysis. Figure 2.10 taken from Papazoglou's thesis shows these temperature variations for the case of HY-130 steel, the material analyzed in this study. The latent heat of fusion was also taken into account in the analysis with a value equal to 118 Btu/lbm (275 kJ/kg).

Two-dimensionality of Problem. Assuming that the welding heat source (arc) is moving at a constant speed along a regular path (e.g., a straight line in a planar weld), that the weld speed in sufficiently high relative to the material's characteristic diffusion rate, and that end effects resulting from either initiation or termination of the heat source can be neglected, the three-dimensional character of the heat transfer problem can be simplified. This can be achieved by analyzing a cross-section of the weldment of unit thickness and located in the mid-length region of the weld.

This approach, which is elaborated in Papazoglou's thesis, was followed in the present analysis resulting in very accurate results.

Molten Pool Modeling. The heat transfer mechanism in the weld metal, when molten, is extremely complex and its physics are not well understood as of today. These complexities arise not only from the

---

10 Hughes, T., "Unconditionally Stable Algorithms for Nonlinear Heat Conduction", Comp. Meth. in Appl. Mech. and Eng., 10, 1977, pp. 135-139.

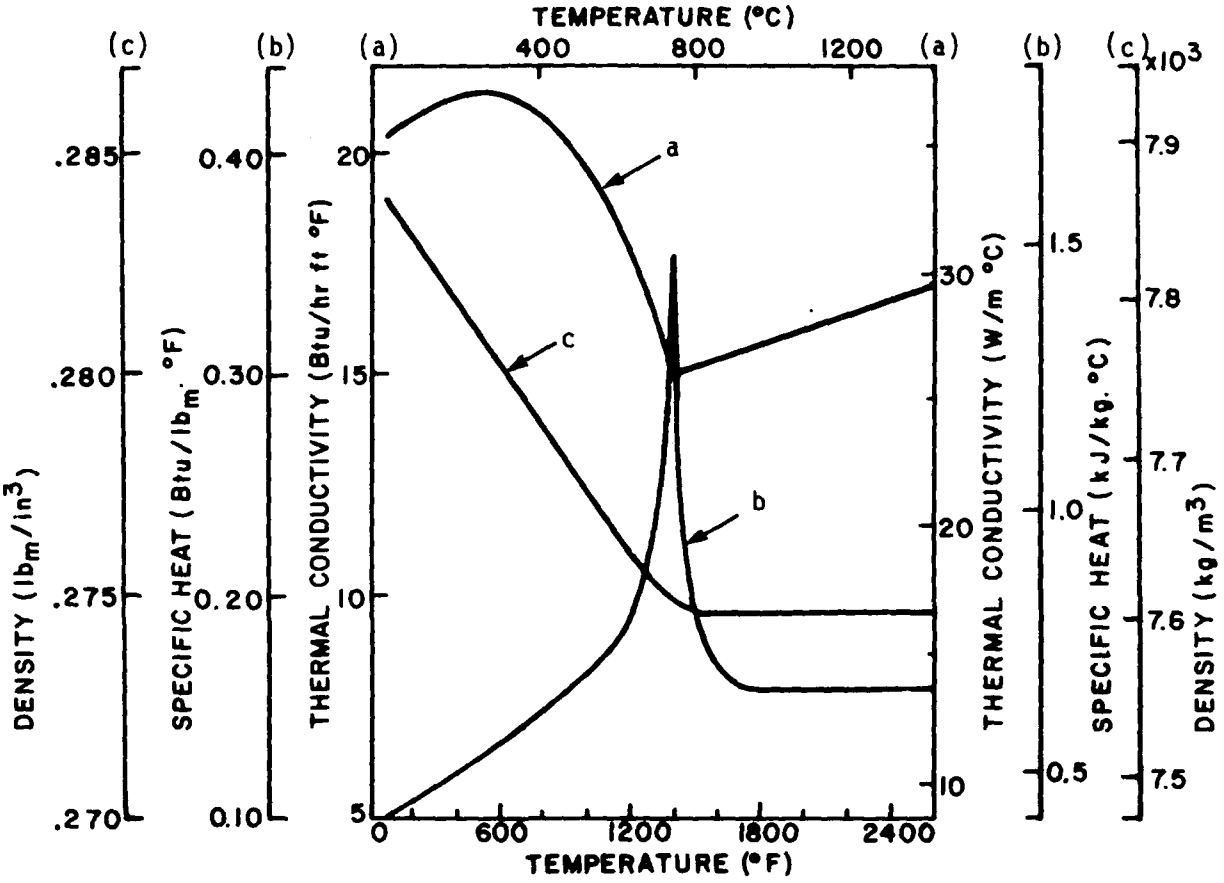

(a) Variation of thermal conductivity with temperature for HY-130

(b) Variation of specific heat with temperature for HY-130

(c) Variation of density with temperature for HY-130

FIGURE 2.10

difficulty involved in modeling the welding arc heat flux correctly, but also from the behavior of the convective motion of the molten metal, the thermal properties of the molten metal (including the phase transformations that take place during melting and solidification), the electric heating due to the current flow in the base metal, the boundary conditions for heat losses, etc. Many investigators have recognized these difficulties and have tried to find ways to approximate the phenomena involved.

A look at the available literature reveals that there are generally three ways for handling the problem. The first one, still at its developing stages, tries to understand and subsequently mathematically model the physical phenomena involved, i.e., the fluid flow, the convective heat transfer, etc.[11] Since no conclusive general results are available yet, this approach was not pursued further.

In the second way the problem is divided into two parts. First the shape of the molten pool is semiempirically determined; then the heat flow equations are solved numerically in the solid metal only using the melting isotherm as a boundary condition.[12] This method could not be used in the present investigation, however, because the temperature distribution in the weld metal has to be calculated too if a stress analysis is to follow (most plastic deformation that causes the formation of residual stresses takes place in this region).

The third and final approach tries to simulate the convective heat transfer mechanism in the molten metal by using a value for the thermal conductivity of the molten metal an order of magnitude higher than that of the material at the solidus temperature. This approach, although strictly not physically correct, was used in the present investigation.

Finally, since the cases analyzed involved multipass welding, it was necessary to find a way to model the laying of the various beads

---

[11] Dilawari, A.H., Szekely, J., and Eagar, T.W., "Electromagnetically and Thermally Driven Flow Phenomena in Electroslag Welding", Met. Trans. B, 9B, 1978, pp. 371-381.

[12] Tsai, C.L., op.cit.

during the welding cycle. This was made possible by the element birth-and-death capabilities of the code used. In other words, the program ADINAT is capable of giving birth to a predetermined number of elements at predetermined time instances, thus enabling one to model the laying of a bead by specifying the appearance of the elements representing it at the time it physically appears.

Comparison of Numerical and Experimental Results. Using the modeling procedures discussed above, a heat transfer analysis of a series of experiments was performed. These experiments involved the multipass GMA welding of 1 in (25.4 mm) thick HY-130 plates. Details of these experiments, which were similar to the ones described in Section 2.3.1 of the First Technical Progress Report to O.N.R., can be found in Papazoglou's thesis.

Figures 2.11a and 2.11b show the finite element mesh used at a cross section of the plate in its mid-length. Note that Figure 2.11a shows the leftmost 11.5 inches (292.1 mm) of the plate with the rightmost 11.5 inches (292.1 mm) being exactly symmetric, whereas Figure 2.11b shows, in different scale, the middle 1 inch (25.4 mm) that includes the weld metal and the heat affected zone.

A total of 37 isoparametric elements were used divided into two groups of 30 and 7 elements, the second group representing the weld metal. Referring to Figure 2.11b, elements 3, 4, and 5 model the first welding pass, elements 1 and 2 the second, and elements 6 and 7 the third.[13] It is once more emphasized that during the analysis of each pass the elements representing the next passes remained inactive using the birth-and-death option of the program. Finally, a total of 72 nodes were used.

It should also be mentioned at this point that due to the fact that only the first welding pass is symmetric, the total cross-section, and not half of it, had to be modelled with finite elements.

---

[13] The general shape of each welding pass was found by cross-sectioning each specimen after all measurements have been made and etching the surface to reveal the weld pass boundaries.

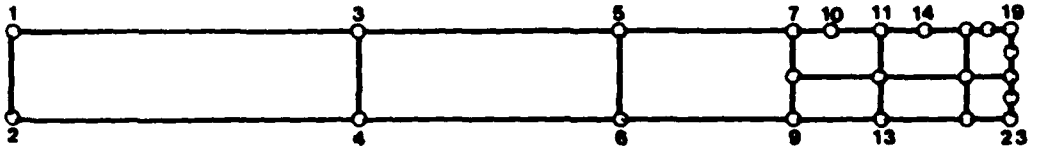

FIGURE 2.11 a Finite element mesh used in heat transfer analysis (rightmost 11.5 in of cross-section)

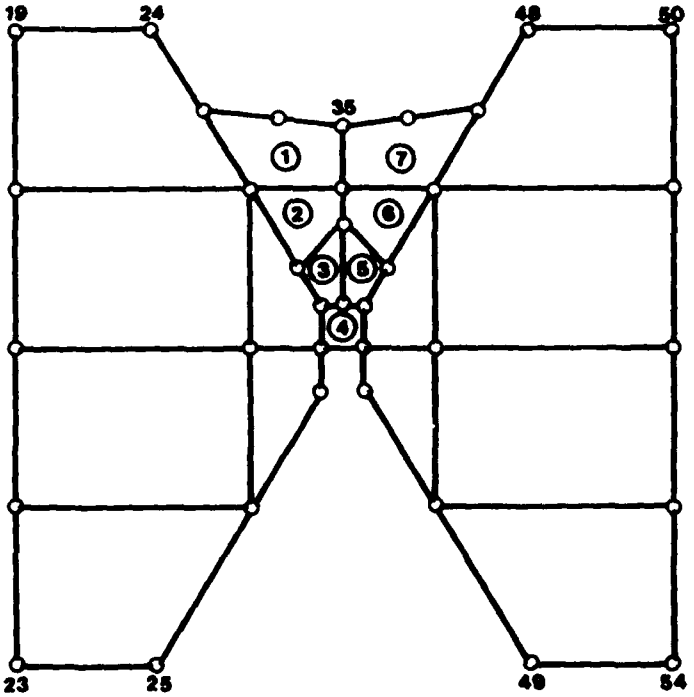

FIGURE 2.11 b Finite element mesh continued (center 1. in)

Table 2.3 summarizes the four analyses performed. Two parameters were varied, the arc efficiency, η_a, and the temperature variation of the convection coefficient, h, given the fact that some uncertainty exists regarding their true values. All other variables were kept constant in the four cases, assuming the values referred to in previous sections.

TABLE 2.3

SUMMARY OF ANALYSES PERFORMED

Analysis	η_a[1]	h case[2]
A1	0.65	1
A2	0.60	1
A3	0.60	2
A4	0.70	3

Notes: [1] η_a is the arc efficiency utilized.

[2] Refers to the case presented in Table 2.2

Cases A2, A3, and A4 are compared with the experimentally obtained results in Fig. 2.12 for a point on the plate's top surface 0.5 in (12.7 mm) away from the weld centerline and for the first welding pass. Considering the same heat input (η_a=0.60), little difference is found between cases A2 and A3. This is due to the fact that although higher values for the convection coefficient were chosen in analysis A3, these values were not high enough to significantly alter the heat losses from the top and bottom surfaces of the plate and consequently the temperature distribution. A substantial increase in the convection coefficient was therefore chosen for case A4; at the same time, however, an increase in the arc efficiency was made to partially compensate for the higher h and thus to obtain a good estimate of the maximum temperature reached. As seen in Fig. 2.12 the combination of values used in this latter analysis succeeded in bringing the cooling rate much closer to the experimental one.

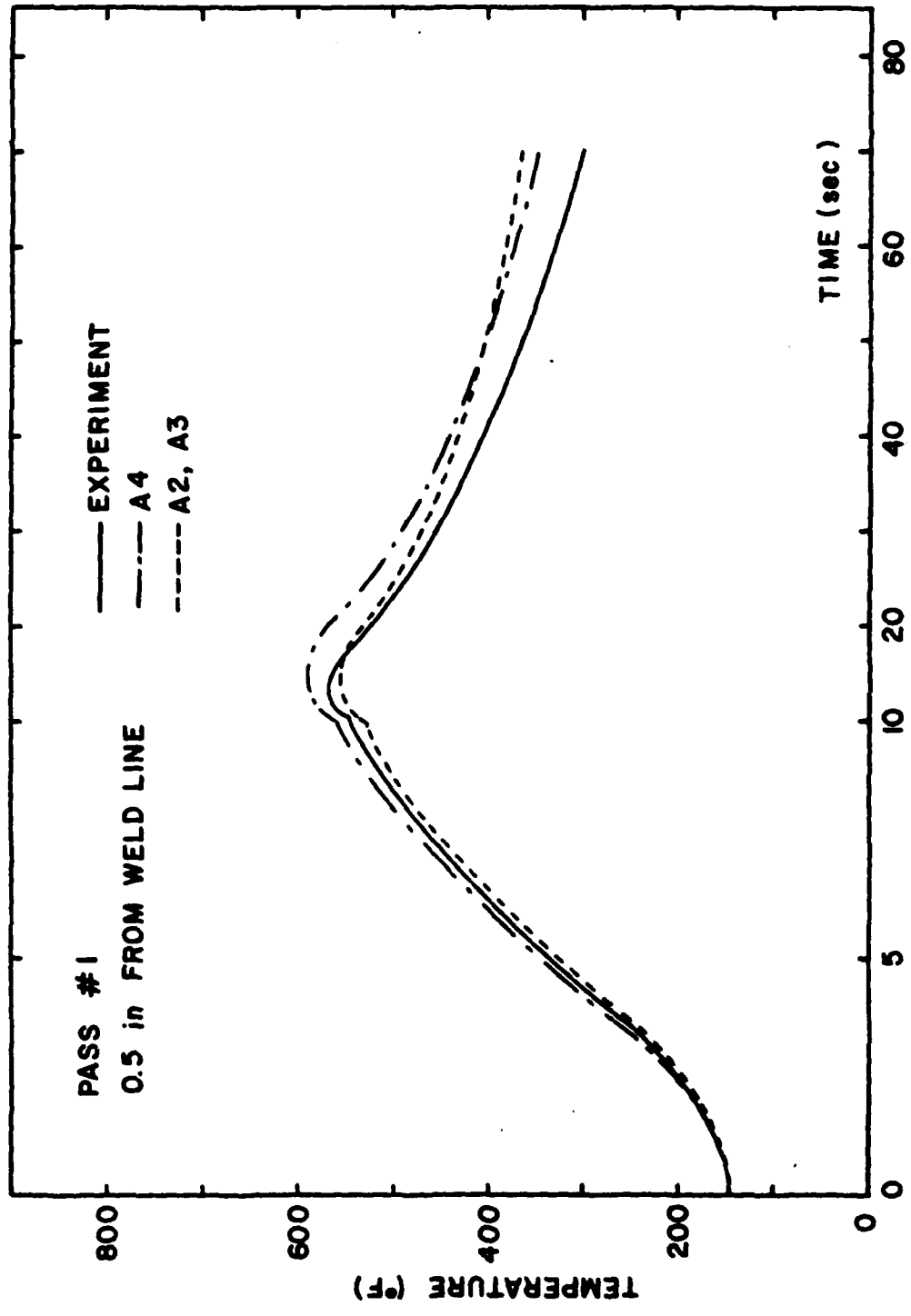

FIGURE 2.12 Comparison of finite element results with experimental data (weld pass no. 1)

At the same time a 4% overprediction of the maximum temperature is observed. The difference, however, was very small so that any further analysis was not felt necessary.

Similar results were found at other points of the plate. Case A4 came always closest at matching the experimentally obtained results.

Temperature distributions for the second welding pass are shown in Figure 2.13. Results for three points on the plate's surface located 0.5, 1.0, and 1.5 in (12.7, 25.4, and 38.1 mm) away from the weld centerline as predicted by cases A3 and A4 are compared with experimental data. As was the case with the first welding pass, analysis A4 comes again closest at matching the experimentally obtained temperature histories.

The temperature histories calculated from analysis A4 were subsequently used as input to the stress analysis discussed in Section 2.4. It should be noted that when this stress analysis failed to give accurate results using the finite element mesh shown in Figures 2.11a and 2.11b, the heat transfer analysis for the first welding pass was repeated with the finer mesh shown in Figures 2.20a and 2.20b. The same conditions as the ones for case A4 were used. No significant difference was observed between the temperatures calculated on this finer mesh and the ones with the more crude one.

Conclusion. Finally, some thoughts regarding the parametric analyses performed should be expressed. To many this would look like an exercise in curve-fitting, trying to match experiments and analysis. In reality, the problem is much more fundamental and has to do with the uncertainties involved in estimating several parameters required as input to the solution. The many complexities and the nonlinearity of the welding problem combined with the state-of-the-art in arc physics and heat transfer, do not allow at present the accurate calculation of, among others, the heat input to the plates being welded and the temperature dependence of the heat convection coefficient. Therefore, and until further developments in these areas are made, some parametric analyses will be necessary to better estimate the temperature distribution during

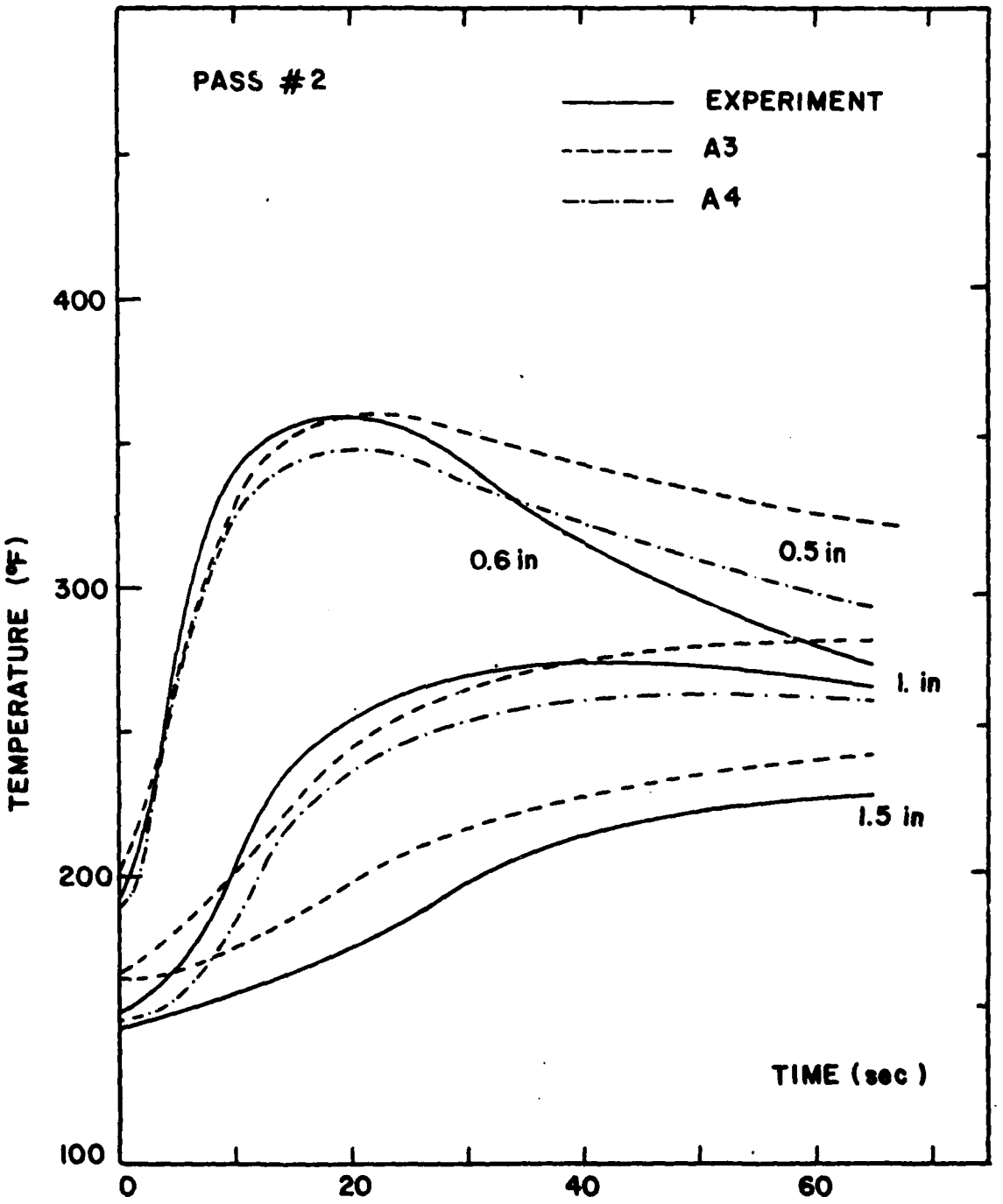

FIGURE 2.13 Comparison of finite element results with experimental data (pass no. 2)

welding. It is nevertheless hoped that analyses similar to the ones performed in this study would help future investigators in better selecting appropriate values for uncertain parameters.

2.4 Thermal and Residual Stress Analysis

Using the predicted temperature distributions one can calculate the transient strains, transient stresses and residual stresses due to welding. The calculation of strains and stresses, however, poses a much more formidable problem than the one encountered in the heat transfer analysis, making the use of numerical techniques a necessity. These difficulties stem from the complicated thermal-elastic-plastic state developed in and around the weld metal during welding.

Two general techniques have been developed to solve the problem. The first one is based on the rather simple one-dimensional analysis.[14] Results using this analysis were reported in the first two technical progress reports to O.N.R. under the present contract.

The second technique is based on the finite element method. This section is devoted to describing how this method was used in the welding case. The discussion is based on the following thesis:

Papazoglou, V.J., "Analytical Techniques for Determining Temperatures, Thermal Strains, and Residual Stresses During Welding", Ph.D. Thesis, M.I.T., May 1981.

2.4.1 Finite Element Formulation

The thermal-elastic-plastic and creep constitutive model (with the phase transformation modification discussed in Section 2.4.2) of the multipurpose finite element program ADINA (Automatic Dynamic Incremental Nonlinear Analysis)[15] will be used for predicting the transient strains,

---

[14] Papazoglou, V.J., "Computer Programs for the One-Dimensional Analysis of Thermal Stresses and Thermal Movement During Welding", Manual # 2 of Report Under Contract N00014-75-C-0469 to O.N.R., M.I.T., 1977.

[15] Bathe, K.J., "ADINA-A Finite Element Program for Automatic Dynamic Incremental Nonlinear Analysis", AVL Report 82448-1, Mech. Eng. Dept., M.I.T., September 1975 (revised December 1978).

transient stresses, and residual stresses due to welding. The model was developed by Snyder and Bathe[16] in 1980. Some features of this model will be described in this section for completeness.

The governing incremental finite element equations for the problem can be written as,

$$ {}^{\tau}\underline{K}\ \Delta\underline{U}^{(i)} = {}^{t+\Delta t}\underline{R} - {}^{t+\Delta t}\underline{F}^{(i-1)} \tag{2.4.1} $$

where ${}^{\tau}\underline{K}$ is the tangent stiffness matrix corresponding to time τ; ${}^{t+\Delta t}\underline{R}$ is the nodal-point external force vector at time $t+\Delta t$; ${}^{t+\Delta t}\underline{F}^{(i-1)}$ is a vector of nodal-point forces that are equivalent, in the virtual work sense, to the internal element stresses at time $t+\Delta t$ and iteration $i-1$

$$ {}^{t+\Delta t}\underline{F}^{(i-i)} = \int_V \underline{B}_L^T\ {}^{t+\Delta t}\underline{\sigma}^{(i-1)}\, dv \tag{2.4.2} $$

and $\Delta\underline{U}^{(i)}$ is the increment in nodal-point displacement in iteration i

$$ {}^{t+\Delta t}\underline{U}^{(i)} = {}^{t+\Delta t}\underline{U}^{(i-1)} + \Delta\underline{U}^{(i)} \tag{2.4.3} $$

The solution using Eq. (2.4.1) corresponds to the modified Newton-Raphson iteration procedure which is helpful in improving the solution accuracy and in many cases in preventing the development of numerical instabilities. The convergence of the iteration can be accelerated using the Aitken method or, in complex material nonlinear cases (like the welding problem), improved using the BFGS (Broyden-Fletcher-Goldfarb-Shanno) matrix updating method.

In the thermo-elastic-plastic and creep model, and assuming infinitesimal strains, the total strain at time τ, ${}^{\tau}e_{ij}$, is assumed

---

16 Snyder, M.D., and Bathe, K.J., "A Solution Procedure for Thermo-Elastic-Plastic and Creep Problems", J. Nuclear Eng. and Design (to be published).

to be given by

$$ {}^{\tau}e_{ij} = {}^{\tau}e^{E}_{ij} + {}^{\tau}e^{P}_{ij} + {}^{\tau}e^{C}_{ij} + {}^{\tau}e^{TH}_{ij} \qquad (2.4.4) $$

where ${}^{\tau}e^{E}_{ij}$ = elastic strain

${}^{\tau}e^{P}_{ij}$ = plastic strain

${}^{\tau}e^{C}_{ij}$ = creep strain

${}^{\tau}e^{TH}_{ij}$ = thermal strain

so that at any time τ during the response the stress is given by the constitutive law for an isotropic thermo-elastic material

$$ {}^{\tau}\sigma_{ij} = {}^{\tau}C^{E}_{ijrs} \left({}^{\tau}e_{rs} - {}^{\tau}e^{P}_{rs} - {}^{\tau}e^{C}_{rs} - {}^{\tau}e^{TH}_{rs}\right) \qquad (2.4.5) $$

with ${}^{\tau}C^{E}_{ijrs}$ denoting a component of the elastic constitutive tensor.

The thermal strains are

$$ {}^{\tau}e^{TH}_{rs} = {}^{\tau}\alpha_{m}({}^{\tau}\theta - \theta_{R})\delta_{rs} \qquad (2.4.6) $$

where ${}^{\tau}\alpha_{m}$ is the average thermal expansion coefficient, θ_{R} is the reference temperature, and δ_{rs} the Kronecker delta. It is this term of Eq. (2.4.5) that will be modified in the next section to take into account the effects of phase transformation.

The creep strains, ${}^{\tau}e^{C}_{rs}$, are determined using the approach proposed by researchers at the Oak Ridge National Laboratory.[17] Given that in the welding problem the time intervals at high temperatures are short, however, creep will not be considered in this study.

---

17 Corum, J.M., et al., "Interim Guidelines for Detailed Inelastic Analysis of High Temperature Reactor System Components", Oak Ridge National Laboratory Report ORNL-5014, December 1974.

For the plastic strains, ${}^{\tau}e^{P}_{rs}$, the situation is more complicated. Although the classical theory of isothermal plasticity is a well tested one, extension of the theory to non-isothermal cases is difficult to experimentally substantiate. Several investigators have proposed modifications but very few experiments have been performed. Corum et al.[18] and Phillips[19] have reported relatively good agreement between theory and experiments, but for temperatures up to about 1000°F only. During welding, though, the temperatures rise to above the A_1 temperature (1210°F for steel) inside the HAZ-base metal boundary and above the liquidus temperature in the weld metal. For lack of any alternative, however, the same non-isothermal theory of plasticity will be used throughout the temperature range encountered in welding problems.

The general form of the yield or loading function for multiaxial stress conditions is

$$ {}^{\tau}F = {}^{\tau}F({}^{\tau}\sigma_{ij}, {}^{\tau}\alpha_{ij}, {}^{\tau}\sigma_{y}) \tag{2.4.7} $$

where ${}^{\tau}\alpha_{ij}$ and ${}^{\tau}\sigma_{y}$ are functions of the history of plastic deformation and temperature. For elastic behavior, ${}^{\tau}F < 0$, and for plastic behavior ${}^{\tau}F = 0$. As a consequence of Drucker's postulate for stable plastic materials, ${}^{\tau}F$ defines a convex surface in the stress-temperature space. It is also assumed that the isothermal normality condition remains valid, so that

$$ {}^{\tau}\dot{e}^{P}_{rs} = {}^{\tau}\lambda \frac{\partial\, {}^{\tau}F}{\partial\, {}^{\tau}\sigma_{ij}} \tag{2.4.8} $$

where ${}^{\tau}\lambda$ is a positive scalar. The selection of a hardening rule is also required for the calculation of ${}^{\tau}\lambda$. In ADINA either isotropic

---

[18] Ibid.

[19] Phillips, A., "The Foundations of Thermoplasticity-Experiments and Theory", Symposium on Topics in Appl. Cont. Mech., Vienna, March 1-2, 1974.

or kinematic hardening can be assumed. Because cyclic plasticity is expected in the welding problem, the kinematic hardening mechanism, thought by many to better model the phenomena involved, was chosen. The assumptions involved in this mechanism are that the size of the yield surface depends on the temperature only, whereas the translation rate of the yield surface in the stress space depends on the plastic strain rate.

A very important aspect of the analysis is the accurate integration of stresses at time t+Δt and iteration i

$$^{t+\Delta t}\underline{\sigma}(i) = {}^{t+\Delta t}\underline{C}\left({}^{t+\Delta t}\underline{e}(i) - {}^{t+\Delta t}\underline{e}^{P}(i) - {}^{t+\Delta t}\underline{e}^{TH}(i)\right) \qquad (2.4.9)$$

where

$$^{t+\Delta t}\underline{e}^{P}(i) = {}^{t}\underline{e}^{P} + \int_{t}^{t+\Delta t(i)} d^{\tau}\underline{e}^{P} \qquad (2.4.10)$$

and where it was assumed that creep strains are zero. The intergration of Eq. (2.4.10) is performed using the α-method where α = 0 and 1 correspond to the Euler forward (explicit) and Euler backward (implicit) methods, respectively. The implicit scheme can display considerably better stability characteristics but is more costly, requiring equilibrium iterations. Furthermore, the accuracy of the integration is enhanced with the use of subincrements in each time step, an important feature considering the rapidity with which some of the solution variables and material parameters vary with time during welding.

2.4.2 *Phase Transformation Effects*

In most previous stress analyses of the welding problem no consideration was given to the phenomenon of phase transformations. The limited efforts reported in the literature are based on the use of a limited number (usually three) of experimentally obtained dilatational

curves for specific cooling rates and do not concentrate on the fundamentals of the phenomena involved.

At the same time in cases where poor agreement is observed between experimental data and analytical results, the discrepancy is attributed exactly to the fact that phase transformation strains are not taken into account.

In this subsection a model developed to calculate the phase transformation strains will be discussed. The model starts from the CCT diagram of the material under consideration which is either known experimentally or can be derived from the TTT diagram. Using the CCT diagram and the temperature distribution during welding, the history of microstructure formation during the cooling stages can be predicted. The combined transformation and thermal strains can then be estimated for each integration point based on the predicted microstructure history, the transformation strains for each allotropic phase change, and the average thermal expansion coefficient appropriate for each phase. Finally, these calculated strains are incorporated into the finite element program ADINA replacing the conventional thermal strains, ${}^{\tau}e_{ij}^{TH}$.

Computed CCT Diagram. Experimentally derived CCT diagrams exist today for several steel alloys, enabling one to predict the microstructure history during the cooling stage of the welding cycle. There are, however, alloys for which CCT diagrams are not available. In such instances the analyst would like to be able to compute a schematic CCT diagram based on available isothermal data and resembling as closely as possible the experimentally obtained one.

Among the methods proposed in the past for such calculations, the most popular ones are those proposed by Grange and Kiefer[20] and

[20] Grange, R.A., and Kiefer, J.M., "Transformation of Austenite on Continuous Cooling and its Relation to Transformation at Constant Temperature," ASM Transactions, 29 (3), 1941, pp. 85-115.

Manning and Lorig.[21] Since both methods utilize linear cooling rate and based on the fact that the welding cooling rates resemble log-linear curves, some modifications had to be made to take account of the latter. Based on these modifications a computer program was written capable of calculating schematic CCT diagrams from isothermal ones.

Figures 2.14 and 2.15 show the experimentally obtained TTT diagram and the calculated CCT one respectively for the case of HY-130 steel. It is believed that the use of log-linear cooling curves results in schematic CCT diagrams that are closer to the ones appropriate for predicting microstructures in the HAZ and the weld metal of a weldment.

It should be pointed out, however, that an even better approximation can be obtained if the microstructure prediction is based on rate equations. Efforts in this direction have been made for a very few steel alloys, primarily of eutectoid composition and much more research in the materials science field is needed for the development of similar rate equations for more complicated alloys, like the quenched and tempered HY-130 steel. Until such developments are made the above described methods with the proposed modifications are thought to be adequate in describing the phase transformations from an applied mechanics (macroscopic) point of view.

The previous discussion pertained to the bainite start, B_s, transformation temperature and can be extended to include any similar nucleation and growth transformation, such as the ferritic one. As far as the martensite transformation is concerned, the situation is different. Austenite transforms to martensite athermally (no thermal activation is involved). This means that once the martensite start transformation temperature, M_s, is known, the extent of the transformation is dependent only on the amount of undercooling below the M_s temperature.

---

21 Manning, G.K., and Lorig, C.H., "The Relationship Between Transformation at Constant Temperature and Transformation During Cooling", AIME Transactions, 167, 1946, pp. 442-463.

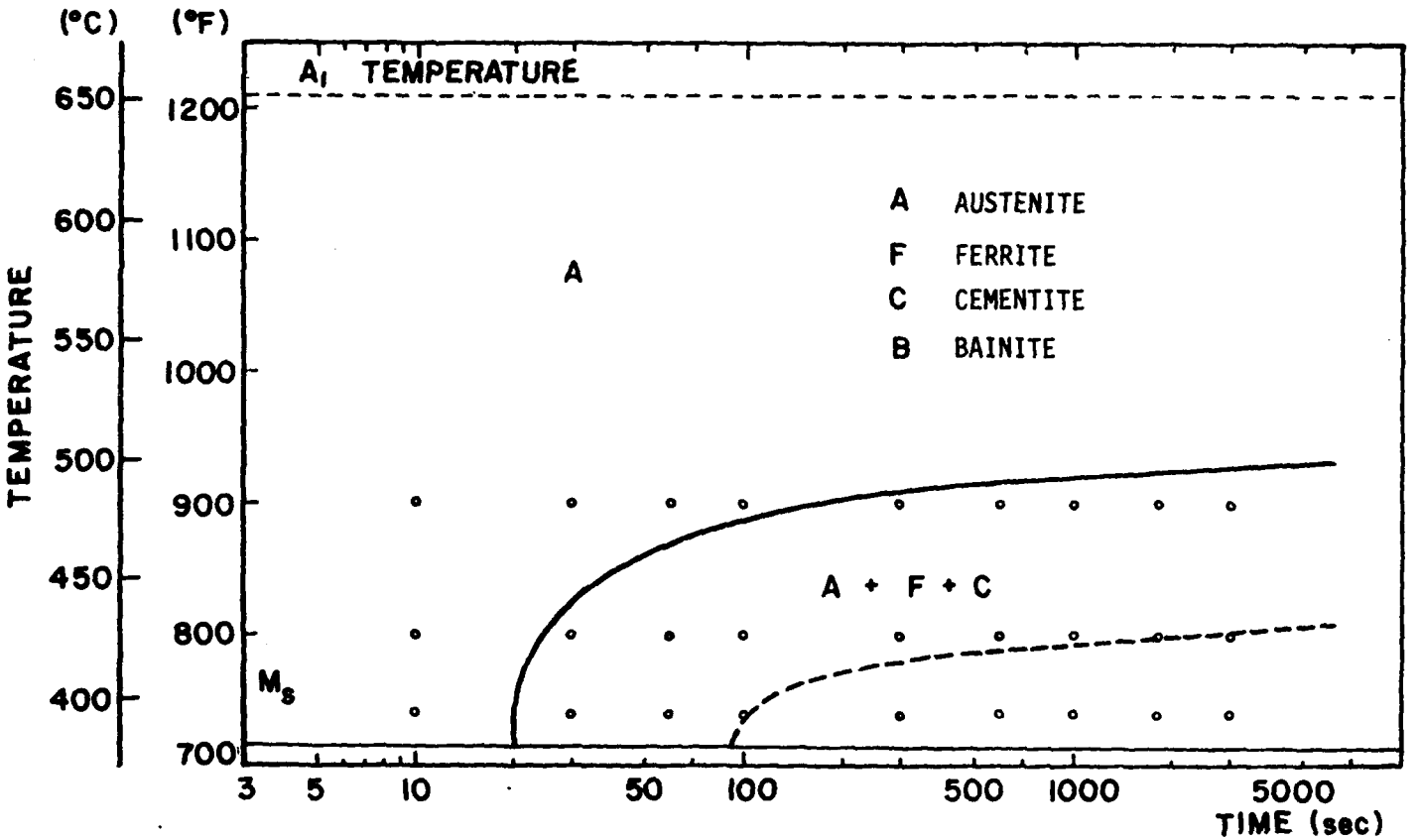

FIGURE 2.14 Isothermal transformation diagram for HY-130 steel

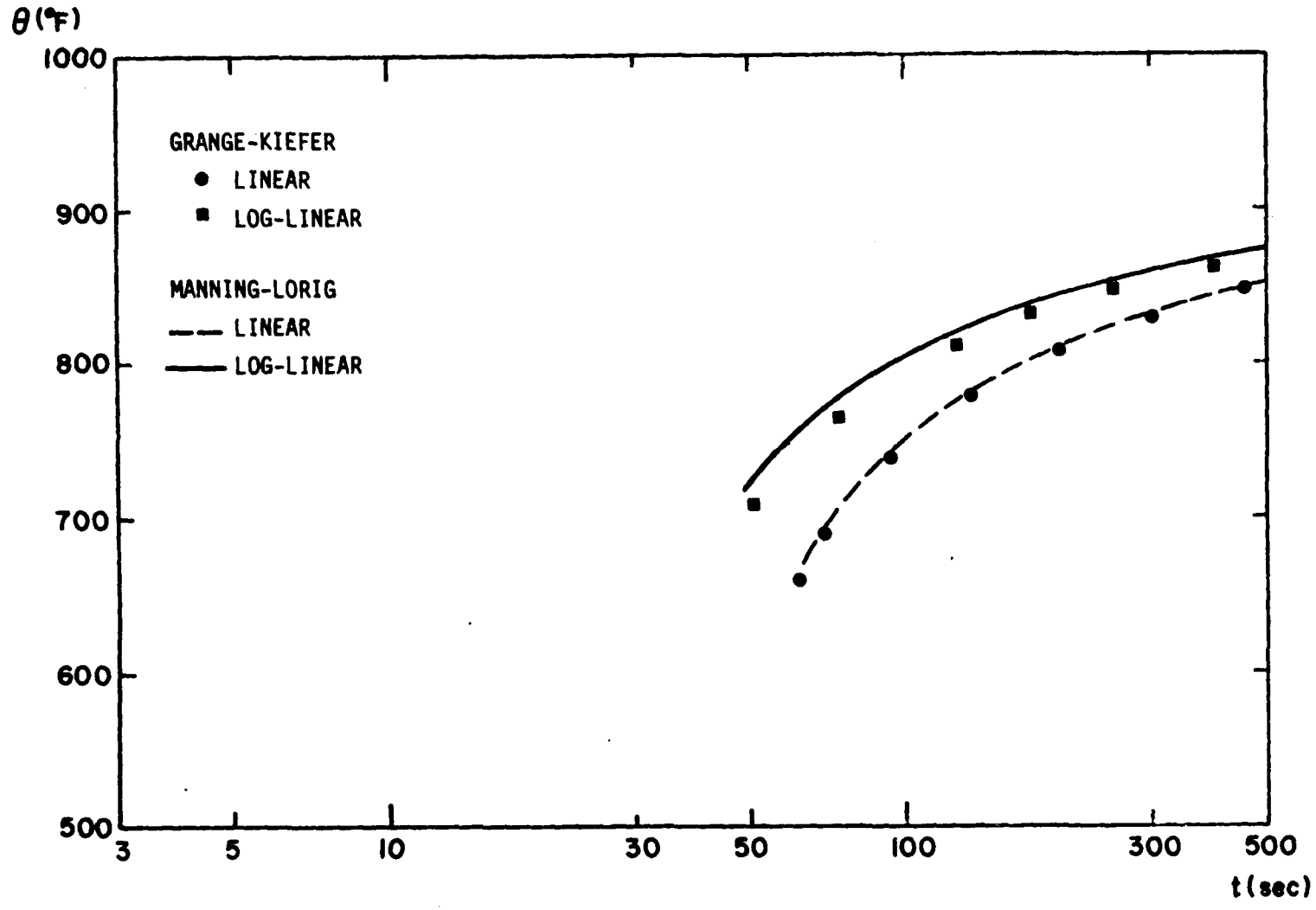

FIGURE 2.15 Schematic CCT diagrams for HY-130 steel
(Bainite start transformation curves)

It can therefore be assumed that the constant M_s temperature found in the TTT diagram can be carried over to the CCT diagram.

Microstructure Prediction. An idealization of the CCT diagram is shown in Figure 2.16. The basic assumption involved is that the bainite start, B_s, and bainite finish, B_f, transformation temperatures are constant, i.e., independent of the cooling rate, the maximum temperature (above the A_1 temperature) reached before cooling commences, and the time held at this maximum temperature. The last two assumptions require that full austenitization has taken place before, upon cooling, the A_1 temperature is reached and is thought to be reasonable for the welding case. Moreover, looking at Fig. 2.15 one notices that the assumption is reasonable for the HY-130 steel.

Furthermore, Figure 2.16 shows the B_f temperature to be in general different than the martensite start, M_s, one. For the case of HY-130, however, the two temperatures can be assumed to be equal. Finally, the assumption of constant M_s and M_f temperature is a completely acceptable one, owing to the athermal nature of the transformation.

To predict the microstructures during the cooling stage of the welding process an incremental strategy is involved so that the model can be compatible with the step-by-step solution of the nonlinear stress analysis using the finite element program ADINA. A procedure has therefore to be established that will enable one to calculate the proceeding of each transformation. The following equation has been used for this purpose:

$$f = f_F \cdot \left[1 - \left(\frac{\theta-\theta_f}{\theta_s-\theta_f}\right)^2\right] \qquad (2.4.11)$$

where f is the fraction of the product transformed at temperature θ, f_F the fraction of the product to be transformed at the transformation finish temperature, θ_f, and θ_s the start transformation temperature. Equation (2.4.11) is applied separately for each allotropic transformation, namely for the martensite to austenite one upon heating

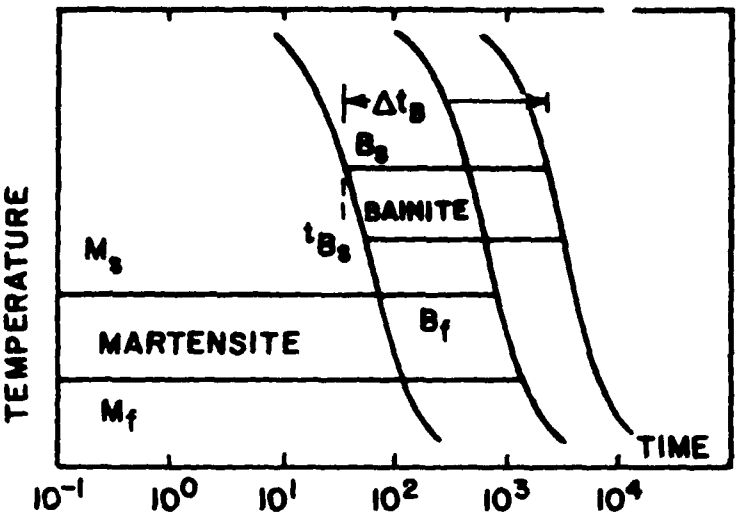

FIGURE 2.16 Idealized CCT diagram

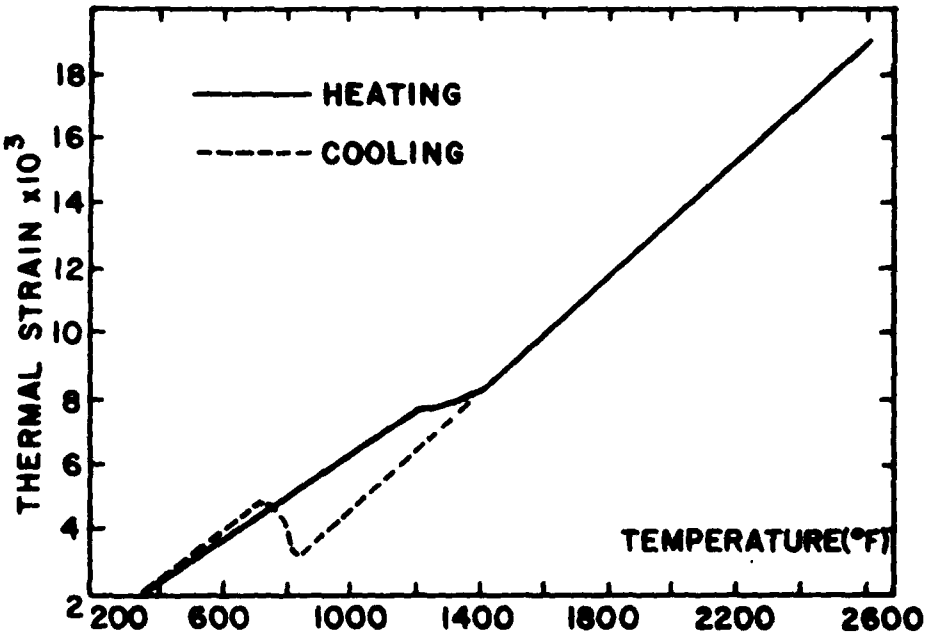

FIGURE 2.17 Typical dialatational curve including phase transformation effects

and for the austenite to bainite and austenite to martensite ones upon cooling.

Details on the calculation of f_p for each transformation are not included here. The interested reader is referred to Papazoglou's thesis.

Calculation of Transformation and Thermal Strains. Based on the microstructure predictions calculated by the methodology outlined above the combined thermal and transformation strains, e_{rs}^{TH}, developed during the welding thermal cycle can be found from

$$e_{rs}^{TH} = (e_1+e_2+e_3) \cdot \delta_{rs} \qquad (2.4.12)$$

where e_1 is the thermal strain in a mixutre of phases, e_2 the transformation strain, e_3 the thermal strain in a single phase, and δ_{rs} the Kronecker delta.

The estimation of the thermal strains e_1 and e_3 requires knowledge of the microstructures present and of the average thermal expansion coefficients of austenite, α_A, bainite, α_B, and martensite, α_M. Similarly, to calculate the transformation strain, e_2, one has to also know the transformation strains for each separate phase change, namely from martensite to austenite, $e_{M\to A}^{TR}$, from austenite to bainite, $e_{A\to B}^{TR}$, and from austenite to martensite, $e_{A\to M}^{TR}$. Table 2.4 shows the values used in this study, taken from a variety of sources.

The equations used for calculating each term in Eq. (2.4.12) depend on the temperature history the considered location (integration point) has undergone. Papazoglou's thesis gives in detail these equations for all possible cases encountered during the welding cycle.

To show the impact the inclusion of phase transformation effects has on the thermal strain of a section which is free to expand or contract, Figure 2.17 is constructed. The solid line depicts for a specific temperature history the thermal strain during the heating stage of this history, including the phase transformation effects

TABLE 2.4

VALUES USED FOR THE CALCULATION OF TRANSFORMATION STRAINS

Transformation temperatures	°F	°C
A_1	1210	654
A_3	1415	768
B_s	840	449
M_s	715	379
M_f	415	213
Thermal expansion coefficients	**in/in °F**	**mm/mm °C**
α_A	8.9×10^{-6}	4.9×10^{-6}
α_M	7.5×10^{-6}	4.2×10^{-6}
α_B	6.7×10^{-6}	3.7×10^{-6}
Transformation strains		
$e^{TR}_{M \to A}$	-0.10×10^{-2}	
$e^{TR}_{A \to B}$	0.25×10^{-2}	
$e^{TR}_{A \to M}$	0.38×10^{-2}	

(phase change from martensite to austenite). This is the usual curve assumed as input in previous stress analyses using the finite element method. Upon cooling, the same curve was usually assumed, thus neglecting the phase changes from austenite to bainite and/or martensite. By contrast, the intermittent line shows clearly the effect the expansion accompanying these transformations has on the thermal strain.

It becomes evident from the previous discussion that the model developed captures the main characteristics of the phase transformation effects. The accuracy of the analysis will, of course, depend on the correct evaluation of the required input.

2.4.3 Weld Model Using the FEM

In this section all the necessary considerations for the modeling of a multipass weldment between two relatively thick plates will be discussed.

Geometry and Boundary Conditions. A cross-section of the weldment in its midlength was used to calculate the transient strains, transient stresses, and residual stresses due to welding. This is rationalized by the fact that for relatively long plates the maximum stresses are developed in this region. Furthermore, the plane strain assumption was used (i.e., all plane sections normal to the weld line remain plane during the entire welding process).

The boundary conditions used in the analysis should be such so as to allow free expansion of the weldment in the transverse direction as well as bending. At the same time the structure should be properly restrained to eliminate all possible modes of rigid body motion; otherwide the stiffness matrix will not be positive definite. Figure 2.18 shows the constraints imposed on the model to satisfy the above conditions.

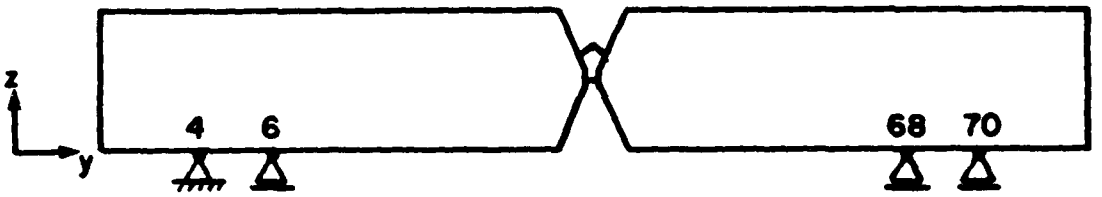

FIGURE 2.18 Constraints applied to the finite element model

Material Properties. The temperature dependence of the Young's modulus, E, Poisson's ratio, ν, virgin yield stress, σ_{vy}, and strain hardening modulus, E_T, are all required input for the thermo-elastic-plastic model used. Figure 2.19 shows this dependence for the HY-130 steel.

A word of caution is appropriate at this point as far as the material properties above the liquidus temperature are concerned. The material does not have any strength when molten since all its mechanical properties are zero. But due to numerical considerations, zero properties cannot be entered as input to the program. Hence to avoid any instabilities (or even divisions by zero) very small values for E, σ_{vy}, and E_T should be used above the liquidus temperature.

Another point is the accumulation of plastic strains in the regions that become molten during the welding cycle. When the temperature reaches the liquidus these plastic strains are physically relieved, starting to accumulate again when the metal solidifies. The presence of nonzero material properties above the liquidus, however, would cause the plastic strains not only to continue accumulating but also to reach artificially high values owing to the very low magnitude of the mechanical properties. It was therefore necessary to modify ADINA by imposing a total relief of plastic strains when the material melts.

Solution Strategy. One of the most important decisions an analyst has to make when performing a nonlinear incremental stress analysis is the solution strategy to be followed, because the accuracy and the convergence characteristics of the solution depend very much on it. This is especially true for complex situations involving highly nonlinear material behavior like the one encountered in the welding problem. Based on previous experience the parameters shown in Table 2.5 were chosen.

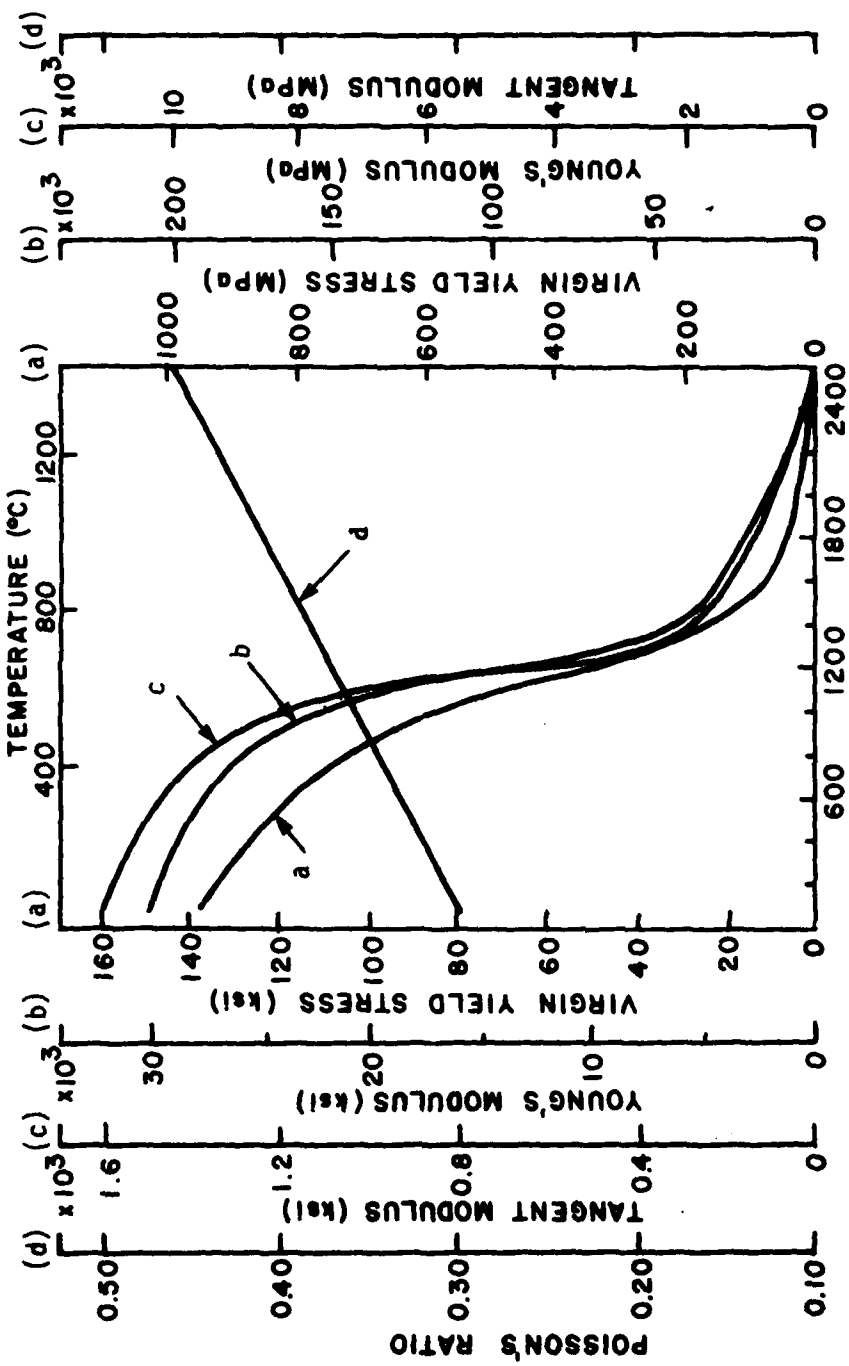

(a) Variation of virgin yield stress with temperature for HY-130
(b) Variation of Young's Modulus with temperature for HY-130
(c) Variation of tangent modulus with temperature for HY-130
(d) Variation of Poisson's Ratio with temperature for HY-130

FIGURE 2.19

TABLE 2.5

SOLUTION PARAMETERS USED WITH ADINA

Equilibrium Iteration Parameters	Stress Integration Parameters
METHØD = 2	ALPHA = 0.0
IATKEN = 0	XISUBM = 150.
DTØL = 0.00001	XNITE = 15.
RTØL = 0.1	XNALG = 2.
STØL = 0.5	TØLIL = 0.005
	TØLPC = 0.1
Note: The above symbols refer to the ones used for the variables in ADINA.	

2.4.4 Results

The same experiments as the ones analyzed for the heat transfer problem were also used in the stress analysis. The finite element mesh shown in Figure 2.11 was initially used. Initial computations, however, showed that the mesh used was too crude for any meaningful results to be obtained. As a consequence, a finer mesh was devised (Figures 2.20a and 2.20b) and used for the analysis.

Four- to six-node isoparametric elements were used; special care was given not to include any triangular elements in the mesh. A total of 77 nodes and 47 elements were utilized. Nodes 2 and 4 were restrained in the z-direction, and nodes 74 through 77 in the y-direction.

Figure 2.21 shows the accumulation of the effective plastic strain, $\bar{e}^p$, for the first welding pass at three points located on the plate's midthickness and at various distances away from the weld centerline. In the weld metal zone, plastic strain is built up rapidly as the

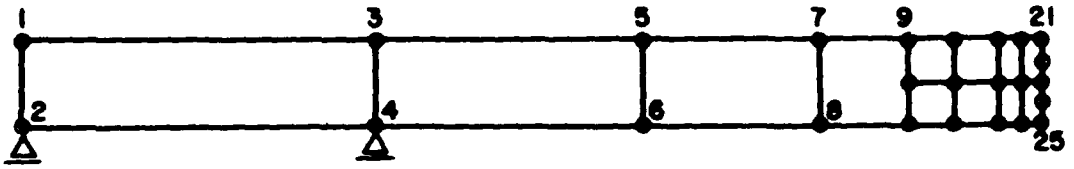

FIGURE 2.20a Finer finite element mesh used in stress analysis of welding problem

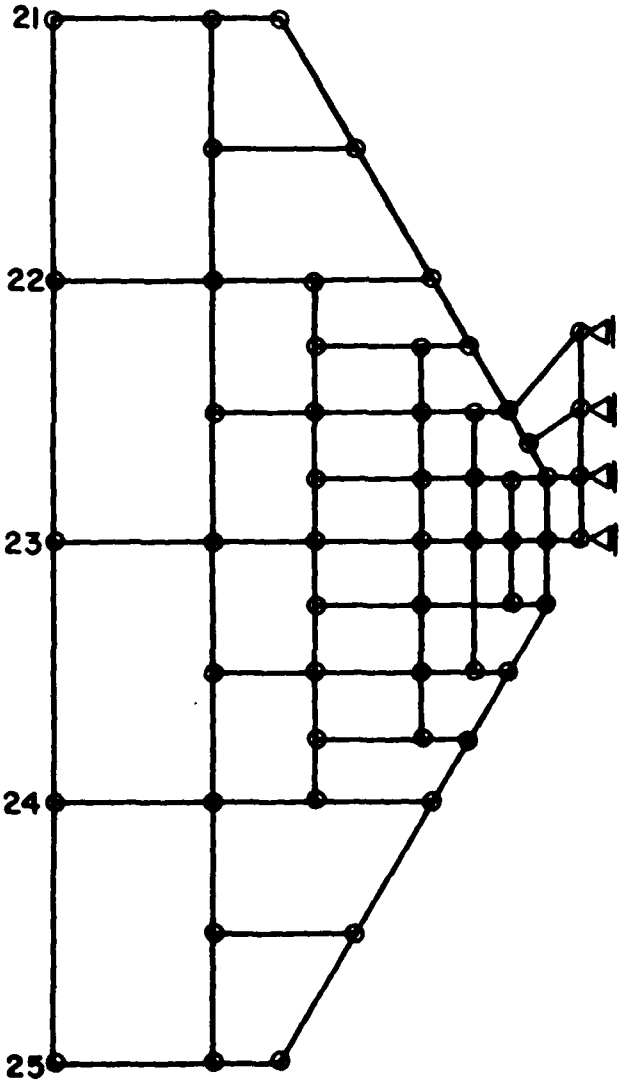

FIGURE 2.20b Finer finite element mesh, cont. (0.5 in to the right of weld centerline)

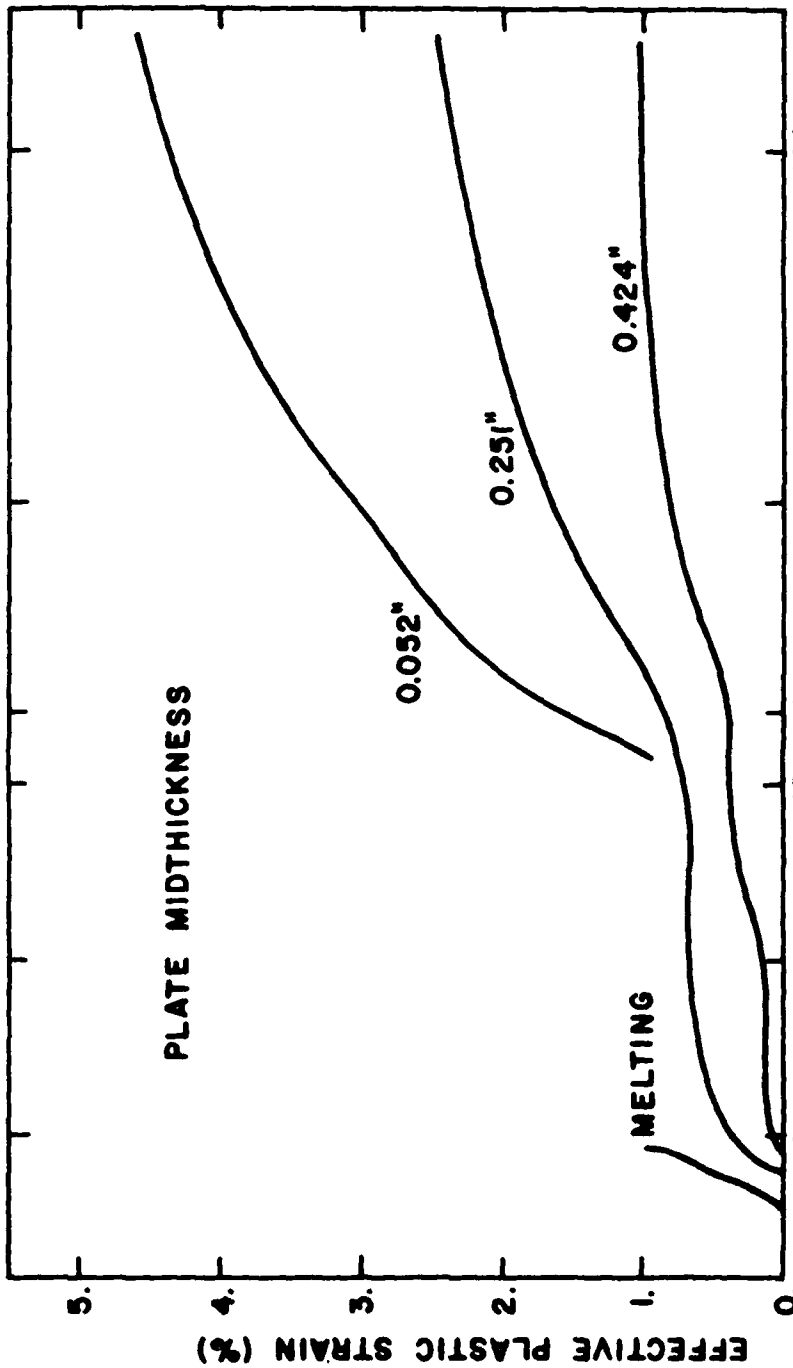

FIGURE 2.21 Accumulated effective plastic strain history at various distances from the weld centerline (first welding pass)

material yields in compression. At the melting region this plastic strain is completely relieved, to rapidly reach again a level in close proximity to that existing prior to melting upon solidification. As cooling continues and yielding in tension progresses, the plastic strain steadily increases but at a smaller rate than before. In the heat-affected zone, plastic strain is accumulated during heat-up in much the same way as in the weld metal zone but not quite as rapidly. As the material cools, it yields in tension and further plastic strain is accumulated.

Figure 2.22 shows calculated transient longitudinal stress distributions. Compressive stresses exist in the weld metal prior to melting. When the metal is in its molten stage, negligible compressive or tensile stresses were calculated.[22] As cooling commences, tensile stresses start appearing in the weld metal. These stresses then build up to the residual stress pattern when ambient temperature is reached. For self-equilibrating purposes, compressive stresses exist in areas removed from the weld centerline. Note in Figure 2.22 the effect of phase transformation, causing a sudden decrease in the tensile stresses.

Comparison of the experimentally measured transverse transient strain history at a point located on the top surface of the plate is made with the numerically obtained results in Figure 2.23. The correlation is relatively good if one takes into account the various assumptions involved in modeling the complex welding problem. A delay in the transition from tensile to compressive and again from compressive to tensile strains is observed in the analysis. The same delay as far as the occurrence of the maximum strain is also exhibited. It is believed that this phenomenon is primarily due to the relative coarseness of the finite element mesh, and the complex loading history present in the welding problem.

Summarizing it can be said that the finite element model developed based on ADINA modified for phase transformation effects captures most

[22] Note that in reality the molten metal has no strength. For numerical reasons, however, a very small amount of strength had to be assumed as explained in previous sections.

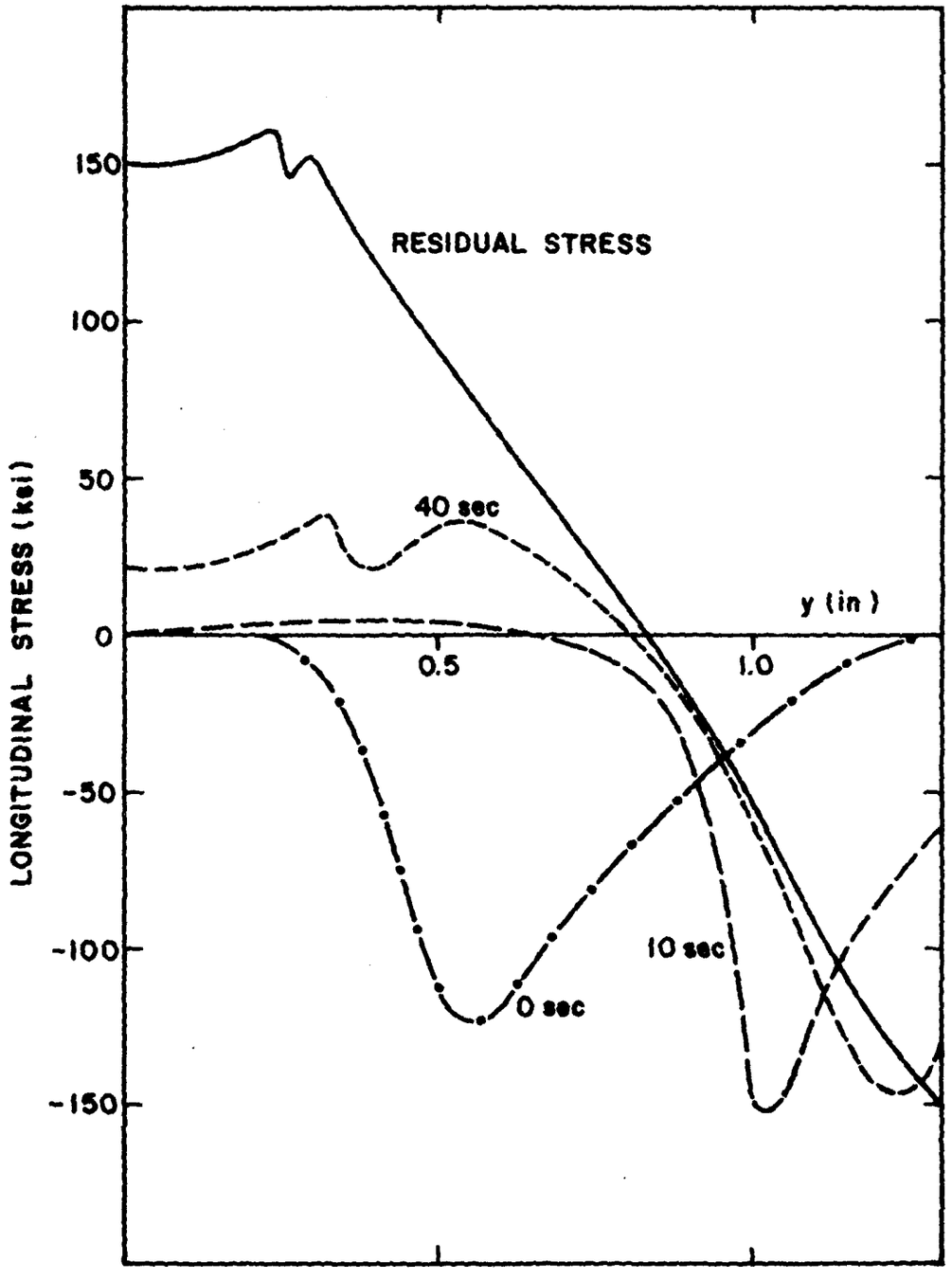

FIGURE 2.22 Longitudinal stress distribution at several time instances (first welding pass)

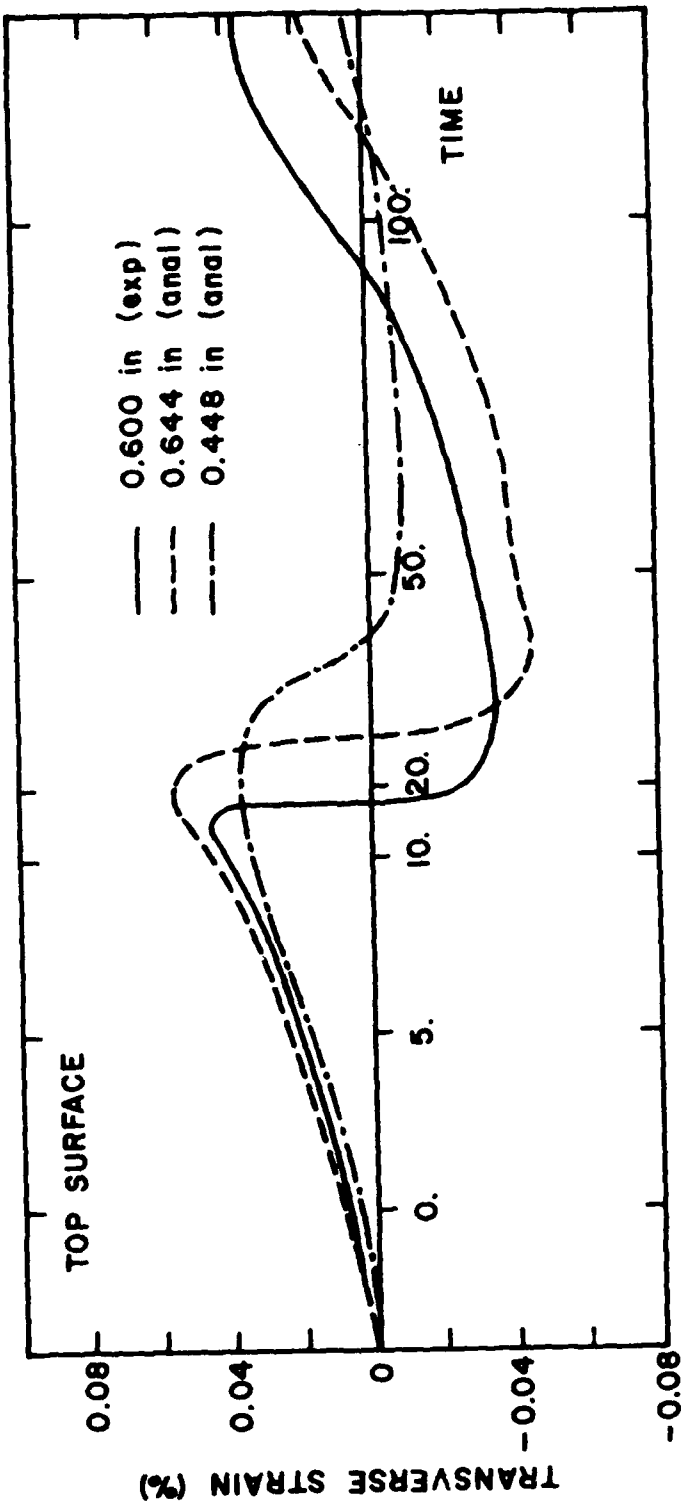

FIGURE 2.23 Comparison of experimentally measured transverse transient strains on the plate's top surface with numerical predictions (first welding pass)

of the important aspects of the welding stress analysis. Although some discrepancies have been observed between the obtained results and experimental data, considerations of cost and the assumptions made do not allow much more sophisticated analyses at present. It is expected, however, that the dramatically decreasing computer costs, together with developments in the areas of coupled thermoplasticity, will enable investigators to perform more accurate analyses in the future.

2.5 Fracture Analysis

Efforts to analyze the fracture experiments described in Section 2.2.2 of this report were completed successfully during the first half of the fourth year of this research program. These efforts consisted of numerically calculating the stress intensity factor and the crack opening displacement using the finite element method and based on a newly developed hybrid crack element.

The work done, a summary of which will be presented in this section, is described in detail in the following thesis to which the interested reader is referred:

Golçalves, E., "Fracture Analysis of Welded Structures", Ph.D. Thesis, M.I.T., May 1981.

2.5.1 Estimation of Residual Stress Field

As emphasized in Section 2.2.2, the fracture experiments were performed in the absence of any externally applied stresses; the only stresses present were the residual stresses due to welding. To successfully analyze these experiments using linear elastic fracture mechanics (LEFM), therefore, it is necessary to know the residual stress field, and in particular the residual stresses perpendicular to the crack surfaces, σ_y.

One way of calculating these residual stresses is through the thermal-elastic-plastic finite element analysis outlined in the previous section. Such an analysis, however, of all eight specimens (see Table

2.1) would be prohibitively expensive due to the high costs involved. Instead a simplified approach was used for determining the surface and through-thickness distribution of the transverse residual stresses. In what follows the through-thickness distribution will be discussed only since this is of importance for the fracture analysis.

Superposition Principle. The proposed approximate method is based on the fact that the COD measured during the fracture experiment was due to the elastic release of the residual stresses present around the notch. Thus by applying the superposition principle the distribution of the transverse residual stresses can be obtained by finding the stress which if applied on the notch surface would result in the same COD values as the experimental ones.

Figure 2.24 shows schematically how the superposition principle is applied. Case a, the experimental case, represents the stress free notch surfaces which result in the measured COD_a. In case b no residual stresses are present; instead, the notch surfaces are acted upon by stresses of the same value but opposite direction to the relieved residual stresses. Resulting from this case is COD_b and a stress distribution in the remaining plate thickness due to the applied stress and the notch stress concentration. Finally, in case c no notch exists and so $COD_c=0$; the stress distribution shown is the one due to the residual stresses that existed prior to the notch introduction.

The previous discussion leads to $COD_b=COD_a$. As a consequence, the experiment can be analyzed by studying the much simpler case b.

Finite Element Code. A finite element code, utilizing several subroutines of the finite element program FEABL[23], was developed for the approximate calculation of the residual stresses.

Figure 2.25 shows the finite element mesh used, where only triangular and quadrilateral assumed displacement elements were used. From symmetry

[23] Orringer, O., French, S.E., and Weinreich, M., "User's Guide for the Finite Element Analysis (FEABL 2, 4 and 5) and the Element Generation Library (EGL)", Aeroelastic and Structure Research Lab., Department of Aero. and Astro., M.I.T., January 1978.

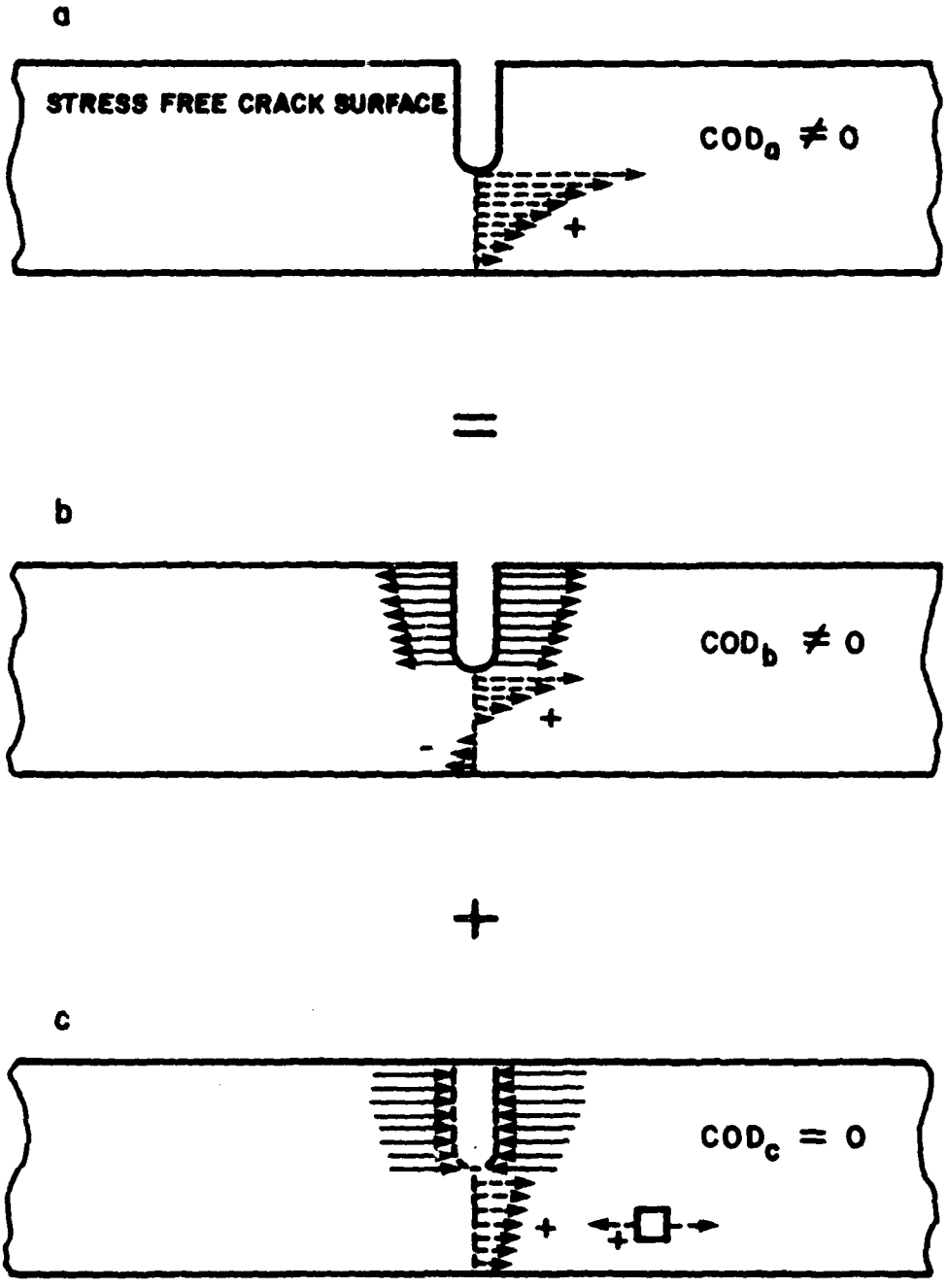

FIGURE 2.24 Superposition principle (schematic representation)

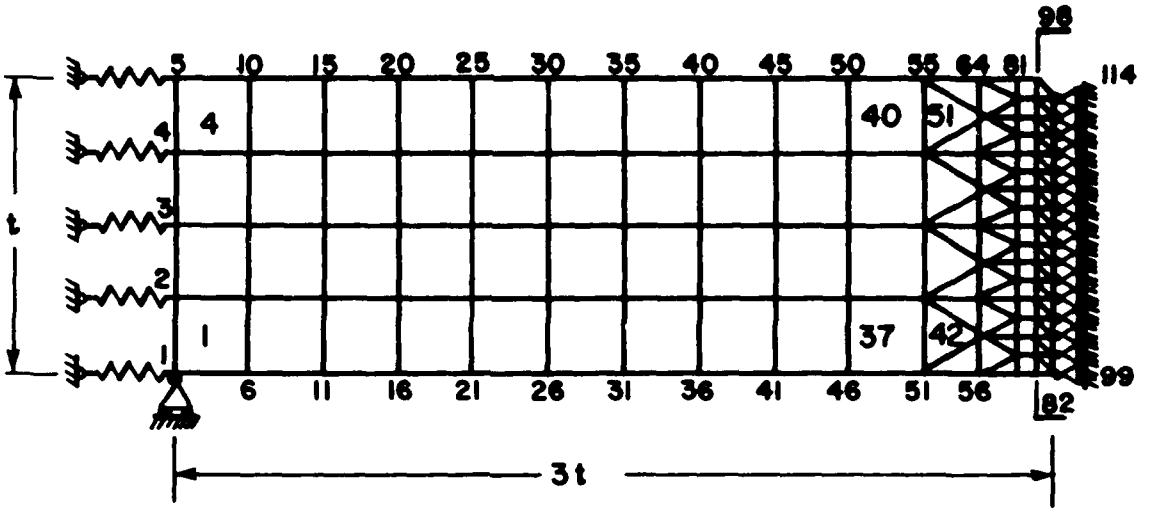

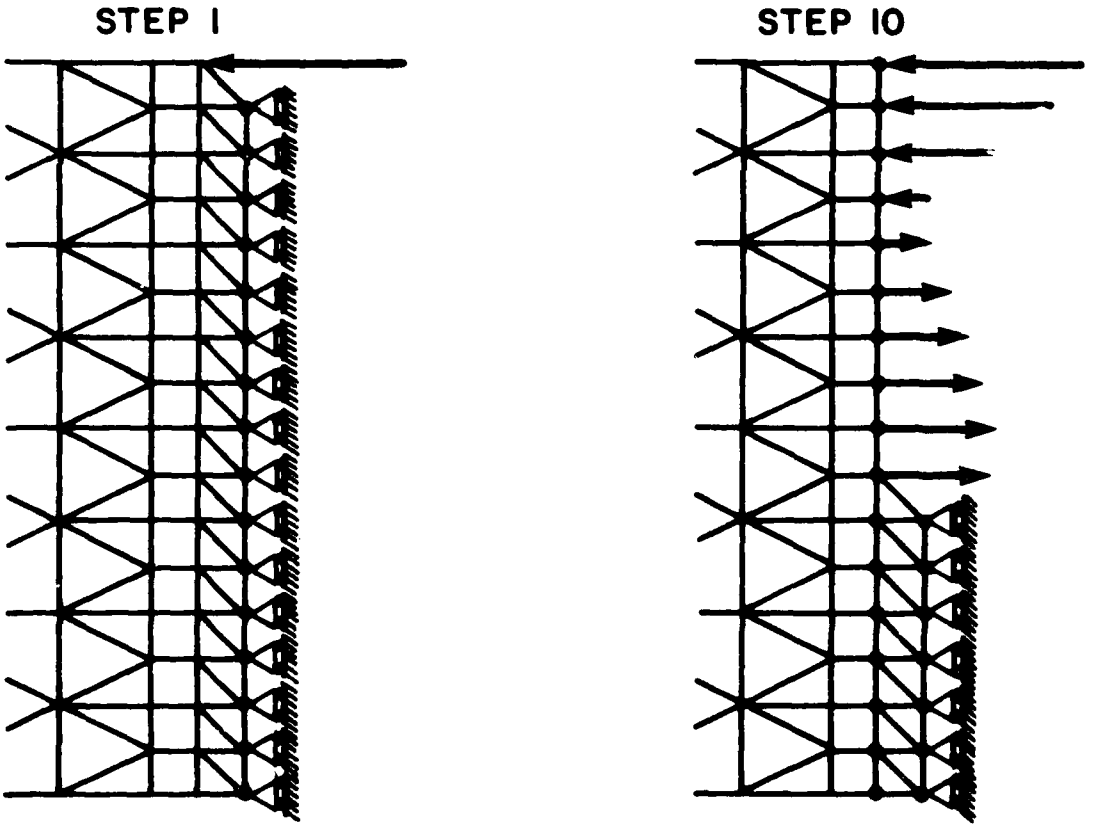

FIGURE 2.25 Finite element mesh used for the approximate calculation of the through thickness residual stress distribution

considerations only one half of each specimen was considered; the restraint was simulated by equivalent elastic springs (see Section 2.7.1 of Second Progress Report).

The notch depth increase was simulated by 16 incremental steps, each equal to 1/16 of the plate's thickness. Steps 1 and 10 are shown in Fig. 2.25. In each step the nodal force distribution that would give the same COD as the experimentally obtained one was calculated iteratively using the method of false position.

Results. Figures 2.26 through 2.28 show the calculated through-thickness transverse residual stress distributions, σ_y, for the three HY-130 specimens (numbers 6 through 8 in Table 2.1). Where COD values were not obtained for the total plate thickness, symmetry with respect to the plate's midthickness was assumed.

Strain Energy. As an additional product of the above analysis, the strain energy released during each notch size increment was calculated by applying the finite element force/displacement solution vector in an algorithm contained in FEABL. Figure 2.29 presents one sample of this analysis. Notice that the curve exhibits a behavior similar to the experimental COD curves presented in Section 2.2.2.

2.5.2 Hybrid Crack Element

To calculate the stress intensity factor for the specimens used in the fracture experiments a linear elastic finite element analysis was performed. Instead of using standard finite elements, however, something that would require up to 1500 degrees of freedom to obtain reasonable accuracy, a hybrid crack element was developed enabling one to simulate the crack growth in a much more inexpensive way. The element developed is an extension of the one proposed by Tong et al.[24] It introduces stresses on the crack surface to simulate the residual stress field, whereas the original element assumed stress free crack surfaces. Figure

[24] Tong, P., Pian, T.H.H., and Lasry, S.J., "A Hybrid Element Approach to Crack Problems in Plane Elasticity", Int. J. of Num. Meth. in Eng., 7, 1973, pp. 297-308.

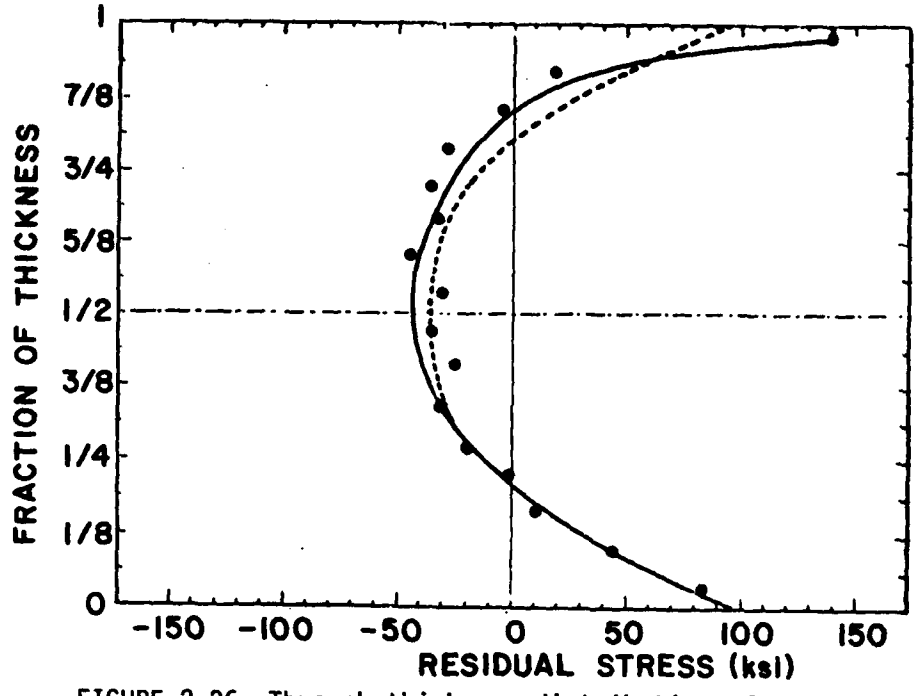

FIGURE 2.26 Through-thickness distribution of transverse residual stress, σ_y (Specimen 6, 7/8 in thick HY-130 plate)

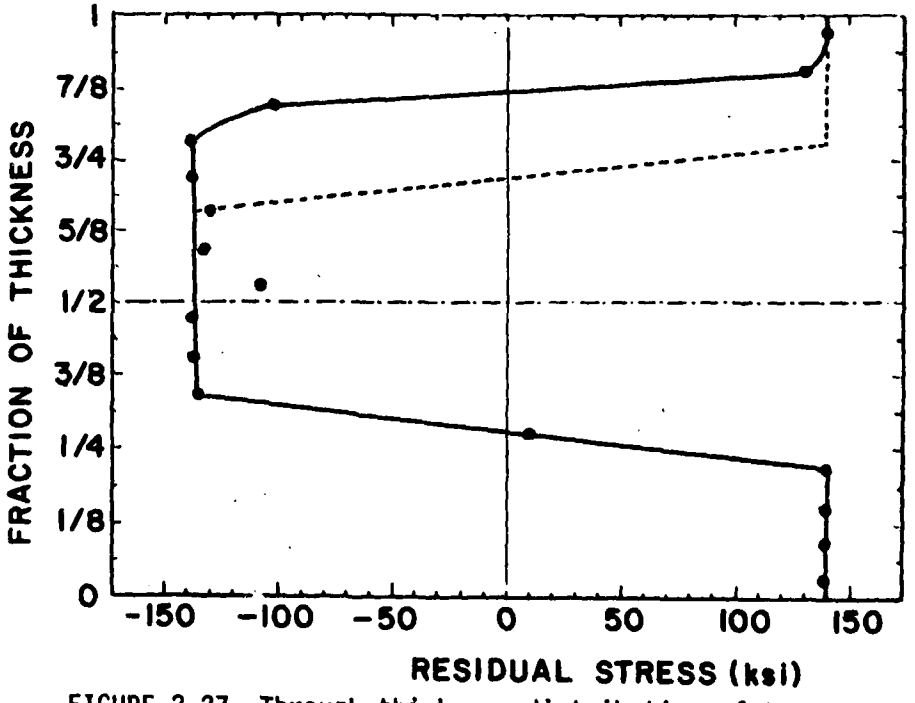

FIGURE 2.27 Through-thickness distribution of transverse residual stress, σ_y (Specimen 7, 7/8 in thick HY-130 plate)

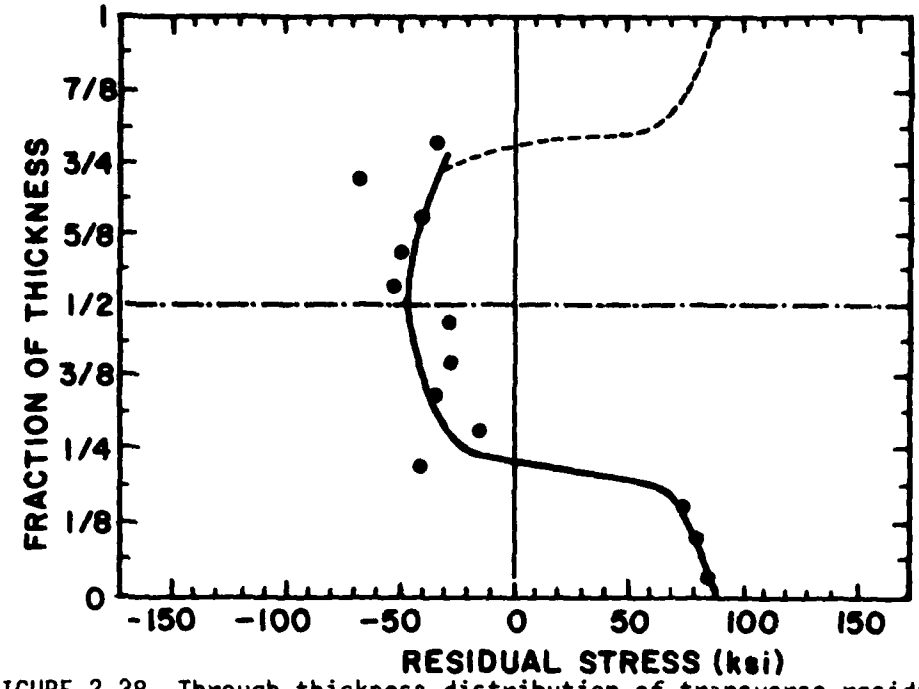

FIGURE 2.28 Through-thickness distribution of transverse residual stress, σ_y (Specimen 8, 2 in thick HY-130 plate)

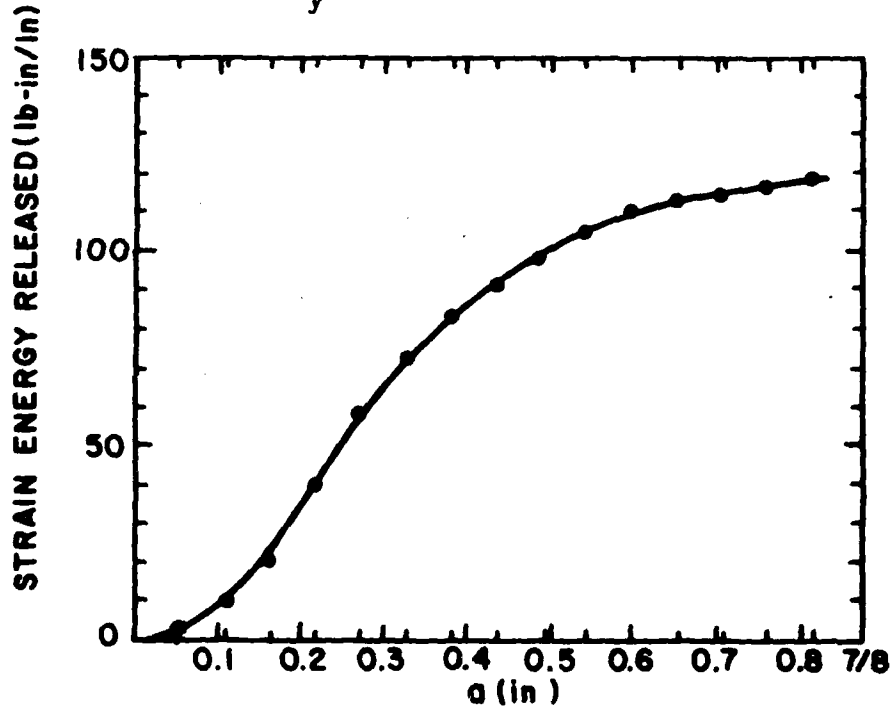

FIGURE 2.29 Strain energy released vs. notch depth (Specimen 7)

2.30 schematically presents the hybrid crack element under the influence of a generic linear stress distribution on the crack surface.

Complex Variable Solution. It is well known from the theory of elasticity that the plane strain or plane stress problem can be reduced to that of determining the Airy stress function which satisfies the biharmonic equation

$$\nabla^4 \Omega(x,y) = 0 \tag{2.5.1}$$

The solution to this equation in the complex domain is given by

$$\Omega(z) = \text{Re}\ \{\bar{z}\phi(z) + \int^z \psi(z)dz\} \tag{2.5.2}$$

where $\phi(z)$ and $\psi(z)$ are suitably chosen analytic complex functions. By neglecting the body forces, the stresses and strains can then be expressed in terms of these analytic functions as follows[25]

$$\begin{aligned} \sigma_x + \sigma_y &= 4\text{Re}\ \{\phi'(z)\} \\ \sigma_y - \sigma_x + 2i\sigma_{xy} &= 2[\bar{z}\phi''(z) + \psi'(z)] \\ 2\mu(u+iv) &= \eta\phi(z) - \overline{\phi'(z)} - \overline{\psi(z)} \end{aligned} \tag{2.5.3}$$

where η is a parameter the value of which depends on whether a plane stress or plane strain analysis is performed.

In the case of the hybrid crack element, the presence of stresses on the crack's surface, assumed to have a linear distribution, results in the following boundary condition

---

25 Muskhelishvilli, N.I., "Some Basic Problems of the Mathematical Theory of Elasticity", Noordhoff Publ., 1969.

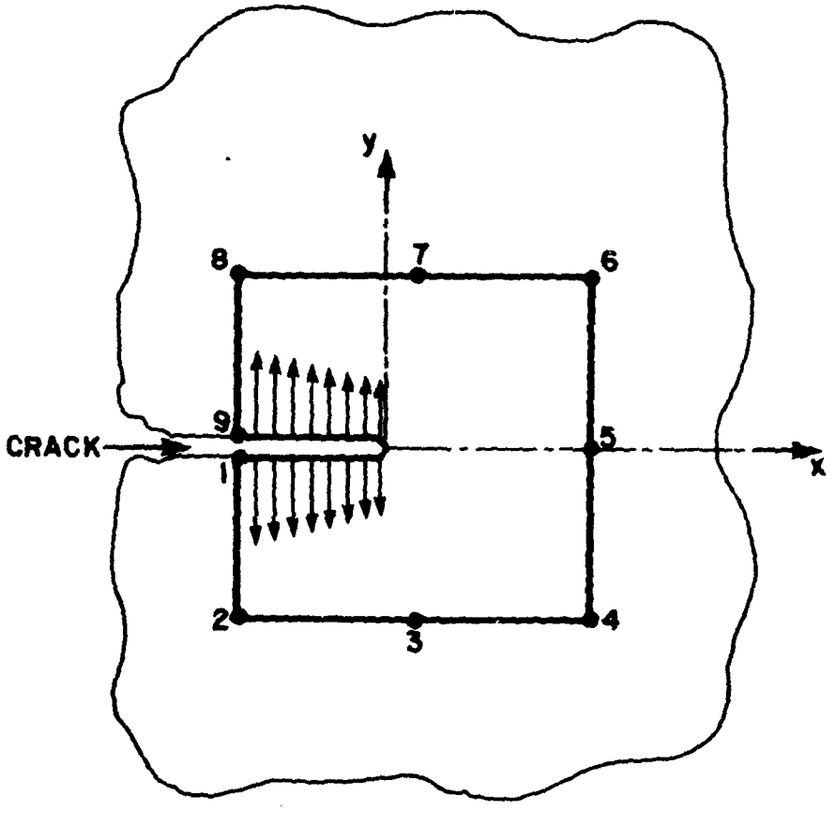

FIGURE 2.30 Hybrid crack element

$$\phi(z) + z\overline{\phi'(z)} + \overline{\psi(z)} = \frac{\alpha_1}{2} z^2 + \alpha_o z \tag{2.5.4}$$

where α_1 and α_o are complex numbers representing the terms of the linear expression for the surface traction components.

In order to choose proper stress and displacement expressions for the crack element taking into account the singularities, a conformal transformation was performed using the following mapping function

$$z = \omega(\zeta) = \zeta^2 \tag{2.5.5}$$

Working in the ζ-phase, with all equations being now a function of ζ, the analytic functions were assumed to have a series-form solution. Skipping some mathematical manipulations that can be found in Gonçalves' thesis, the following final expressions were found, expressed here in matrix form, for the stresses and displacements:

$$\underline{\sigma} = \underline{A}\ \underline{\beta} + \underline{B} \tag{2.5.6}$$

$$\underline{u} = \underline{U}\ \underline{\beta} + \underline{C} \tag{2.5.7}$$

where $\underline{\beta}$ is a matrix containing the undetermined parameters of the series expansions of ϕ and ψ, and $\underline{A}$, $\underline{B}$, $\underline{U}$, $\underline{C}$ known matrices containing elements that are functions of ζ.

Element Hybrid Functional. For a particular element the following hybrid functional can be defined

$$\pi = \int_{\partial A} (\bar{u}_i - u_i)\ T_i\ ds - \int_{S_\sigma} \bar{u}_i\ \bar{T}_i\ ds$$

$$+ \frac{1}{2} \int_A [\sigma_{ij}(u_{i,j} + u_{j,i}) - S_{ijkl}\ \sigma_{ij}\ \sigma_{kl}]\ dS \tag{2.5.8}$$

where A is the element area, ∂A its boundary, S_σ the portion of the boundary where tractions are prescribed, T_i the surface traction, $\bar{T}_i$ the prescribed surface traction over S_σ, u_i the displacement within A, $\bar{u}_i$ the displacement field along ∂A, σ_{ij} the stress, and S_{ijkl} the elastic compliance tensor.

Applying the equilibrium condition within each element, the interior compatibility equation, and integrating by parts, the above functional can be written in matrix form as

$$\pi = \int_{\partial A'} [\underline{T} + \bar{\underline{T}}]^T \bar{\underline{u}} \, ds - \frac{1}{2} \int_{\partial A} [\underline{T} + \bar{\underline{T}}]^T \underline{u} \, ds \tag{2.5.9}$$

where $\partial A'$ is the part of the element boundary on which tractions are not prescribed and where

$$\underline{T} = \underline{R} \ \underline{\beta} \tag{2.5.10}$$

The element boundary displacement matrix is then approximated in terms of generalized displacements $\underline{q}$ as

$$\bar{\underline{u}} = \underline{L} \ \underline{q} \tag{2.5.11}$$

where for the interpolation matrix $\underline{L}$ linear interpolation is assumed in our case between two consecutive nodes. The generalized displacment matrix for the 9-node hybrid crack element (see Fig. 2.30) is given

$$\underline{q} = \{u_1 \ v_1 \ u_2 \ v_2 \ \cdots \ u_9 \ v_9\}^T$$

Substituting Eqs. (2.5.7), (2.5.10), and (2.5.11) into the hybrid functional (2.5.9), and setting the variation equal to zero, an equation for the unknown $\underline{\beta}$ is obtained. Finally, using this latter expression the functional takes the form

$$\pi = \frac{1}{2} \underline{q}^T \underline{K} \underline{q} - \underline{q}^T \underline{Q} + \underline{M} \tag{2.5.12}$$

where $\underline{K}$ is the element stiffness matrix, $\underline{Q}$ the nodal force vector and $\underline{M}$ the element mass matrix.

Stress Intensity Factors. In the Linear Elastic Fracture Mechanics theory the stress distribution around the tip of a plane crack can be obtained in series form containing the stress intensity factor. By comparing these expression with the ones obtained using the analytic function theory, i.e., Eq. (2.5.6), equations for calculating the mode I and II stress intensity factors were obtained.

Finite Element Code. Based on the formulation described above, a finite element code, compatible with the FEABL subroutines, was developed. This code, named CRALOD, can be found in Gonçalves' thesis.

To test the code, mode I stress intensity factors (K_I) were calculated for cracks of variable size having a uniform distributed stress normally applied to their surface. Extremely close agreement was found between the obtained results and previously developed analytical solutions.

2.5.3 Linear Finite Element Fracture Analysis

The hybrid crack element described in the previous section was used in conjunction with FEABL to perform a linear finite element fracture analysis of the experiments described in Section 2.2.2.

Figure 2.31 shows the finite element mesh used in the analysis. Only the central part of a specimen is represented in the mesh; a series of springs applied on both sides of the mesh simulates the restraint the rest of the specimen exhibits on this central portion of the plate.

The crack growth was simulated by two ways: first, by increasing the size of the crack in the hybrid crack element without changing the rest of the mesh; and second, by moving the hybrid crack element deep into the mesh, something that required changes in the position of some

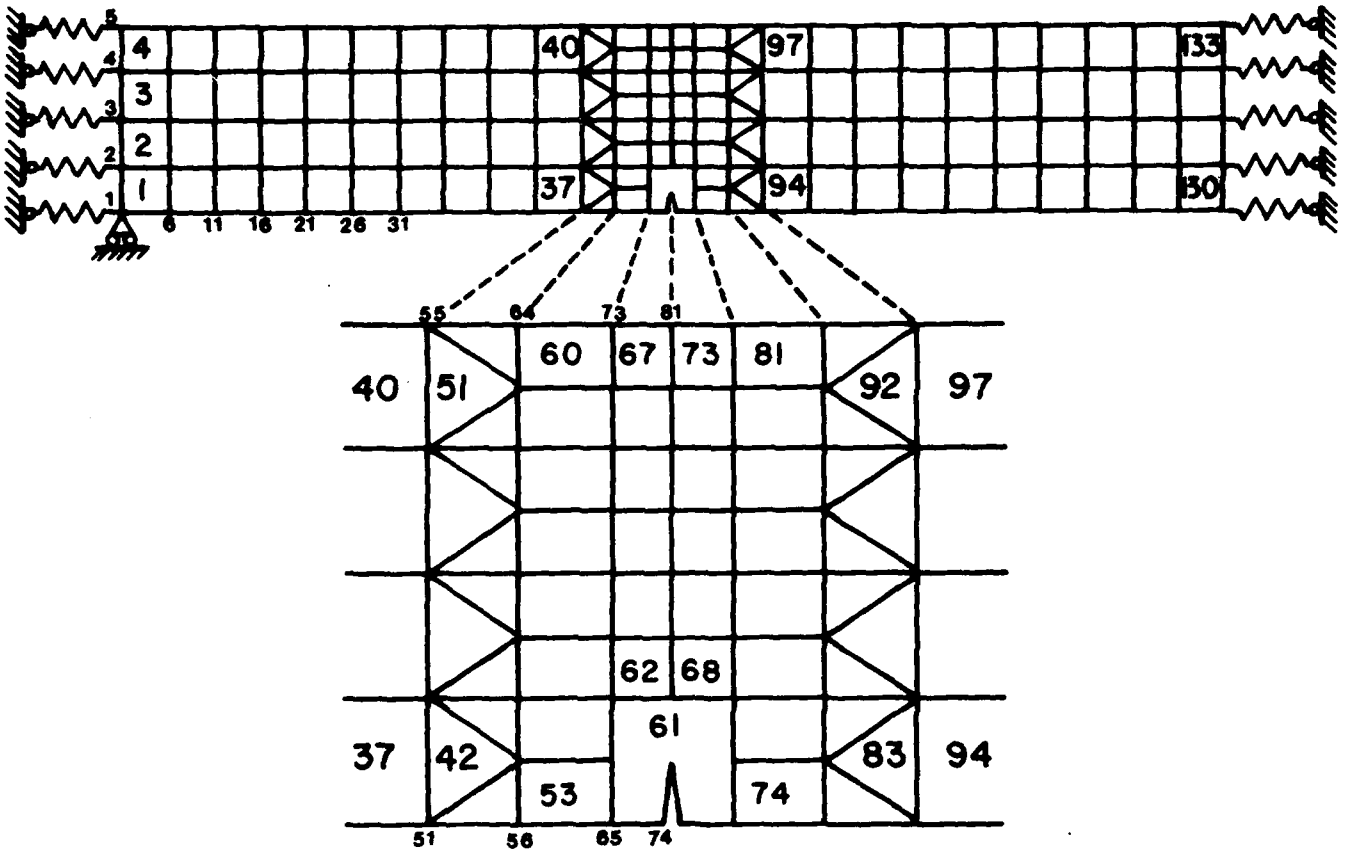

FIGURE 2.31 Finite element mesh used for the analysis of the fracture experiments

of the other elements, increases in the number of nodes, and a r
of approximately half of the nodes in the mesh. The crack growt
automatically by the program in increments of 1/16 of the plate
t, from 1/16t to 14/16t. Figure 2.32 presents schematically sev
these crack growth steps.

Equivalent nodal forces and distributed stresses on the cra
were determined and prescribed automatically by the program at e
they were based on the procedure described in Section 2.5.1.

Results. Numerical results of the Mode I stress intensity
K_I obtained by the finite element analysis are presented in Figu
through 2.36, where K_I is plotted versus the crack depth, a.

It is interesting to note the nonlinear character of the cu
which usually show high values of K_I for cracks with depths equa
about one quarter of the plate's thickness; some of the curves e
negative values for K_I.

Figures 2.37 through 2.40 present the calculated values of
opening displacement at a distance 0.25 in (6.35 mm) from the cr
centerline and compare them with the experimentally obtained one
Section 2.2.2). Close agreement between the two is observed for
case of small cracks. The divergence between the numerical and
curves observed for longer cracks is probably due to three-dimen
effects as the crack grows deeper.

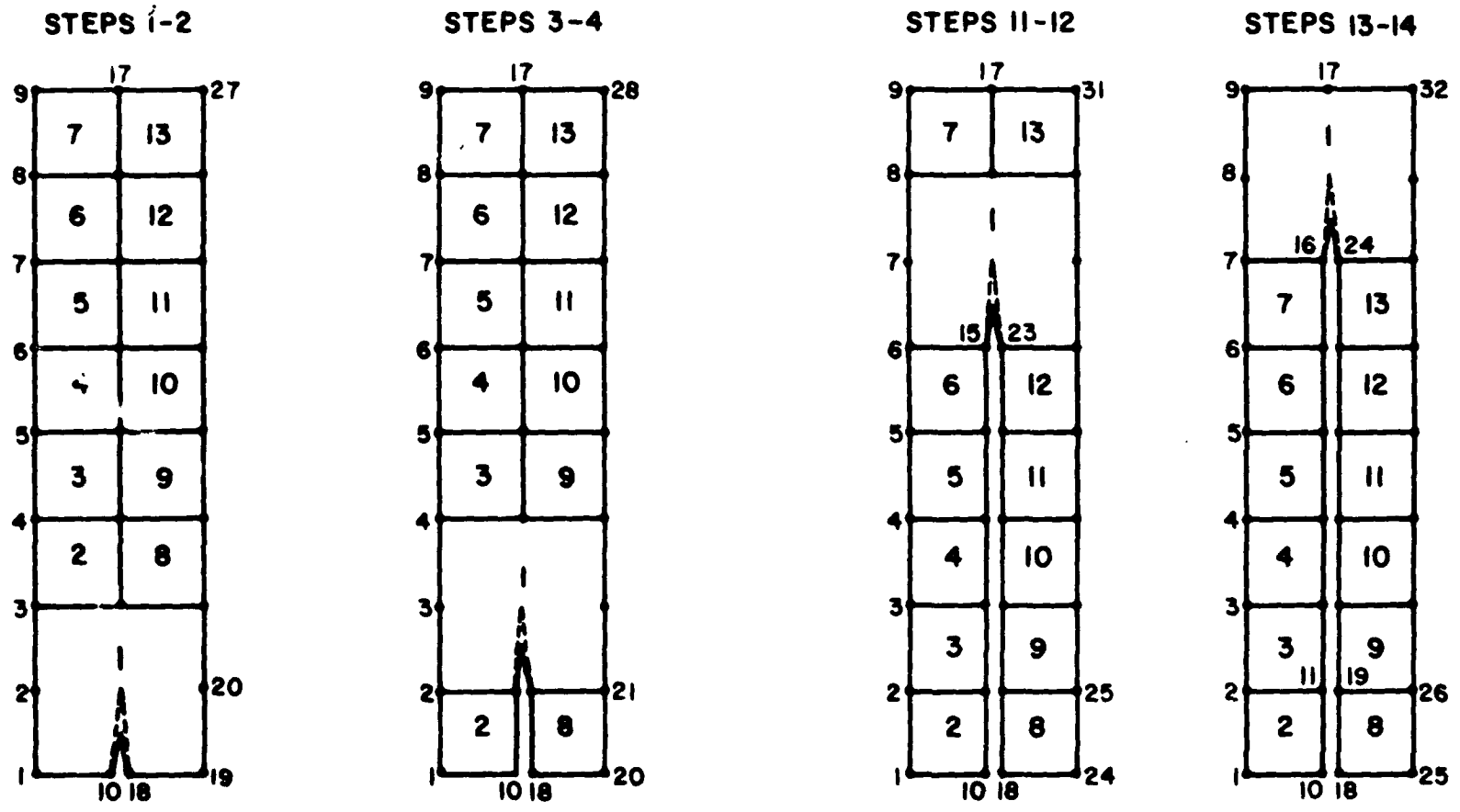

FIGURE 2.32 Schematic representation of crack growth process

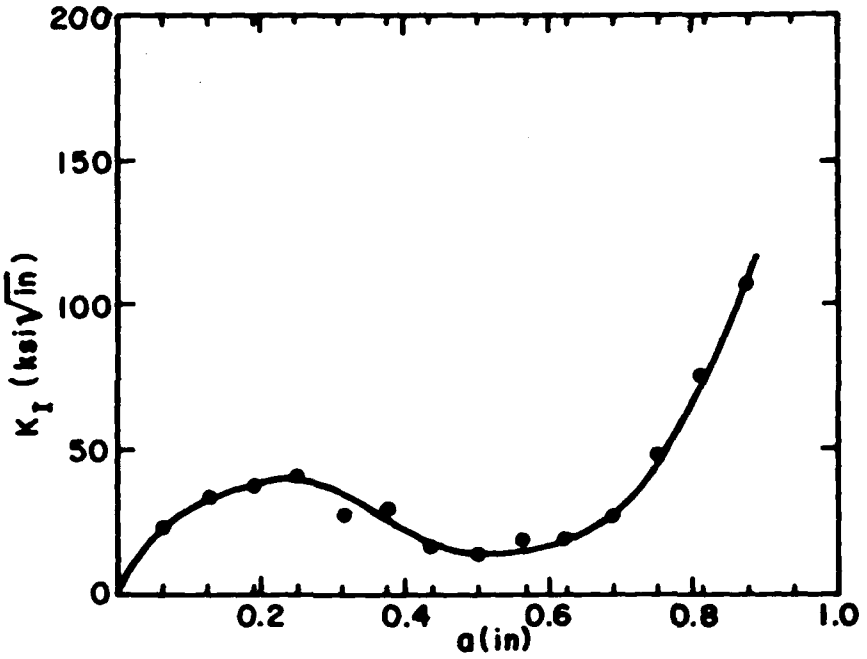

FIGURE 2.33 Stress intensity factor vs. crack depth (Specimen 3)

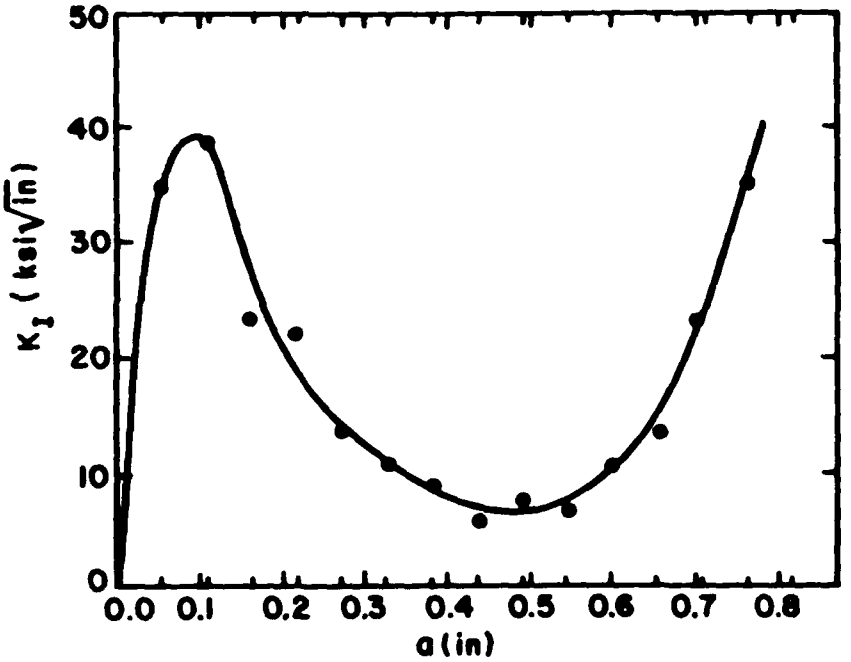

FIGURE 2.34 Stress intensity factor vs. crack depth (Specimen 6)

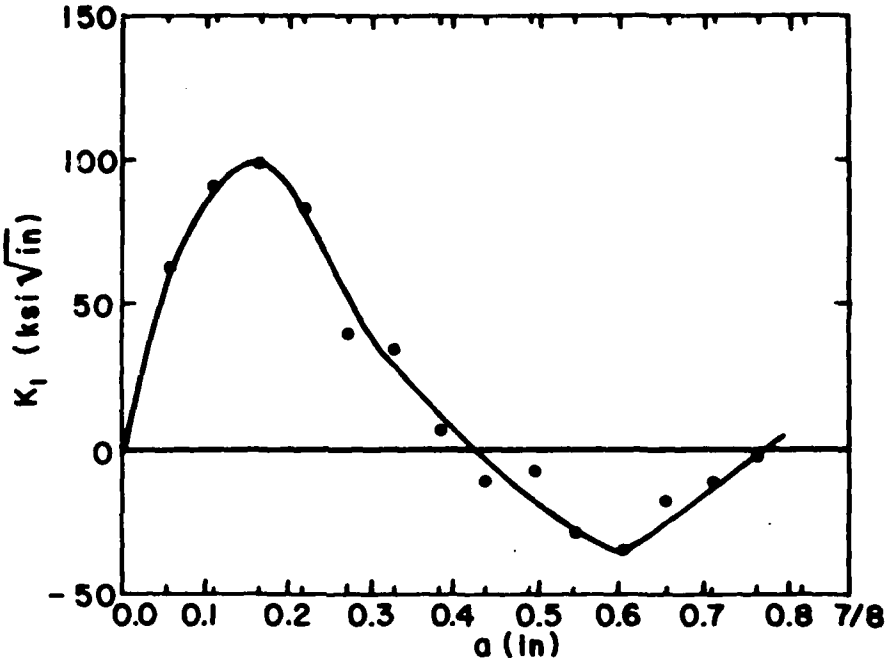

FIGURE 2.35 Stress intensity factor vs. crack depth (Specimen 7)

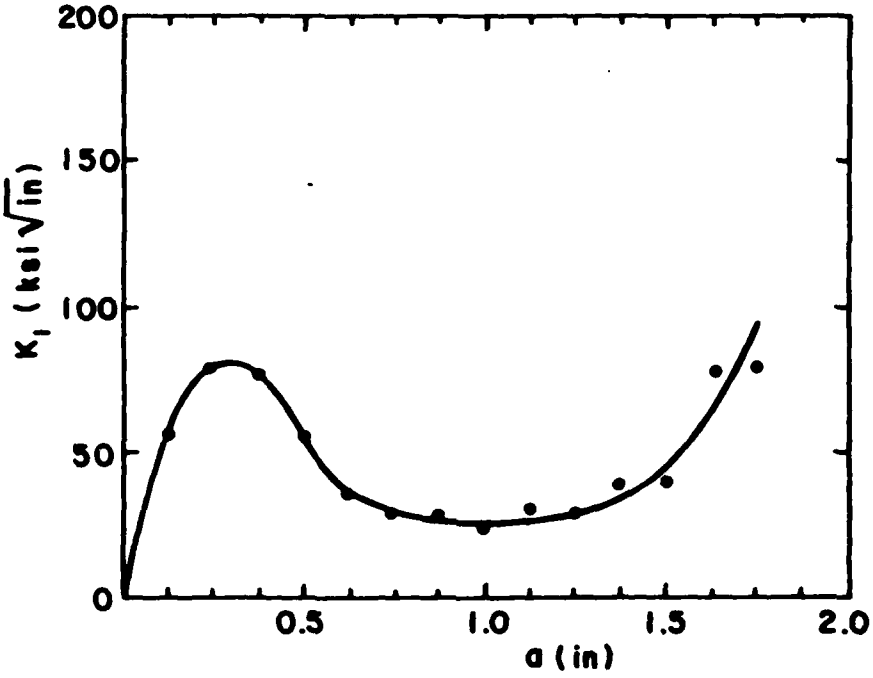

FIGURE 2.36 Stress intensity factor vs. crack depth (Specimen 8)

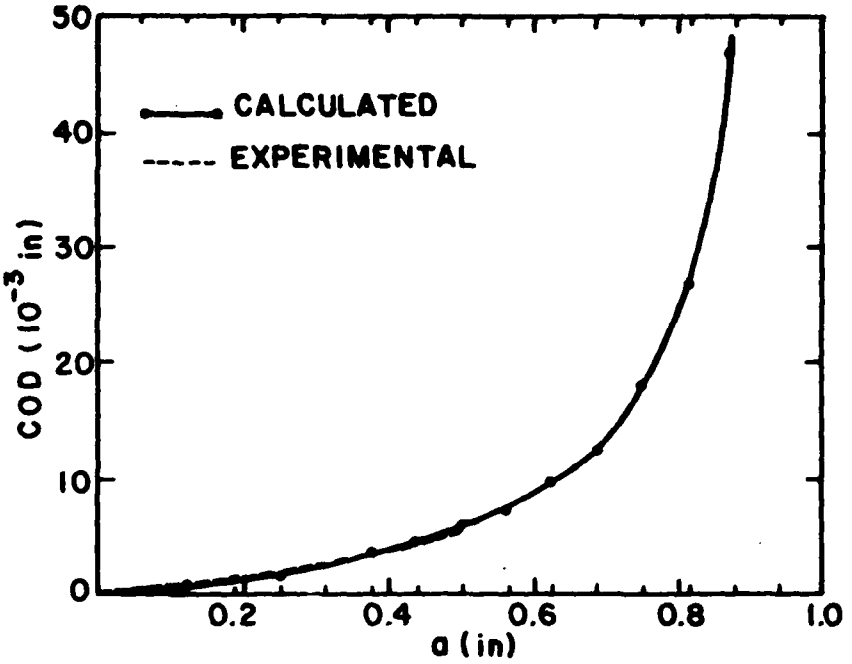

FIGURE 2.37 FEM and experimental COD vs. a results (Specimen 3)

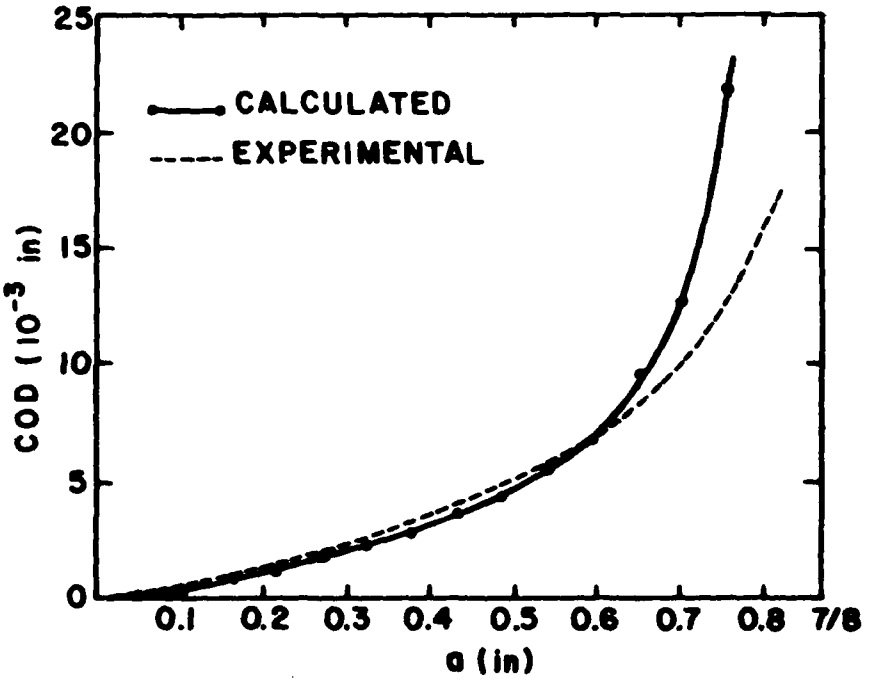

FIGURE 2.38 FEM and experimental COD vs. a results - (Specimen 6)

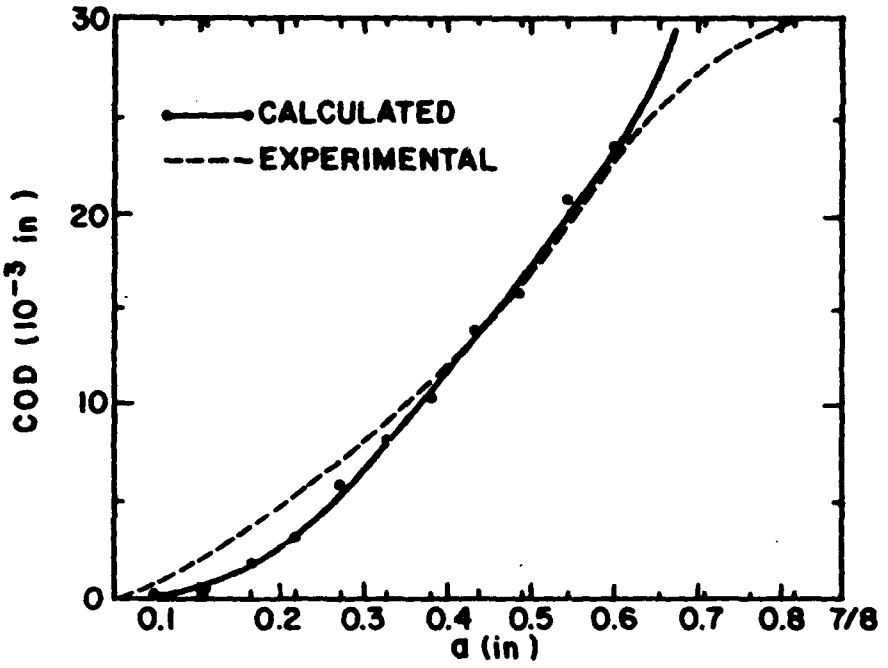

FIGURE 2.39 FEM and experimental COD vs. a results (Specimen 7)

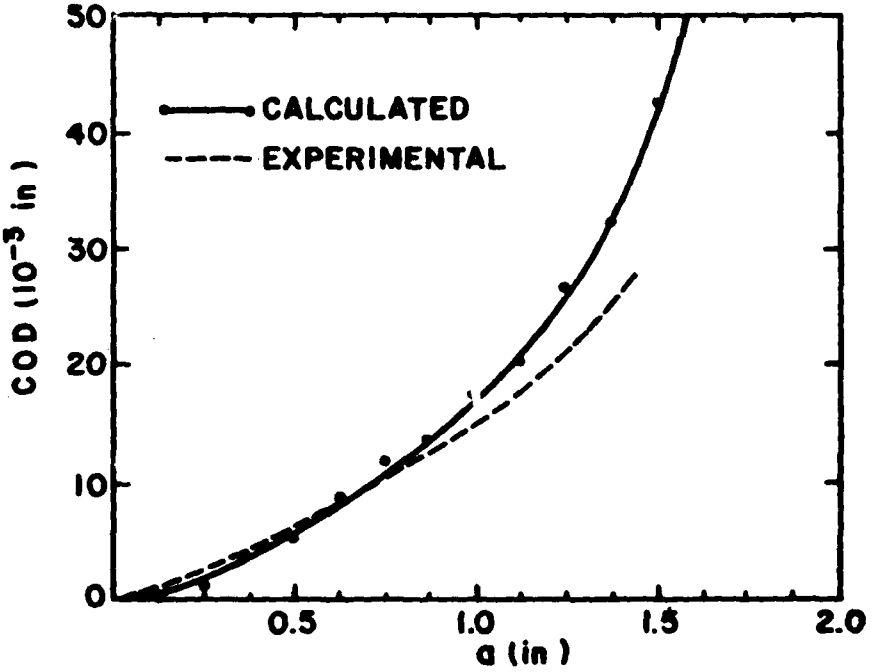

FIGURE 2.40 FEM and experimental COD vs. a results (Specimen 8)

3. PROGRESS OF TASK 2 - CYLINDRICAL SHELLS
(December 1, 1980 to November 30, 1981)

3.1 General Status

The objective of Task 2 of this research program is to experimentally and analytically study temperatures, thermal strains, residual stresses and distortion in girth welded high strength steel (specifically HY-130) unstiffened cylindrical shells. All steps of this task (see Table 1.1) has been completed as originally planned.

The work on this Task has already been completed during the first three years of the research program. Details of this work can be found in the first two technical progress report to O.N.R. In what follows a brief summary of the work performed is outlined for completeness purposes.

3.2 Experimental Program

An initial experiment was performed outside M.I.T. on butt welding two unstiffened low carbon steel cylindrical shells. This exploratory experiment was of great value, providing the M.I.T. investigators with experience that was later utilized in a similar experiment conducted at M.I.T. using HY-130 steel cylinders.

The second experiment, performed at the M.I.T. facilities, involved HY-130 cylindrical shells. The shells were formed from 60 in x 63 in x 3/4 in HY-130 flat plates by first bending them to semi-circular cylindrical shells and subsequently seam-welding the two halves together using the GMA welding process. After completion of the seam weld, the 60 in long, 18 in OD cylinder was sawn into three equal sections and preparations of the grooves were made for the joining of two of these sections. Finally, the two cylindrical sections were girth welded together using the GMA welding process.

Temperature changes and transient strains in the axial and circumferential directions were measured at preselected locations during both the seam and girth welding operations using thermocouples and

electric resistance strain gages respectively. The radial distortion at two points was also continuously measured during the girth welding of the two cylinders.

Finally, using electric resistance strain gages and the strain relaxation technique, the residual stresses on the outer surface of the welded cylinders were measured. The axial and tangential stresses, as distributed in both the axial and circumferential directions, were determined and compared with data from other investigators.

3.3 Analytical Program

The problem of welding two unstiffened cylindrical shells was analyzed using existing computer programs developed at M.I.T. during the past several years. A program based on the analytical solution for a moving point heat source was used for the heat flow analysis. Then, strains, stresses, and distortion during welding were analyzed using an axisymmetric finite element program.

Good correlation was observed between the numerically and experimentally obtained temperature distributions. This was not the case, however, for the strain and stress analysis. It is believed that if adequate funding was available better results would have been obtained using the modified finite element programs ADINAT and ADINA (see Sections 2.3 and 2.4 of this report).

4. PROGRESS OF TASK 3 - BRONZE WELDMENTS
(December 1, 1980 to November 30, 1981

4.1 General Status

The objective of Task 3 of the current research project is to experimentally generate information on temperature changes, transient strains and distortion on bronze weldments. In particular, Nickel-Aluminum (Ni-Al) bronze was chosen as the material to be investigated because of the problems encountered in controlling distortion during the manufacturing of propeller blades using this material. It should be pointed out that this investigation was prompted from the fact that, to the best of our knowledge, no published information is available on the subject.

The proposed research was carried out as originally proposed. A literature survey was first conducted to obtain material properties on Ni-Al bronze. Experimental studies were then carried out to determine temperature, strain, and displacement changes resulting from the welding of Ni-Al bronze plates. The experiments consisted of bead-on-plate and edge welds on one quarter inch thick specimens. The experimental results were finally compared with baseline data to determine the effects of restraint, block welding, preheating, postheating, and grinding on the final distortion.

The following thesis, dealing with Task 3, has already been completed:

McCord, R.S., "An Investigation of Strain, Distortion, and Heat Flow Distribution during Welding of Nickel-Aluminum Bronze", Ocean Engineer's Thesis, M.I.T., June 1981.

4.2 Material Properties of Ni-Al Bronze

Nickel-Aluminum bronze exhibits good strength, extremely good corrosive resistance in salt water, and is often selected for use in the construction of ship's propellers. Cold rolled Ni-Al bronze has a

minimum yield stress of 50 ksi (345 MPa), whereas as cast it exhibits a minimum yield stress of 40 ksi (276 MPa). In this study cold rolled material was used.

Due to phase transformations, Ni-Al bronze exhibits "hot shortness" (loss of ductility) from 600° to 1100°F. Therefore the material has to be either cold worked at temperatures less than 600°F or hot worked or annealed at temperatures above 1100°F.

Table 4.1 provides the typical chemical composition ranges for Ni-Al bronze. A comparison of the mechanical and physical properties of cold rolled Ni-Al bronze, hot rolled AISI-SAE-1035 steel, and cold rolled copper is shown in Table 4.2 for reference purposes.

TABLE 4.1

CHEMICAL COMPOSITION OF Ni-Al BRONZE
(weight %)

Copper, Cu	75.9 to 84.5
Aluminum, Al	8.5 to 9.5
Nickel, Ni	4.0 to 5.0
Iron, Fe	3.0 to 5.0
Manganese, Mn	3.5 max.
Silicon, Si	0.10 max.
Lead, Pb	0.02 max.
Other	0.5 max.

NOTES:
(1) Fe content shall not exceed Ni content
(2) Excessive Pb or Si will cause hot shortness in weld joints
(3) Excessive Mn will reduce corrosion resistance

TABLE 4.2

MECHANICAL AND PHYSICAL PROPERTIES OF STEEL, Ni-Al BRONZE AND COPPER

Property	Steel (hot rolled, AISI-SAE-1035)	Ni-Al Bronze (Cold Rolled)	Copper (Cold Rolled)
Yield Stress, ksi	39	40	48-55
Ultimate Tensile Stress ksi	72	46	93-105
Young's Modulus, 10^3 ksi	30	17	17
Shear Modulus, 10^3 ksi	11.5	6.4	6.4
Elongation in 2 inches, %	18	18	5
Poisson's Ratio	0.3	0.328	0.328
Hardness, Brinell R_b	143	92-99	100
Density, lb/ft^3	0.284	0.276	0.323
Thermal Conductivity, BTU/hr.ft.-°F	26	22.5	21
Specific Heat, W-s/lb.-°F	118	110.7	97
Coefficient of Expansion, in/in-°F	6.7	9.0	9.4
Melting Temp, °F (°C)	2768 (1520)	1940 (1040)	1981 (1043)

Estimates of the temperature dependence of the mechanical and physical properties of Ni-Al bronze were also made using various data found in several sources. Knowledge of this temperature dependence is necessary for the numerical analysis of heat flow and stresses during welding. The obtained estimates are shown in Table 4.3.

4.3 Description of Experimental Procedures

Two series of experiments using a total of eight specimens were conducted to measure temperature, thermal strain, and distortion changes during the welding of Ni-Al bronze plates. Emphasis was placed on comparing the final distortions of the plates after welding. Table 4.4 gives a summary of the welding parameters used in these experiments.

The first series of experiments consisted of laying a bead-on-plate weld in two passes. Specimens 1 through 6, all measuring 24 in x 12 in x 1/4 in, were welded in this manner, with the heat input being held approximately constant for all specimens. Specimens #1 and #2 were welded in the unrestrained condition so that baseline data could be gathered for comparison purposes with other conditions. Specimen #3 was restrained during both weld passes using C-clamps, as shown in Fig. 4.1. Specimen #4 was block welded in four blocks; in each block, measuring 6 in in length, both passes were completed before moving on to the next one. Specimen #5 was welded in the unrestrained condition; it was however preheated and postheated using oxyacetylene torches, and finally the weld was ground down at preselected locations. Specimen #6 was welded in the restrained condition; steel plates and C-clamps were used for this purpose, as shown in Figure 4.2.

The second series of experiments consisted of laying in two passes a bead on the edge of two specimens, #7 and #8, each measuring 21 3/4 in x 5 3/4 in 1/4 in. Heat input as well as all other parameters were kept constant in both cases.

TABLE 4.3

TEMPERATURE DEPENDENCE OF MATERIAL PROPERTIES FOR Ni-Al BRONZE

Temperature, θ	70.	300.	500.	700.	900.	1100.	1300.	1500.	1700.	1900.
Yield stress, σ_{ys}	50.	49.2	47.4	43.	18.2	10.2	6.3	3.6	2.6	0.2
Young's modulus, E	17.	18.	17.	10.	7.	5.7	4.	2.7	1.4	0.3
Density, ρ	0.276	0.274	0.273	0.271	0.270	0.269	0.267	0.266	0.264	0.263
Specific heat, c	110.8	116.	137.1	126.6	126.6	128.5	130.	131.9	131.9	131.9
Thermal conductivity, k	0.513	0.626	0.724	0.823	0.921	1.019	1.117	1.216	1.314	1.412
Average thermal, expansion coefficient, α	8.84	9.64	10.18	10.63	11.07	11.45	11.81	12.16	12.42	12.75

Units: $[\theta]$ = °F $[c]$ = W.sec/lb_m.°F

$[\sigma_{ys}]$ = ksi $[k]$ = W/in.°F

$[E]$ = 10^2 ksi $[\alpha]$ = 10^{-6} in/in °F

$[\rho]$ = lb_m/in^3

TABLE 4.4

SUMMARY OF WELDING PARAMETERS IN Ni-Al BRONZE EXPERIMENTS

Specimen	Current (A)	Voltage (V)	Travel Speed (in/sec)	Heat Input (kJ/in)	# of passes	Preheat Interpass (°F)	Remarks
1	145	29	0.273	15.40	2	60-168	Unrestrained
2	145	29	0.263	15.98	2	60-168	Unrestrained
3	142	29	0.267	15.44	2	60-150	C-Clamp Restraint
4	142	29	0.264	15.64	2 (8 blocks)	60-150	Unrestrained, Blockwelded
5	142	29	0.260	15.84	2	150-175	Unrestrained, Preheated, Post-heated, Grind
6	145	29	0.252	16.69	2	60-146	Steel Plate Restrained
7	110	32	0.635	5.54	2	60-140	Unrestrained
8	110	32	0.635	5.54	2	60-140	Unrestrained

NOTES: (1) Type of weld was bead-on-plate for specimens 1 through 6 and edge for specimens 7 and 8.

(2) All specimens were welded using the semiautomatic d.c.r.p. gas metal arc welding process.

(3) Wire used was 1/16" diameter Ampco Trode 10 for all specimens.

(4) The wire feed rate was 0.458 in/sec for specimens 1 through 6 and 1.097 in/sec for specimens 7 and 8.

(5) The shielding gas used had a composition of 98% Argon and 2% Oxygen.

MASSACHUSETTS INST OF TECH CAMBRIDGE DEPT OF OCEAN E--ETC F/G 13/
STUDY OF RESIDUAL STRESSES AND DISTORTION IN STRUCTURAL WELDMEN--ETC(U)
NOV 81 V J PAPAZOGLOU, K MASUBUCHI N00014-75-C-0969
UNCLASSIFIED NL

2 OF 2
AD
A113813

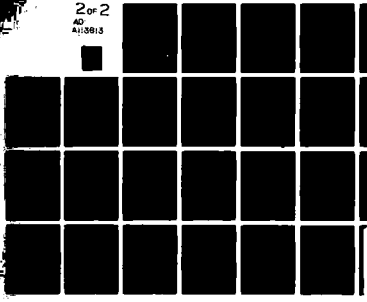

END
DATE FILMED
5 82
DTIC

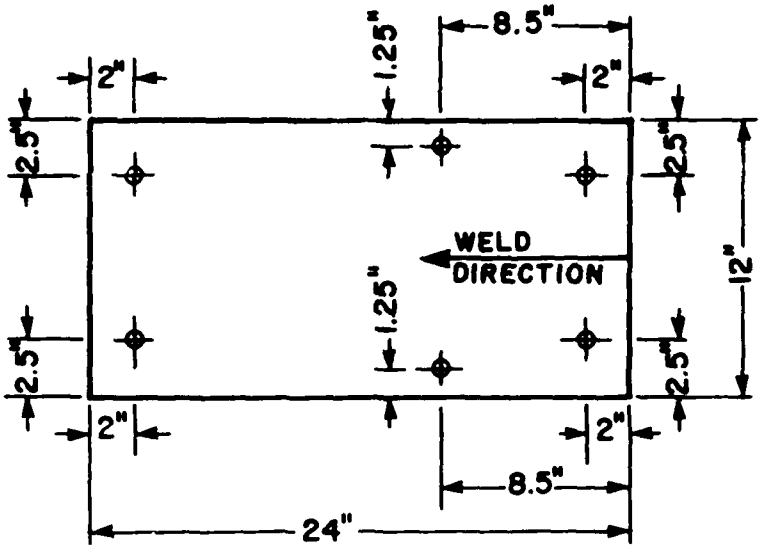

FIGURE 4.1 Location of C-Clamp restraints
Specimen #3

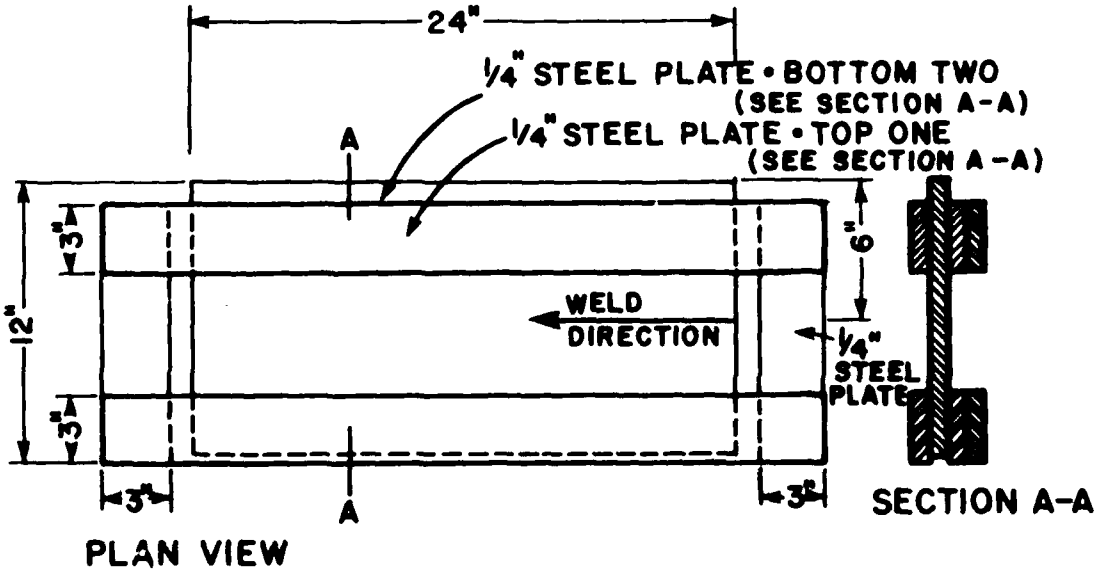

FIGURE 4.2 Location of restraints
Specimen #6

Temperature, strain, and distortion changes were recorded continuously during the welding of all specimens using chromel-alumel thermocouples, electric resistance strain gages, and dial indicators respectively. The locations at which these measurements were taken are shown in Figures 4.3 through 4.7.

The effect of heat input due to a weld grinding operation on the plate's distortion was also studied. Specimens #5 and #8 were chosen for this purpose. After welding and subsequent cooling, a portion of the weld metal was ground down in these two specimens as shown in Figure 4.8. The temperature and distortion changes resulting from this operation were measured.

4.4 Obtained Results and Discussion

Some of the results obtained during the experimental program will be presented and discussed in this section. For more details one is referred to McCord's thesis.

4.4.1 Temperature Distributions

Figures 4.9 through 4.14 show the temperature distributions for specimens #2, 5, and 8. The following conventions are used in these figures: time in the horizontal axis starts at the time a welding pass commences; the time duration of each welding pass is denoted by a horizontal arrow, whereas the time instance at which the welding arc passes the instrumentation area is denoted by a vertical arrow; finally, note the scale changes in the horizontal axis.

The temperature distributions for specimens #2 and 5 are shown in Figures 4.9 through 4.12 (for the thermocouple locations refer to Fig. 4.3). Measurements at point b were taken for both the plate surfaces (top and bottom) to check the usual assumption made of uniform through-thickness temperature distributions in the case of thin plates. The obtained results indicate that such an assumption is valid, at least for points located some distance away from the weld centerline. Furthermore, Figures 4.11 and 4.12 show the effect the preheating and postheating operations carried out on specimen #5 had on the temperature distributions.

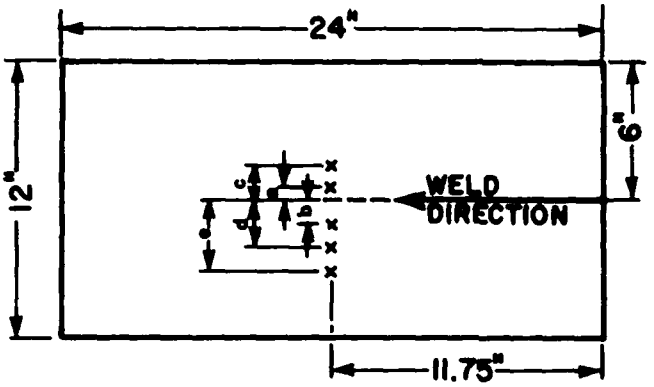

DISTANCES IN INCHES

SPECIMEN	a	b	c	d	e
1	0.5	1.0	1.5	2.0	3.0
2	0.4	1.0*	1.4	2.0	-
3	0.65	0.75	1.7	1.7	2.7
4	0.45	1.0	1.45	2.0	3.0
5	0.45	0.95*	1.45	1.9	-
6	0.5	1.0	1.5	2.0	3.0

FIGURE 4.3 Thermocouple locations for Specimens #1 through #6

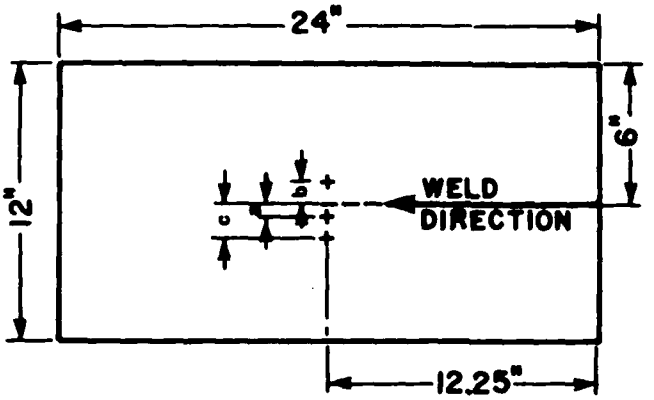

DISTANCES IN INCHES

SPECIMEN	a	b	c
1	0.5*	1.0*	1.5
2	1.0*	1.4*	
3	0.7*	1.7*	
4	1.0*	1.4*	
5	1.0*	1.5*	
6	1.0*	1.5*	

FIGURE 4.4 Strain gage locations for Specimens #1 through #6

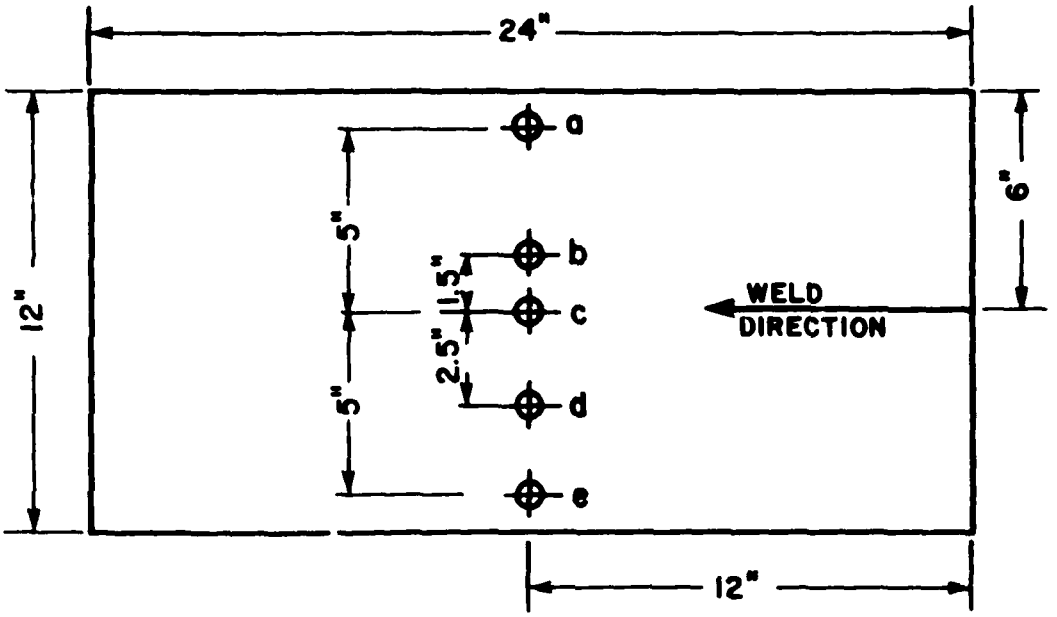

FIGURE 4.5 Dial indicator locations for Specimens #1 *through #6*

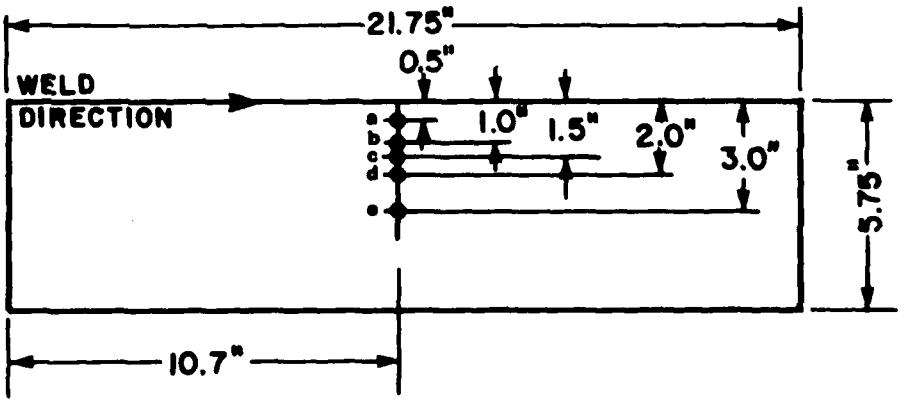

FIGURE 4.6 Strain gage and thermocouple locations for Specimens #7 and #8 (strain gages installed on back side and thermocouples on front side)

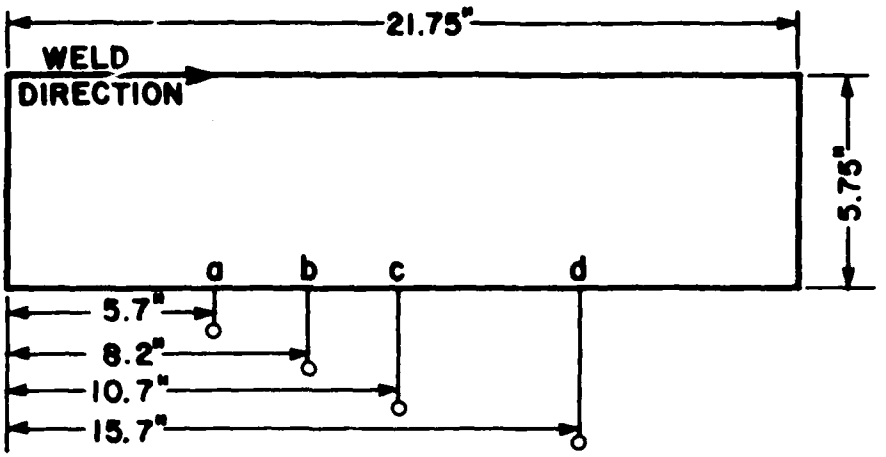

FIGURE 4.7 Dial indicator locations for Specimens #7 and #8

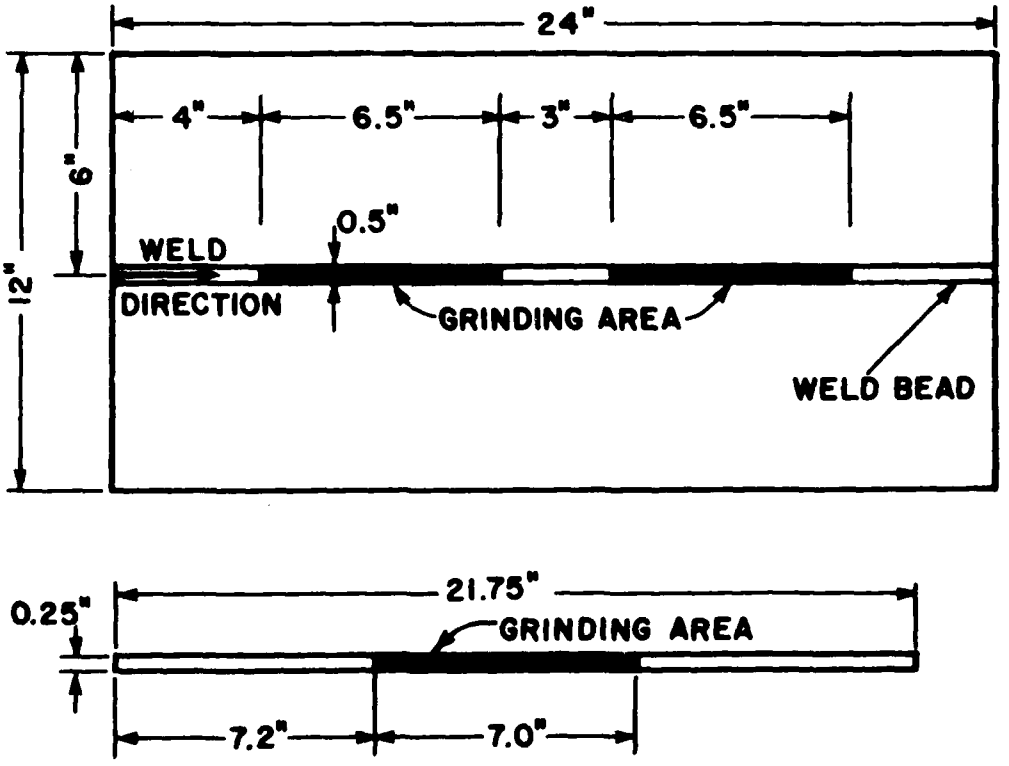

FIGURE 4.8 Grinding areas in Specimens #5 and #8

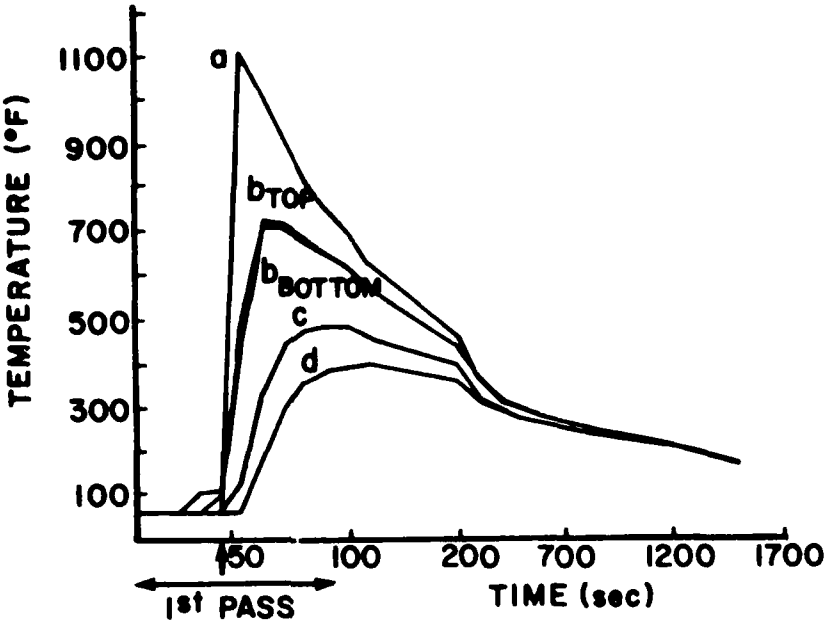

FIGURE 4.9 Temperature distribution in Specimen #2 (Pass #1)

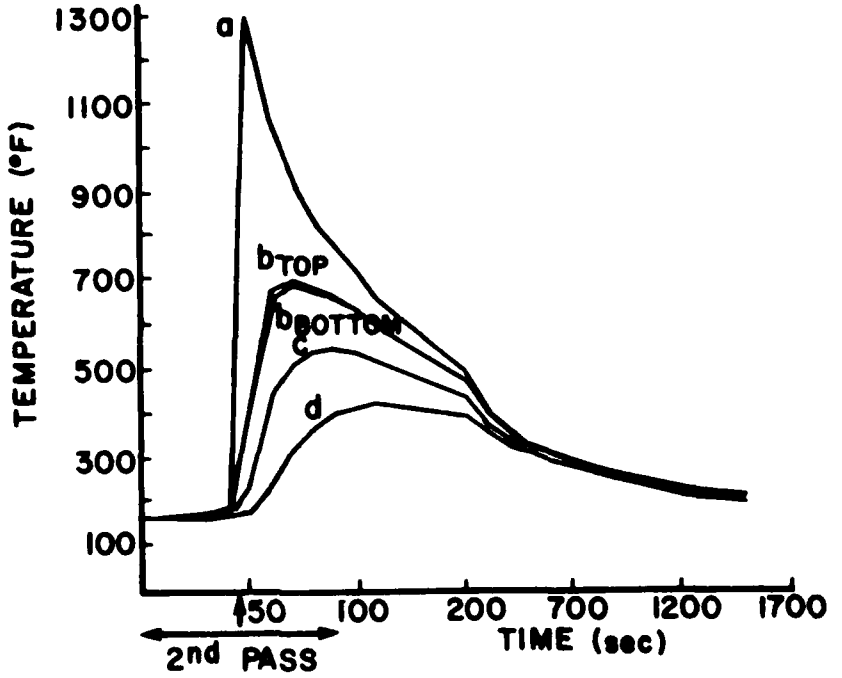

FIGURE 4.10 Temperature distribution in Specimen #2 (Pass #2)

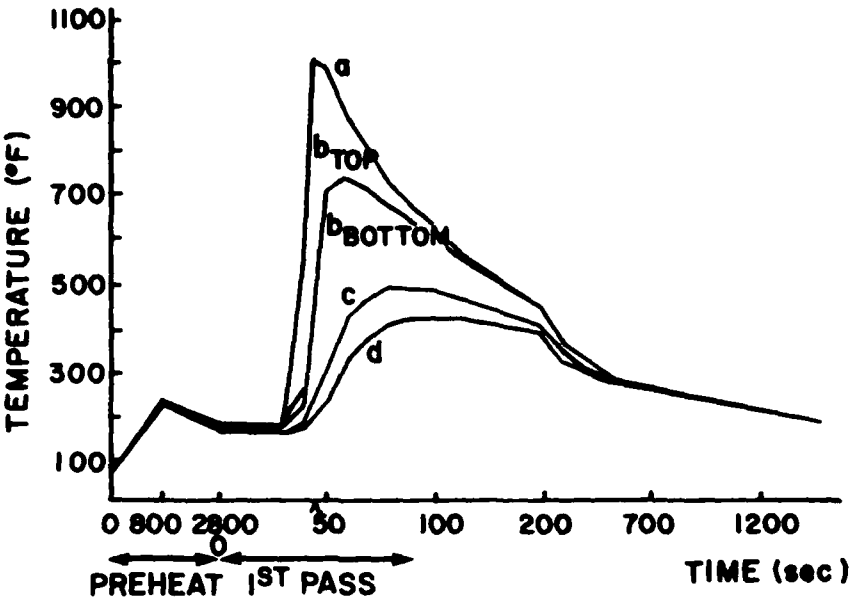

FIGURE 4.11 Temperature distribution for Specimen #5 (Preheating and Pass #1)

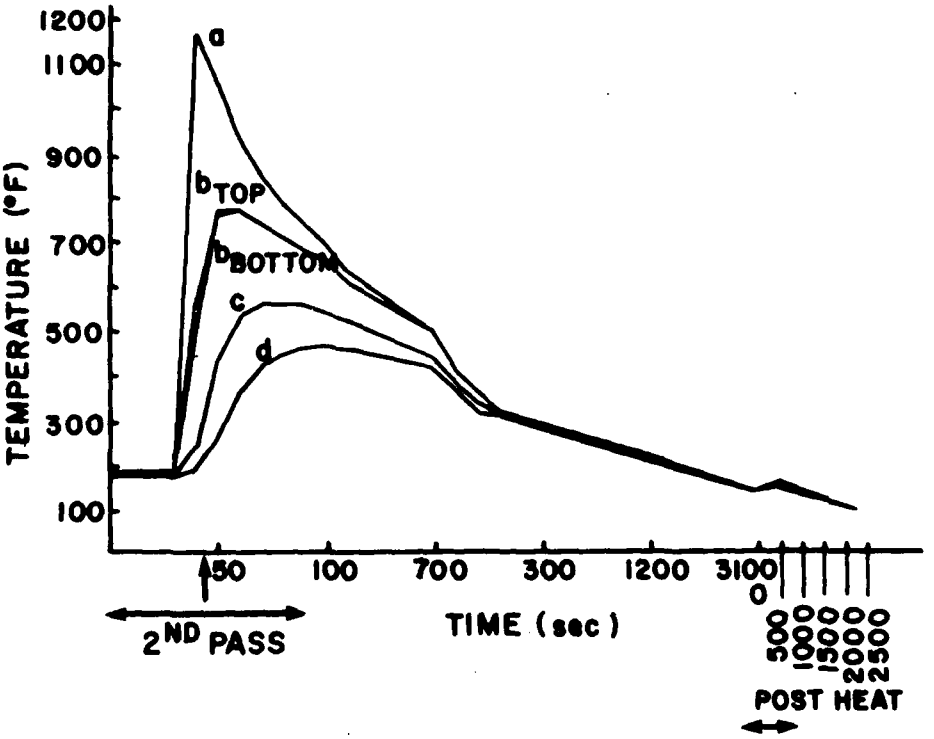

FIGURE 4.12 Temperature distribution for Specimen #5 (Pass #2 and Postheating)

The effect of the grinding operation on the temperature distribution is shown in Figures 4.13 and 4.14 for specimens #5 and 8 respectively. Note that there is a substantial difference between the maximum temperatures reached in the two specimens. This difference can be explained by referring to Fig. 4.8. In the bead-on-plate welded specimen #5 the area ground down was very large, whereas in the edge welded specimen #8 the grinding operation was contained to a much smaller area, thus giving rise to higher temperatures. Furthermore, comparing Figures 4.3, 4.6, and 4.8 it becomes apparent that the thermocouple location area was closer to the grinding area in the latter specimen.

4.4.2 Transient Strains

The time variation of the total transient strain was also measured during the experiments. Representative results are shown in Figures 4.15 through 4.18, where the same conventions as the ones for the temperature distribution are used. Note that the strains shown are total strains, that is they also include strains due to plate bending.

Although dissimilar procedures were used for the various specimens, a definitive pattern of strain history emerged. As the welding arc approached the gage location the strains became compressive. This was caused by the increasing temperature resulting in a tendency for the heated material to expand; this expansion was, however, hindered by the surrounding bulk of relatively cooler metal. As the arc passed the gages, the strains became less compressive or even tensile owing to the melting of the weld metal and the subsequent strain release in this region. As the welding arc continued to travel the strains once again became more negative (compressive). This happened as long as the temperature kept increasing at the observation points. As each point reached its maximum temperature and subsequently started cooling down, the strain became less negative. This phenomenon can be seen clearly by comparing Figures 4.9 and 4.15. Point c in the first and points b_{top} and b_{bottom} in the latter figure are all located at a distance 1.5 in from the weld centerline. The maximum temperature at this location is

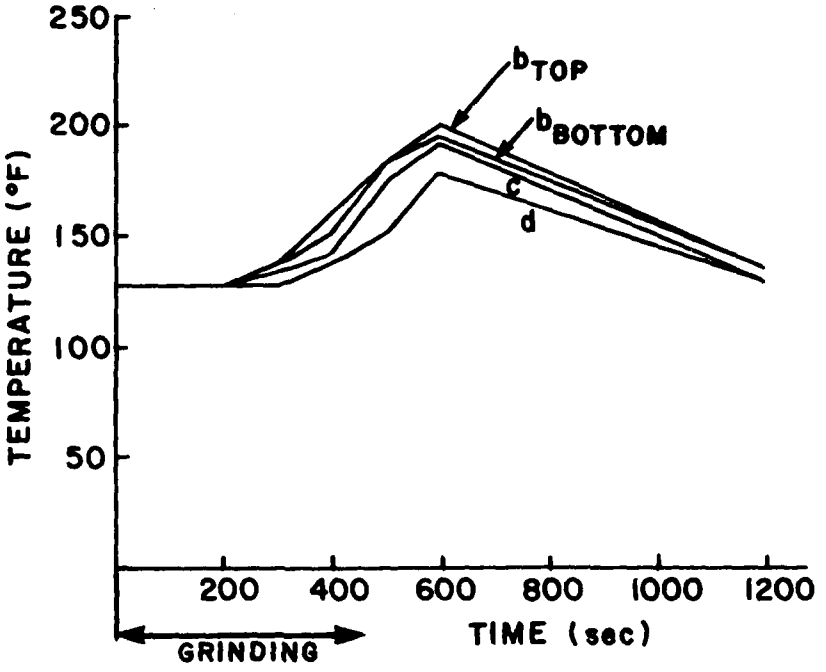

FIGURE 4.13 Temperature distribution due to grinding operation on Specimen 5

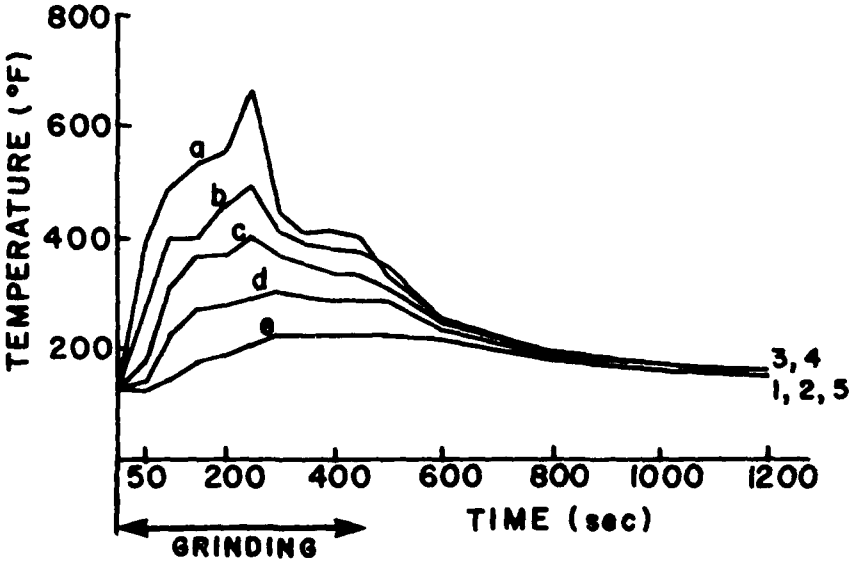

FIGURE 4.14 Temperature distribution due to grinding operation on Specimen 8

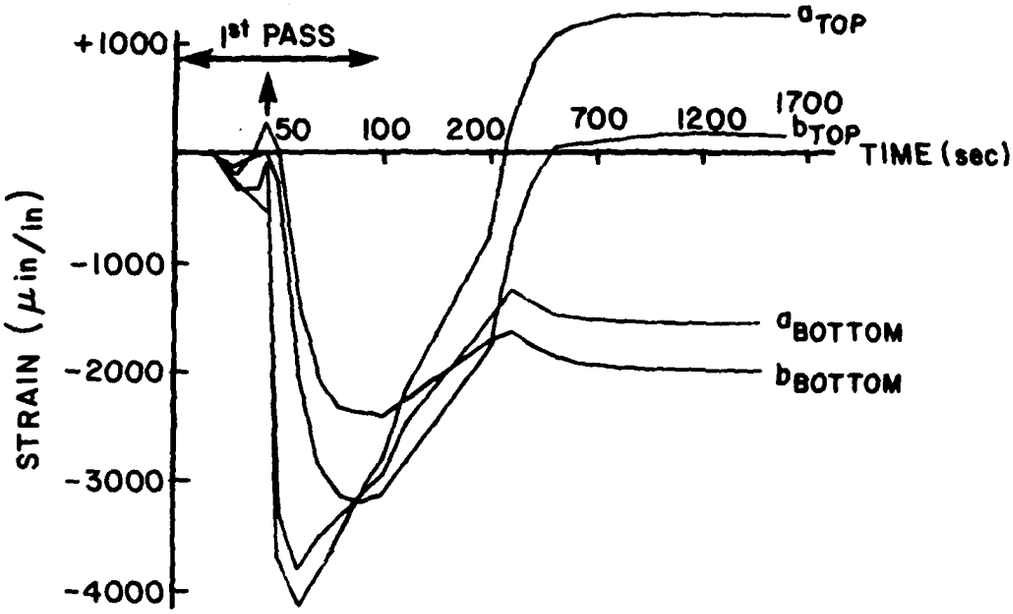

FIGURE 4.15 Transient strain history for Specimen 2 (Pass #1)

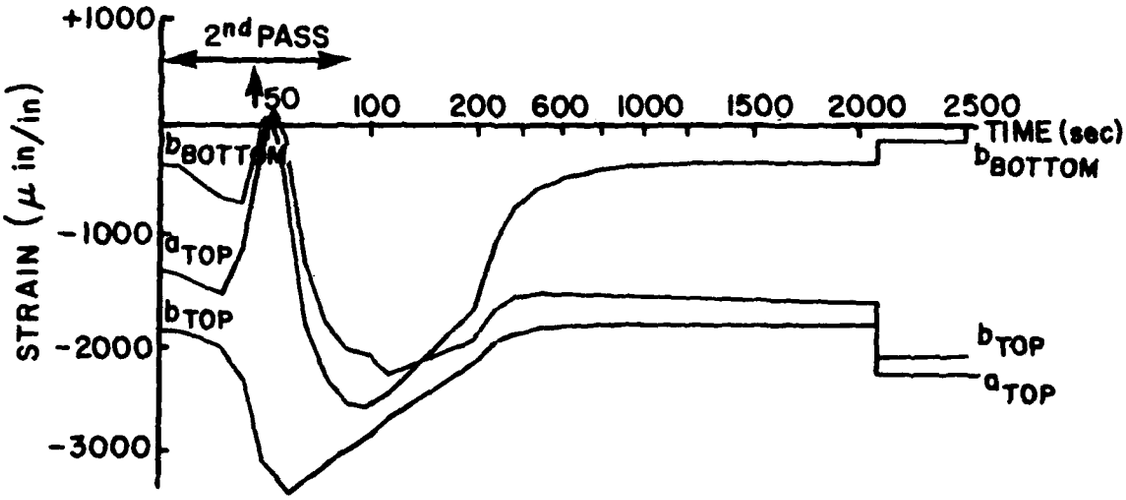

FIGURE 4.16 Transient strain history for Specimen 3 (Pass #2 and release of restraint)

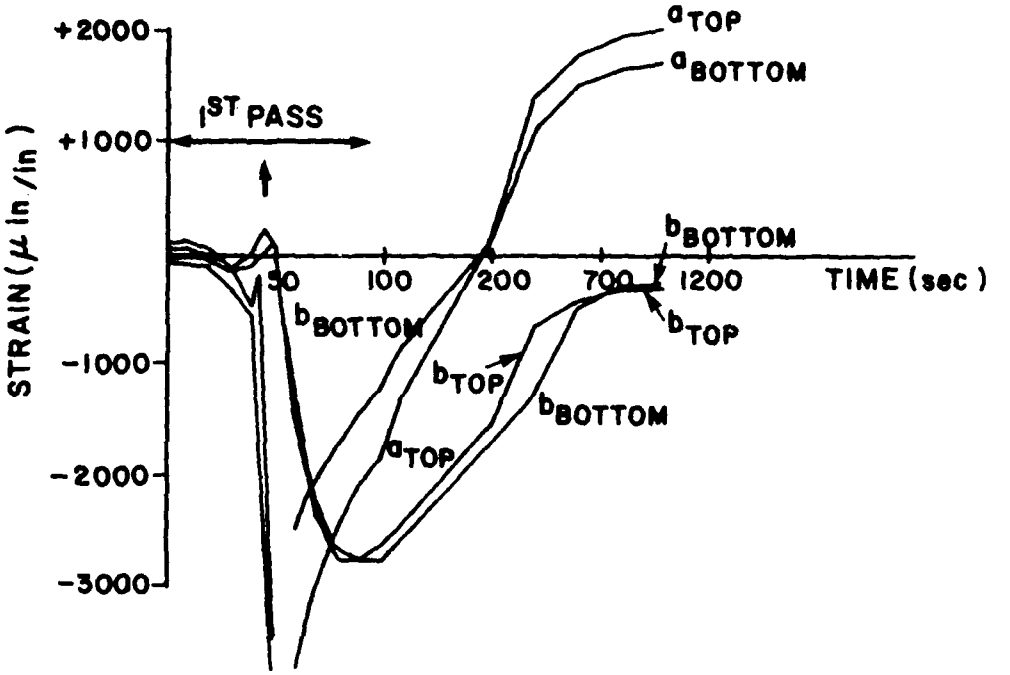

FIGURE 4.17 Transient strain history for Specimen #6 (Pass #1)

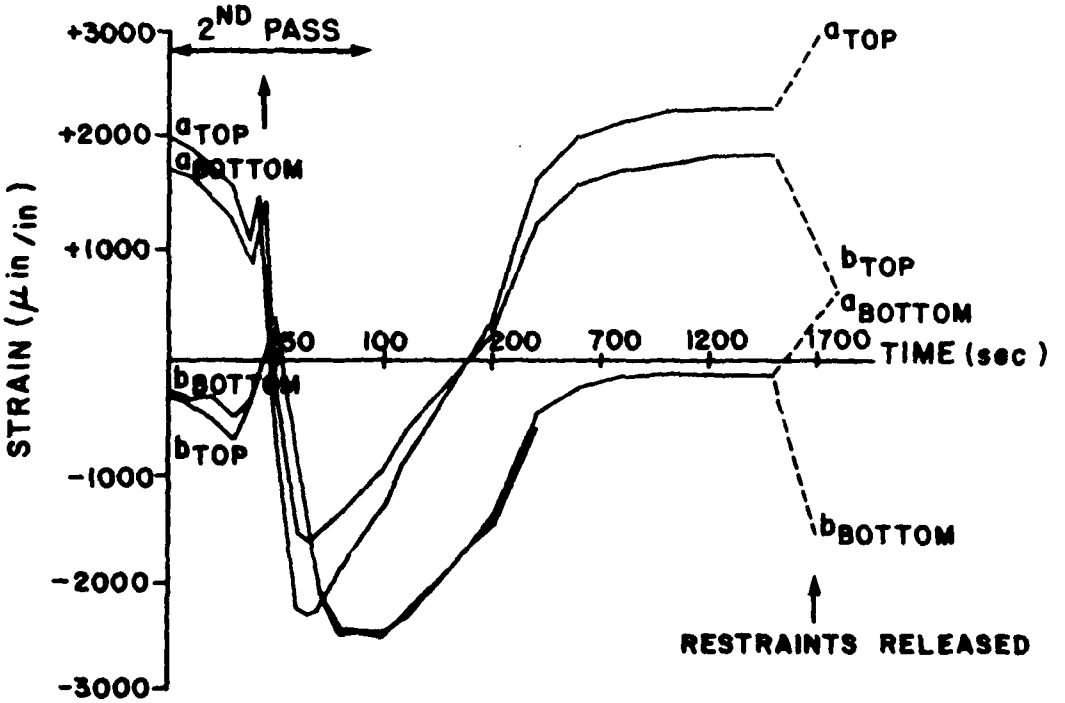

FIGURE 4.18 Transient strain history for Specimen #6 (Pass #2 and release of restraint)

reached 90 sec after the start of the welding operation (Fig. 4.9); at about the same instance the maximum compressive strain is reached (Fig. 4.15). From then on as the temperature decreases so does the strain (in absolute value). At 300 sec however after the commencement of welding the strain becomes slightly more negative at the plate's bottom. This is caused by the plate bending, resulting in tensile bending strains on the top and compressive strain on the bottom surfaces.

The effect of releasing the C-clamp restraint after the plate has cooled down is shown in Figure 4.16 for specimen #3. If this is compared with Figure 4.18 for specimen #6, it can be noted that much more strain was stored in the combination of C-clamps and steel plate restraint than in the C-clamp only restraint.

Assuming that the total strain is the summation of the mechanical and bending strains, that the mechanical strain has a uniform through-thickness distribution, and that the bending strain varies linearly through the plate thickness, McCord was able to calculate the mechanical and bending strains for the specimens for which total strains were measured on both the top and bottom surfaces of the plate (specimens #1, 2, and 5). Graphs of these strains can be found in his thesis.

4.4.3 Distortion History

Figures 4.19 through 4.22 are plots of distortion history for specimens #1, 2, 5, 7, and 8. Note that the latter two specimens show much smaller distortion values than the other ones. This is due to the much higher section modulus (moment of inertia divided by the maximum distance from the neutral axis) and much lower welding heat input exhibited by specimens #7 and 8.

It can be seen from the above figures that little distortion occurs until after the weld is complete, the plate reaches a uniform temperature and then starts to cool down. At this point the bending strains begin to increase in magnitude, whereas the mechanical strains approach a constant value.

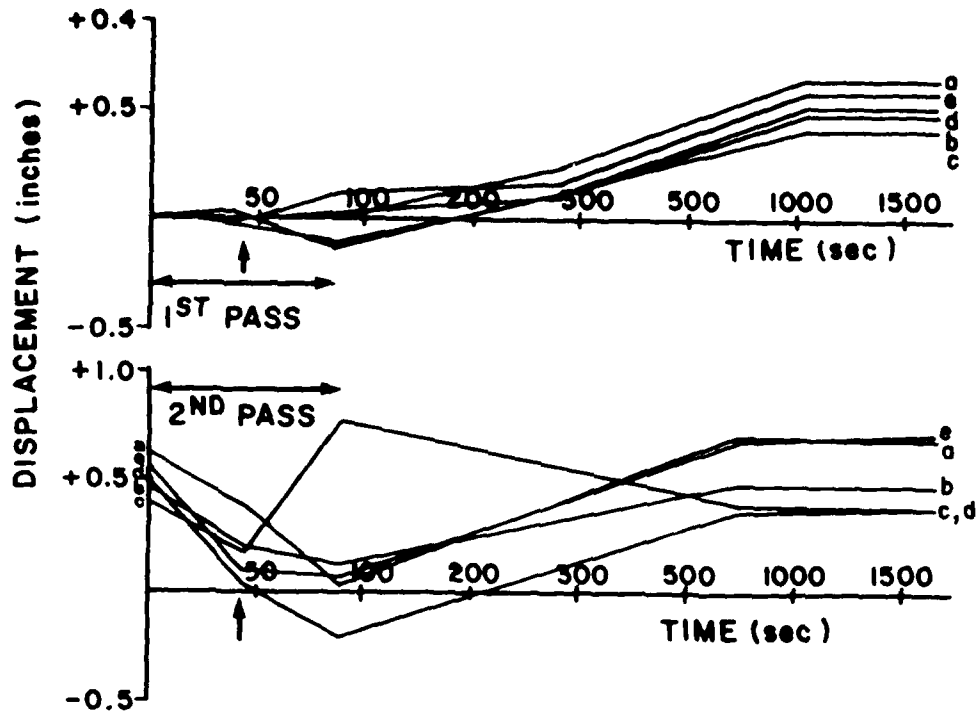

FIGURE 4.19 Distortion history for Specimen #1

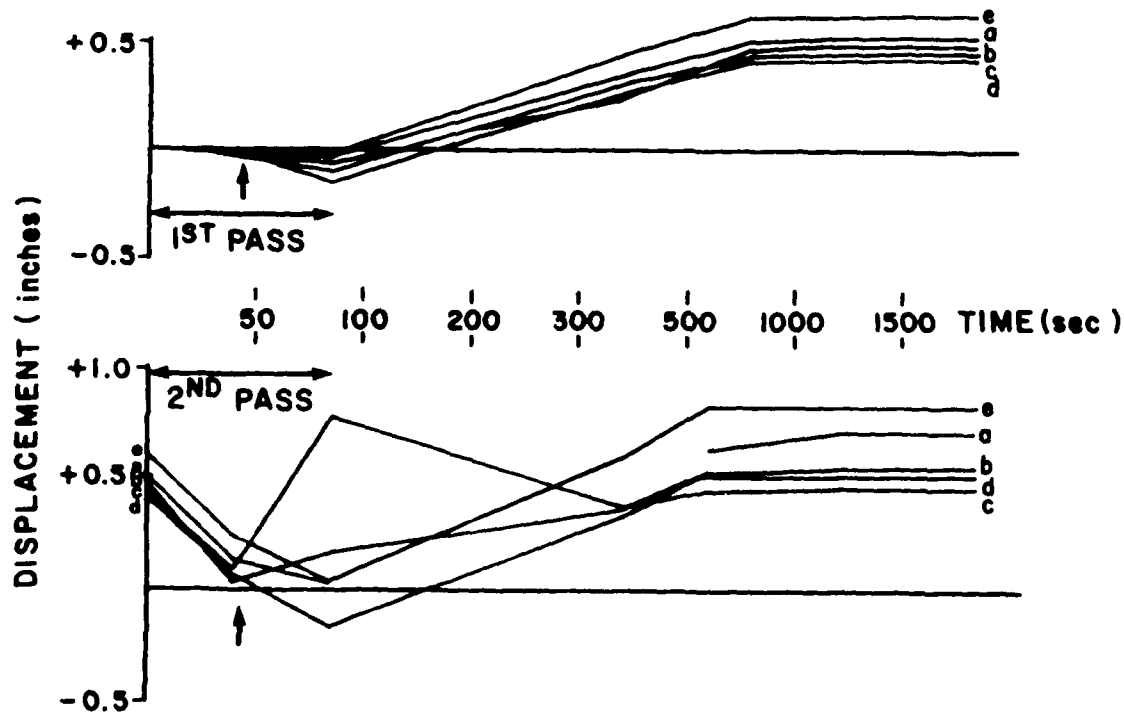

FIGURE 4.20 Distortion history for Specimen #2

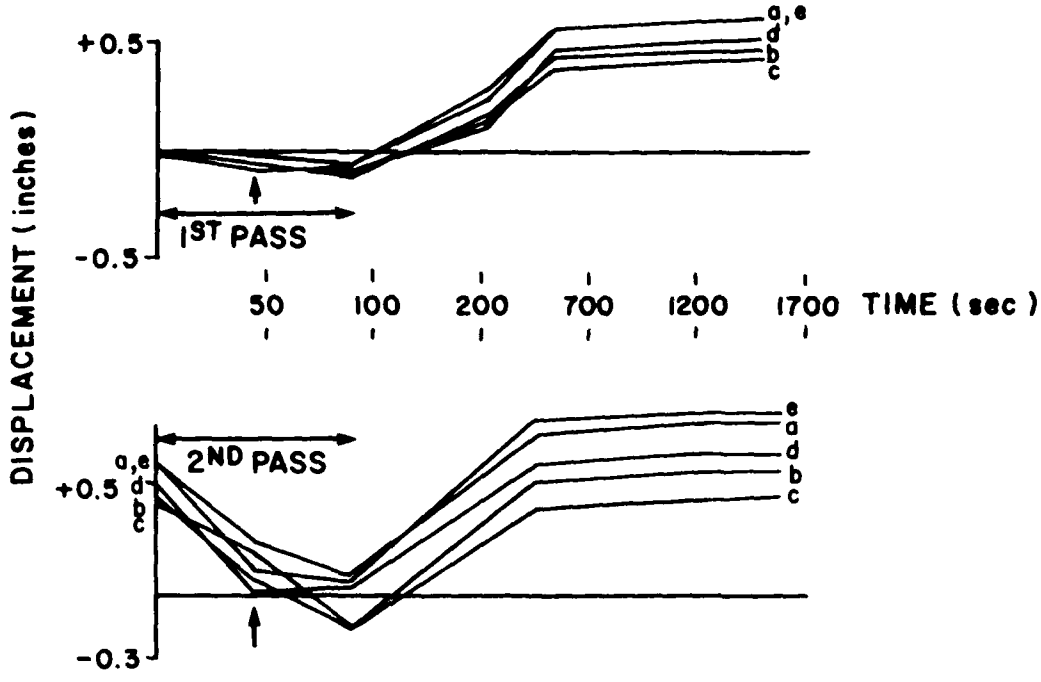

FIGURE 4.21 Distortion history for Specimen #5

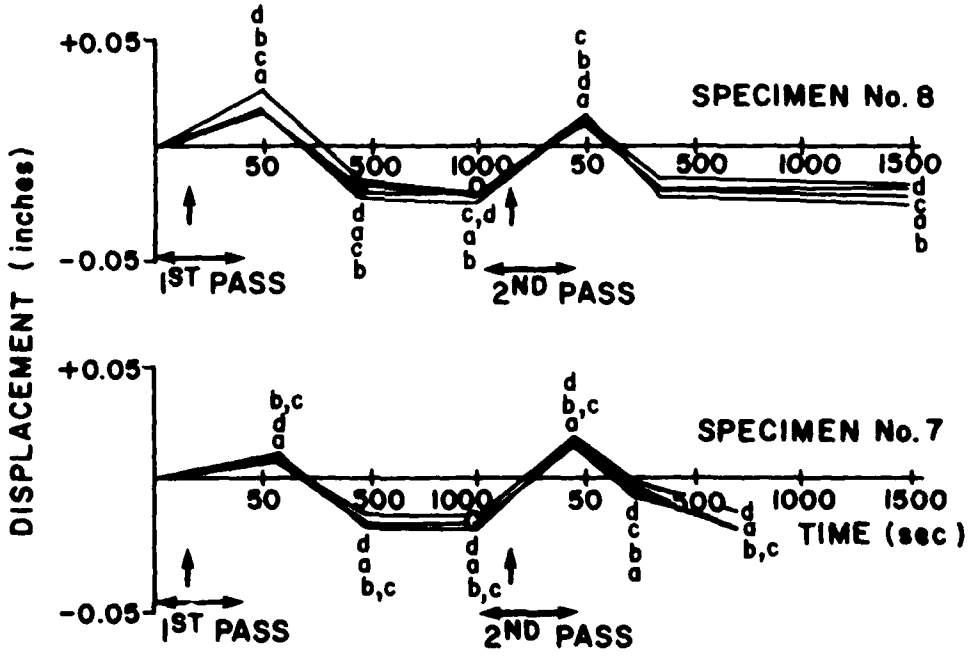

FIGURE 4.22 Distortion history for Specimens #7 and #8

Comparing the graphs of distortion and bending strain histories, McCord observed that their shapes closely follow each other. Based on this observation and using simple beam theory he was able to develop an approximate procedure for predicting the welding distortion from a knowledge of the bending strains. His model is reasonably accurate for the case of unrestrained plates, giving an error of less than $\pm$ 10%. For better predictive capabilities it is recommended that the model be modified using plate bending theory and values of bending strains in both the x and y directions.

4.4.4 Final Distortion

Figure 4.23 shows the final displacements for specimens #1 through #6. For specimens #1 and 2 the final displacements are plotted after the first and second weld pass. The final displacements for specimens #3 and #6 are shown only after the restraints are released. The displacement plot of specimen #4 is a plot of final displacement after each weld block has cooled. The graph for specimen #5 shows the effect of preheating, postheating, and grinding, as well as welding two passes, on the final displacements.

These graphs may be used to construct a three-dimensional representation of the plate. From the graphs in Figure 4.23 both longitudinal displacements and transverse displacements may be found.

Figure 4.23 shows pictorially the following results. Good correlation between specimen #1 and specimen #2 exists, and thus there is good confidence in these results as a baseline. The other specimens should then be compared to specimens #1 and #2 to evaluate the effect of different weld conditions on distortion. Specimen #3 buckled in the opposite direction than all other cases. This deflection is roughly equivalent in magnitude to specimens #1 and #2 but in the opposite direction. Specimen #3 buckled in this manner due to the way it was clamped allowing the ends to rotate only up and not down. Specimen #4 shows a marked decrease in final displacements over those of specimens #1 and #2 (as much as a 60% decrease). Preheating and postheating of specimen #5

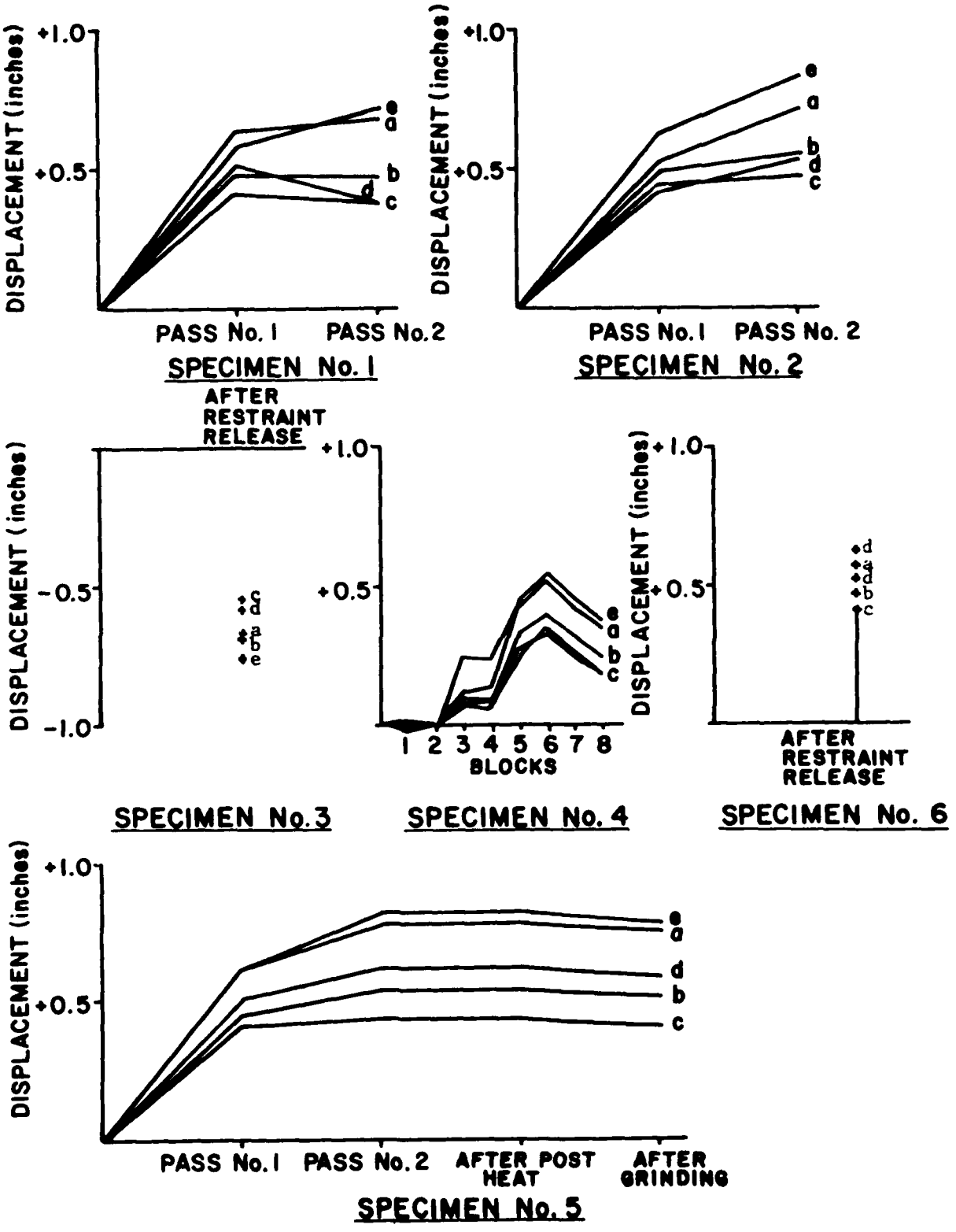

FIGURE 4.23 Final distortion measurements for specimens #1 through #6

had no effect on the final displacements, while grinding the weld tends to reduce the displacements slightly. The restraints used in specimen #6 reduced the final displacements only slightly (approximately 10%).

4.4.5 Comparison with Analysis

The experimentally obtained results were compared with predictions made using the M.I.T. one-dimensional computer program capable of analyzing thermal stresses and metal movement during welding. Only the unrestrained specimens were analyzed due to the program's limitations. Very good correlation was observed between experiments and analysis.

4.5 Conclusions

Based on the results obtained in this study, the following conclusions can be drawn:

1. The lower the temperature of the weld and the surrounding base metal, the lower the generated strains will be. A decrease in strain results in a decrease in distortions of the piece. However, the temperature must be high enough to produce an adequate weld.

2. Block welding is one way of reducing strains and greatly reducing the amount of distortion in the specimen.

3. Caution must be exercised when restraining a specimen during welding in order to reduce distortions. Specimens #3 and #6 of this study showed the effects that different types of restraint have on the final distortion.

4. By being able to resolve the total strain into mechanical strain and bending strain at a particular point in the specimen, a quick and economic method of monitoring the bending strain in the specimen is available. If the strain gage inputs are fed through a digital-to-analogue converter to a computer, which separates the total strain signal into bending strain and mechanical strain, it is possible to obtain real time data of the bending strain present in the specimen. If the correct structural modeling is then used, the bending strain can be further resolved into displacement.

5. By knowing the strain history of a typically welded (or mass produced) specimen, it is possible to identify a given value of strain at a certain point that corresponds to a certain distortion. If, for example, a specimen is required to deflect by no more than X amount, then a strain corresponding to this deflection can be found. By being aware of the strain history, by monitoring a specimen during welding, and by identifying upper limits of allowable strain, the welding operation could be monitored and operations ceased as a strain threshold is approached. This method could save time and money by eliminating the need to rework a specimen in order to reduce welding-caused distortions.

5. PROGRESS OF TASK 4 - THERMAL STRESS RELIEVING (December 1, 1980 to November 30, 1981)

5.1 General Status

The objective of Task 4 of this research project is to study the mechanisms of thermal stress relieving in weldments. Task 4 consists of the following subtasks:

Task 4.1: Initial Analysis and Verification Tests

Task 4.2: Further Analyses and Experiments

In the most part progress has been made as originally proposed. An extensive literature survey was initially performed covering thermal, mechanical, and vibratory stress relieving treatments. Special attention was given to the applicable military and industrial codes.

An initial analysis of the effect of both mechanical and thermal stress relieving treatments was then performed for the case of long, thin plates butt or edge welded. The one-dimensional computer program earlier developed at M.I.T. was modified for this purpose. Currently efforts are being carried out to also include creep calculation capabilities.

Experiments to verify the analytical results have not been conducted yet but are currently under way with anticipated completion date January 1982. The delay was due to plate shipment problems. Details on these experiments will be discussed in Section 5.4.

In what follows information on the progress made so far will be provided. This information is largely taken from the following thesis under preparation:

Agapakis, J., "Fabrication of High Strength Steel Structures - A Study on Stress Relieving and Weld Metal Strength", S.M. Thesis, M.I.T. (in preparation).

5.2 Literature Survey

General Background. It is a well established fact that during the fabrication of welded structures residual stresses are developed having peak values that reach the yield stress of the material being welded. This fact

was confirmed by both analysis and experiments for the case of HY-130 steels in the course of the present research program.

These residual stresses, however, can have detrimental effects on the service behavior of welded structures. As a consequence, several methods have been proposed and are currently in use aimed at reducing residual stresses. These methods include both mechanical (overstressing and vibratory) and thermal treatments.

Thermal stress relieving involves heating of the structure to a temperature at which the material yield stress has fallen to a value lower than the room temperature one and where the mechanism of creep can also take effect. High welding residual stresses can therefore no longer be supported. If temperatures are high enough, the stress distribution will become rather uniform. At the same time, the thermal stress relief treatment will usually involve some tempering or aging effects. That is the microstructures will be changed to an extent depending on the material under consideration, the heat treatment temperature, and the time spent at this temperature.

Stress relief heat treatment can be either applied to the structure as a whole or to specific portions of it if the size in prohibitively large. In the former case electric and fossil-fired furnaces are generally used, whereas the localized heat treatment is effected by means of electric resistance, induction, and high velocity gas techniques.

Experience has shown that in the case of a butt weld in plate structures satisfactory relief of residual stresses can be expected if uniform heat input is applied over a bandwidth equal to twice the weld length. According to British codes, this bandwidth becomes equal to $5\sqrt{Rt}$ for a circumferential girth weld on a cylinder of radius R and thickness t (see Figure 5.1)[26]. Different specifications, however, are spelled out in different welding codes.

---

[26]Burdekin, F.M., "Heat Treatment of Welded Structures", The Welding Institute, Abington, England, 2nd edition, 1969.

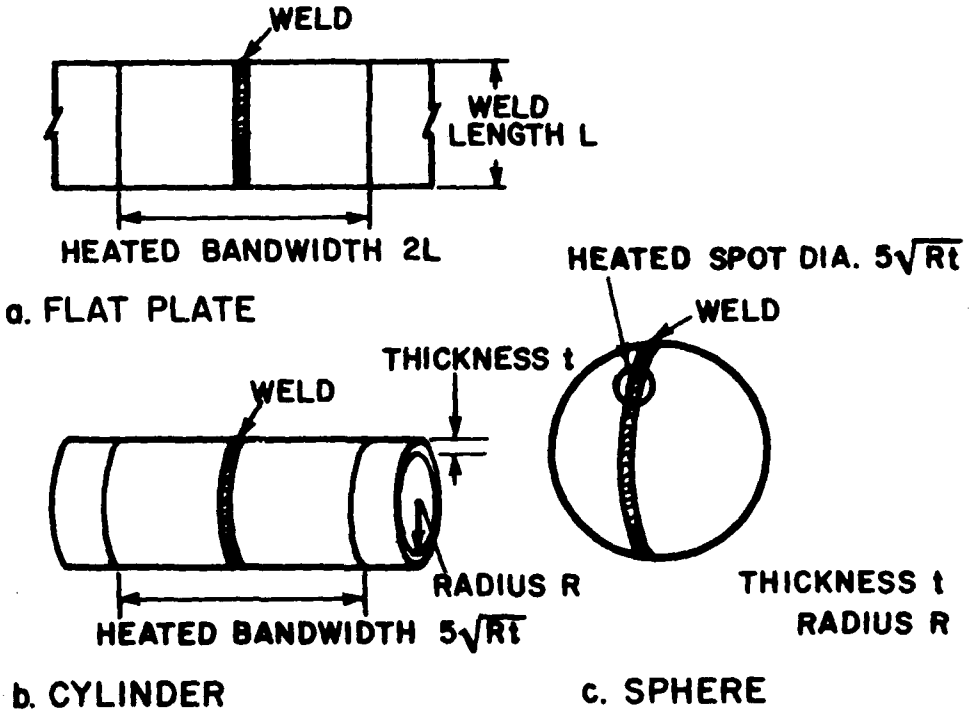

FIGURE 5.1 Band widths for local heat treatments to achieve stress relief in: (a) flat plate situations, (b) circumferential butt joints in cylinders, and (c) butt joints in spheres

Nevertheless, there are generally three main requirements that govern the heat treating method:

(a) It should be able to produce the required temperature.

(b) The required temperature should be controlled within specified limits (e.g., $\pm$ 10° to 20°F for steels).

(c) It should be possible to achieve a uniform and even heating and cooling rate throughout the heaviest section to be treated.

The last requirement is especially important for the case of joints of complex geometry and variable thickness.

Effects of Thermal Stress Relieving. Stress relief heat treatments should in general be avoided unless necessary to obtain adequate service performance of a joint. In some codes, however, such treatments are mandatory. Nevertheless, their effects are different for different materials.

Specifically for C/Mn steels, stress relief treatments are beneficial for the fracture toughness of the HAZ. A treatment would permit these steels to operate at considerably lower temperatures than those of the as-welded structures of the same material. Moreover, the stress corrosion cracking characteristics would have a marked improvement since the total stress level present close to the weld will be reduced. The effect on fatigue characteristics will in general be secondary.

For low alloy steels, however, the effect of heat treatment is different. These types of steel are usually supplied in a heat treated condition, e.g., normalized and tempered, quenched and tempered, etc. Therefore, if postweld stress relief treatments are necessary, they must be carefully applied so that the optimum welded joint properties are developed without destroying the inherrent properties of the parent material. For the cases of stress corrosion cracking and fatigue characteristics of low alloy steels, the effects of the thermal treatments are similar to the ones for C/Mn steels. This is not the case, however, as far as brittle fracture is concerned where the effects are not always beneficial if the heat treatment is incorrectly stipulated.

For creep resisting steels the behavior is similar, the only difference being that higher stress relieving temperatures are required. It should nevertheless be stressed that the metallurgical effects are extremely important for these secondary hardening steels.

For austenitic steels the post weld heat treatment is necessary in some cases but can give rise to problems. For complete stress relief the treatments should be carried out at temperatures above 1500° to 1600°F

(800° to 850°C), whereas for the removal of stress peaks treating to below 900°F (500°C) is adequate. In these steels stress relief treatments are beneficial for the prevention of stress corrosion and reheat cracking.

For other steels and alloys various effects of stress relief treatments are reported in the literature. It should be pointed out that in several cases these effects are unfavorable.

To assess the desirability and effectiveness of stress relief treatments Commission X of the International Institute of Welding (I.I.W.) established in the late 1960's a working group on "Stress Relief by Heat Treatment". The principal objective of this research effort was:

"To study the recommendations on stress relief heat treatment and collect results relating to the effects of such treatment on the properties of the welded joint".

Various reports from this working group appear in the bibliography, the latest one published in 1979.[27]

Postweld Heat Treatment of HY-130 Steel. Extensive work has been performed at the Materials Laboratory, DTNSRDC aimed at evaluating the effectiveness and desirability of post weld stress relief heat treatments for the HY-130 base metal and compatible weld metal. Basic results from these studies can be summarized as follows:[28]

(1) Stress relief cycles are cumulative in nature. This was demonstrated by the similar tensile and Charpy properties resulting from tests on specimens given several short-duration stress relief heat treatments and a long-duration one, both histories having equal time at the stress relief temperature.

---

[27] I.I.W. Working Group on Stress Relief by Heat Treatment, "Final Report: Desirability of Post Weld Heat Treatments in Welded Construction," I.I.W. Document X-913-78, February 1979.

[28] Private communication with representatives of the Material Laboratory, DTNSRDC.

(2) A degradation of notch toughness, not accompanied by any change in conventional tensile properties, occurs during stress relief treatments at 950°F (510°C), both isothermally and during cooling. Isothermal degradation is dependent upon time at temperature, with longer times leading to greater embrittlement. The degradation upon cooling is dependent upon rate of cooling, slower cooling rates leading to greater embrittlement. Usually the embrittlement obtained during cooling constitutes the major portion of degradation after short times at temperature but only a minor portion of the degradation after longer times.

(3) At the tempering temperature of 1050°F (565°C), softening at temperature and embrittlement on cooling take place. Thus the resulting properties depend on the cooling rate and on time at temperature.

(4) The toughness degradation may be recovered by retempering to a lower strength level.

(5) Minimum degradation of base metal is observed at stress relieving temperatures approaching the tempering temperature of 1050°F (565°C). The most desirable stress relieving temperature for the weld metal, however, is the lowest possible that still results in sufficient stress relief.

Based on several factors,including maintenance of overmatching weld metal, substantial amount of stress relief within a reasonable time, and considerations of the base and weld metal toughness as a function of stress relief temperatures, a compromise was finally reached regarding the practical temperature range for effecting stress relief in HY-130 weldments. This range is generally accepted to be 1000° to 1025°F (538° to 552°C).

Mechanical Stress Relieving. When the metallurgical effects of thermal treatments are undesirable, it is possible to achieve stress relief by mechanical means.

One such method is the well known overstressing above yield. In general, loading the welded structure to a level higher than its intended service loading will reduce the effect of the existing residual stresses on its service performance. Additionally, a first overloading succeeds in producing compressive residual stresses around any undetected defects,

resulting in what are believed to be beneficial effects on the fatigue characteristics of the weldment. The mechanical treatment, however, does not produce any improvement in the fracture toughness of the HAZ as opposed to the thermal treatments.

An alternative to overstressing is the vibratory stress relief (V.S.R.) treatment. Experimental work on this method started in the 930's and initially gave rise to very optimistic predictions. During the last decade both experimental and analytical work was intensified in an effort to investigate the mechanisms and effectiveness of the V.S.R. Although this technique is currently used in the industry with some success, there still remains much to be learned about its mechanism or even if it actually does relieve stresses as claimed. Nevertheless, the energy savings accrued in comparison to thermal stress relief treatments is a sufficient enough reason to exploit its use.

For the purposes of this study, however, no further consideration was given to mechanical stress relieving techniques. Instead, the method of thermal stress relief treatment was examined both analytically and experimentally.

5.3 Analysis of Thermal Stress Relieving

Various approaches have been adopted in the published literature by several investigators for the analysis of thermal stress relief treatments. Very simple uniform residual stress distributions are usually assumed for the weld metal so that the unidimensional stress-strain curves can be directly employed.[29] For more complex cases numerical models have been proposed, often using the finite element method for performing the thermal-

[29] Tanaka, J., "Decrease in Residual Stresses, Change in Mechanical Properties and Cracking due to Stress Relieving Heat Treatment of HY80 Steel", Welding in the World, 10 (1/2), 1972.

elastic-plastic and creep analysis required.[30, 31]

For the purposes of the current study it was decided that the analysis of the thermal stress relieving operation be accomplished using the simple one-dimensional computer program, successfully employed in the past at M.I.T. for the prediction of residual stresses in long, thin, butt or edge welded plates.[32] Some modifications had to be made in this program to more accurately handle the case of thermal stress relieving. These modifications will be dealt with below at the appropriate places.

Description of One-Dimensional Model. Before considering the mathematical details of the one-dimensional model used, a general description will be given.

In the welding case the computer program calculates the temperature distribution assuming it to be two-dimensional (i.e., the through-thickness distribution is assumed to be uniform since only thin plates are considered). The well-known Rosenthal moving line heat source model is used for this purpose. For the analysis of the heat treatment operation, on the other hand, the temperature distribution is assumed to be uniform over the entire plate. Moreover, Figure 5.2 shows how this temperature distribution changes with time.

---

[30] Ueda, H., and Fukuda, K., "Analysis of Welding Stress Relieving by Annealing Based on Finite Element Method", Trans. of Japan Weld. Res. Inst., 4 (1), 1975.

[31] Cameron, I.G., and Pemberton, C.S., "A Theoretical Study of Thermal Stress Relief in Thin Shells of Revolution", Intl. J. for Num. Meth. in Eng., 11, 1977, pp. 1423-1437.

[32] Papazoglou, V.J., "Computer Programs for the One-dimensional Analysis of Thermal Stresses and Metal Movement during Welding", M.I.T., January 1977.

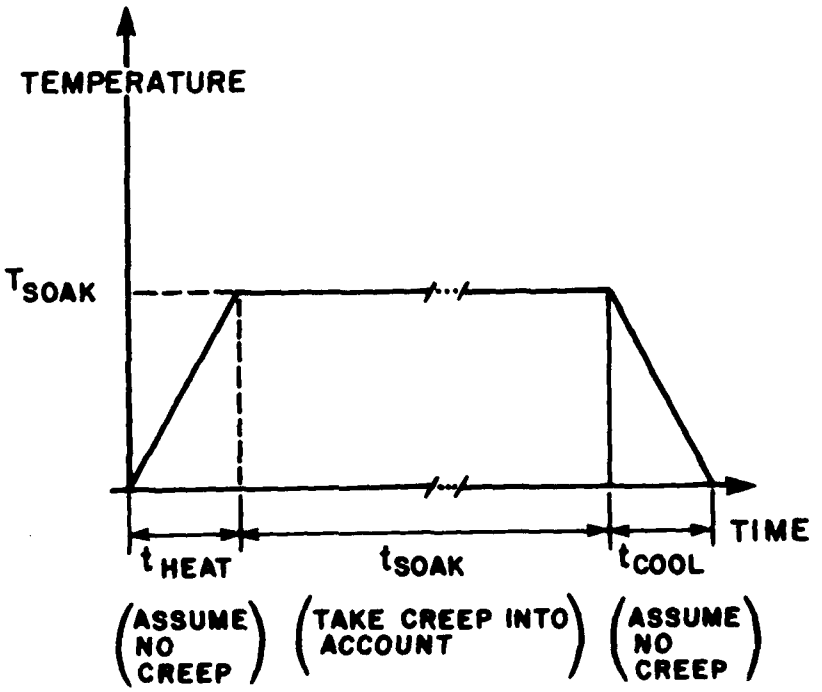

FIGURE 5.2 Stress relieving temperature history

Nevertheless, it should be pointed out that any arbitrary two-dimensional temperature distribution and any time history can be accomodated by the model.

For the stress analysis during welding the following assumptions are made:

(1) Stress is non-zero only in the direction parallel to the weld centerline.

(2) These stresses are a function of the transverse distance from the weld centerline only.

Additional assumptions for the analysis of thermal stress relief treatment were made as follows:

(3) During the heating stage residual stresses decreased due to the decrease of the yield stress and other material properties at high temperatures. Because of the relatively fast heating rate, however, it was assumed that no creep occurred during this period.

(4) During the holding or soaking period at the stress relieving temperature, residual stresses can only decrease due to creep. In other words, if creep is not included in the model, no change in stresses will take place during this period.

(5) During the cooling stage the stresses increase again but end up having smaller values and peaks than before.

To describe the model in mathematical terms, assume an infinite plate of width 2c having a general temperature distribution $\theta(y)$ (see Figure 5.3).

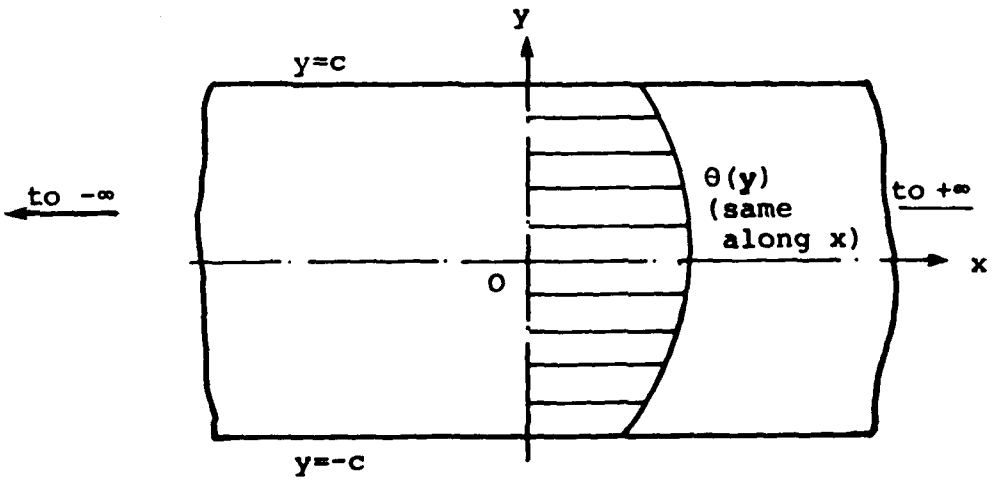

FIGURE 5.3 Thin infinite strip with temperature distribution across the width

The only non-zero stress and strain are assumed to be $\sigma_x = \sigma_x(y)$ and $\varepsilon_x = \varepsilon_x(y)$.

From compatibility considerations[33]

$$\varepsilon_x = c_1 + c_2 y \tag{5.1}$$

where c_1 and c_2 are constants to be determined. The above equation states that plane sections will always remain plane.

Considering an incremental approach, at the end of a time interval Δt the following will hold

$$\varepsilon_x = \frac{\sigma_x}{E} + \alpha \cdot \Delta\theta + \varepsilon_x^{IN} + \Delta\varepsilon_x^{IN} \tag{5.2}$$

or

$$\sigma_x = E(\varepsilon_x - \alpha \cdot \Delta\theta - \varepsilon_x^{IN} - \Delta\varepsilon_x^{IN}) \tag{5.3}$$

where

σ_x/E = elastic part of strain, ε_x^{EL}

$\alpha \cdot \Delta\theta$ = thermal strain, ε_x^{TH}

ε_x^{IN} = accumulated inelastic strain = $\varepsilon_x^{PL} + \varepsilon_x^{c}$

ε_x^{PL} = plastic strain

ε_x^{c} = creep strain

$\Delta\varepsilon_x^{IN}$ = change in inelastic strain during the time increment Δt

From global equilibrium (no external forces and moments acting on the plate)

$$\int_{-c}^{+c} \sigma_x \, dy = 0 \tag{5.4a}$$

---

[33] Papazoglou, V.J., 1977, op.cit.

$$\int_{-c}^{+c} \sigma_x \, y \, dy = 0 \tag{5.4b}$$

Substituting Eqns. (5.1) and (5.3) into (5.4) a set of linear equations is obtained for the determination of the unknown coefficients c_1 and c_2. Solving this system and substituting back into Eqn. (5.1) the following expression is obtained for the total strain:

$$\varepsilon_x(y) = (A_1 - yA_2) \int_{-c}^{+c} E(\alpha \cdot \Delta\theta + \varepsilon_x^{IN} + \Delta\varepsilon_x^{IN}) \, dy$$

$$- (A_2 - yA_3) \int_{-c}^{+c} E(\alpha \cdot \Delta\theta + \varepsilon_x^{IN} + \Delta\varepsilon_x^{IN}) \, y \, dy \tag{5.5}$$

where

$$A_1 = \left[\int_{-c}^{+c} Ey^2 dy\right]/B$$

$$A_2 = \left[\int_{-c}^{+c} E \, y \, dy\right]/B \tag{5.6}$$

$$A_3 = \left[\int_{-c}^{+c} E \, dy\right]/B$$

and

$$B = \left[\int_{-c}^{+c} Edy\right] \cdot \left[\int_{-c}^{+c} Ey^2 dy\right] - \left[\int_{-c}^{+c} Eydy\right]^2$$

Equations (5.3) and (5.6) are not enough to solve the problem. What is still needed is a stress-strain law and a relation between stress and creep strain increments.

To proceed further the assumption is made that creep will only take place during the soaking stage of the temperature history. Thus during this period the accumulated plastic strain, ε_x^{PL}, will remain constant.

Furthermore, it will be assumed that no creep takes place during the heating and cooling stages, resulting in these periods being treated exactly the way the welding problem is handled by the program.

Details on the way the calculations are performed during the soaking period, when creep is taken into account, are given below. They are based on the method of successive elastic solutions:[34]

(a) At the start of the first time interval of the soaking period (see Fig. 5.2)

$$\varepsilon_x^{IN} = \varepsilon_x^{PL}$$

where ε_x^{PL} is the total accumulated plastic strain up to that instant which, as mentioned before, will remain constant during the whole soaking period. To get a first approximation of the total strain after Δt, it is assumed that $\varepsilon_x^{IN} = 0$ in Eqn. (5.5).

(b) This first approximation of the total strain is then substituted for ε_x in Eqn. (5.3) (with $\varepsilon_x^{IN} = \varepsilon_x^{PL}$ and $\Delta\varepsilon_x^{IN} = 0$) to obtain a first approximation of the stress σ_x.

(c) Using this stress approximation and the appropriate creep law (see below for further details), a second approximation for the creep strain increment, $\Delta\varepsilon_x^c = \Delta\varepsilon_x^{IN}$, is obtained (it is reminded that as a first approximation it was assumed that $\Delta\varepsilon_x^c = 0$).

(d) This second approximation for $\Delta\varepsilon_x^c$ is used in conjunction with Eqn. (5.5) to obtain a new approximation for the total strain, ε_x, which is subsequently substituted into Eqn. (5.3) to get a second approximation to the stress, σ_x, and hence reevaluate $\Delta\varepsilon_x^c$. The procedure is repeated until convergence to the correct solution is reached.

(e) For the second and any subsequent time increment, the initial total strains are known from

$$\varepsilon_x^{IN} = \varepsilon_x^{PL} + \sum_{i=1}^{n-1} \Delta\varepsilon_x^c$$

---

34 Mendellson, A., "Plasticity: Theory and Applications", McMillan Publ. Co., New York, 1968.

where the n^{th} time step is considered above. The procedure then follows exactly along the lines described in (a), (b), (c), and (d) above.

It should be noted that for the computer implementation of the outlined procedure all necessary integrations are performed numerically. Furthermore, the temperature variation of the material properties is also taken into account using an iterative procedure.

Finally it is worth pointing out that, since in the stress relieving operation temperature is assumed to be constant over the whole plate during each time step, the form of all the above equations is considerably simplified.

Creep Law. Very limited information on the creep properties of HY-130 steel is available in the literature. Therefore, in order to test the computer model it was decided that a limited number of experiments be performed on 304 stainless steel for which extensive creep data exist in the literature.[35]

The following creep law was used for this material

$$\varepsilon_x^c = A(1 - e^{-Rt}) + St$$

where t is time, and A, R, S are constants that depend on the applied stress and temperature. Note that for the case of thermal stress relief treatment temperature remains constant during the soaking period for which creep is important.

---

[35] Clinard, J.A., et al., "Verification by Comparison of Independent Computer Program Solutions", in Pressure Vessel and Piping Computer Program Evaluation and Qualifications, ASME, PVP-PB-024, 1977.

Model Results. Currently, the creep model is in the process of being implemented in the M.I.T. one-dimensional computer program. Initial trial runs have been made, however, simulating the whole temperature history of the thermal stress relief treatment without taking creep into account. The purpose of these trials was to investigate the effect of plastic flow alone on the stress relieving operation.

A sample of the obtained results is shown in Figures 5.4 through 5.6. The transverse distribution of the longitudinal residual stresses as predicted by the welding part of the 1-D program is shown in Fig. 5.4 for the case of an edge weld performed on a thin low-carbon steel plate. As expected, tensile residual stresses as high as the material yield stress are predicted near the weld centerline, compressive stresses further away, and tensile stresses near the other edge of the plate.

Figure 5.5 presents the stress distribution attained during the soaking period of the heat treatment cycle. Since no creep was present, this distribution remained constant throughout this period regardless of the time spent at the soaking temperature. Note that the stress level is generally lower than in the previous figure, owing to the fact that the material properties (especially the yield stress) are lower at higher temperatures.

The final stress distribution obtained after the plate has cooled to room temperature is shown in Figure 5.6. A general reduction of stresses as compared to the as-welded condition and a leveling-off of the tensile residual stresses near the weld centerline is observed. It is once more emphasized that these results are due to plastic flow only.

It is expected that results showing also the effect of creep will be available in January, 1982. They will be included in the final report to O.N.R.

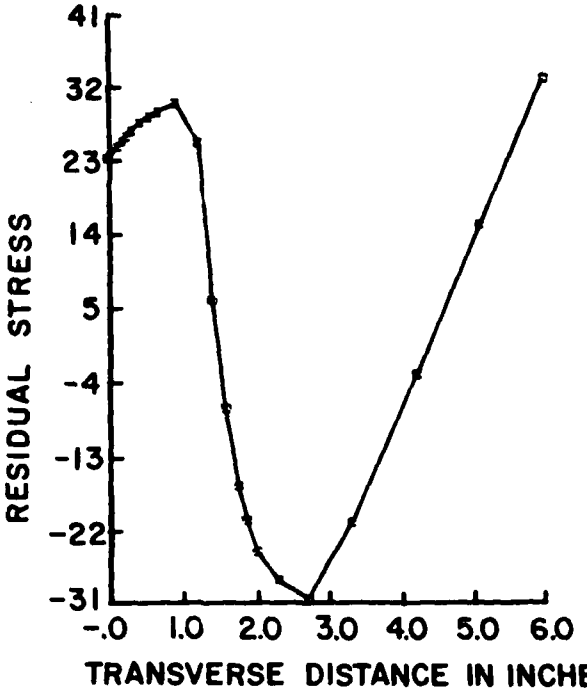

FIGURE 5.4 Transverse distribution of longitudinal residual stresses (as-welded condition)

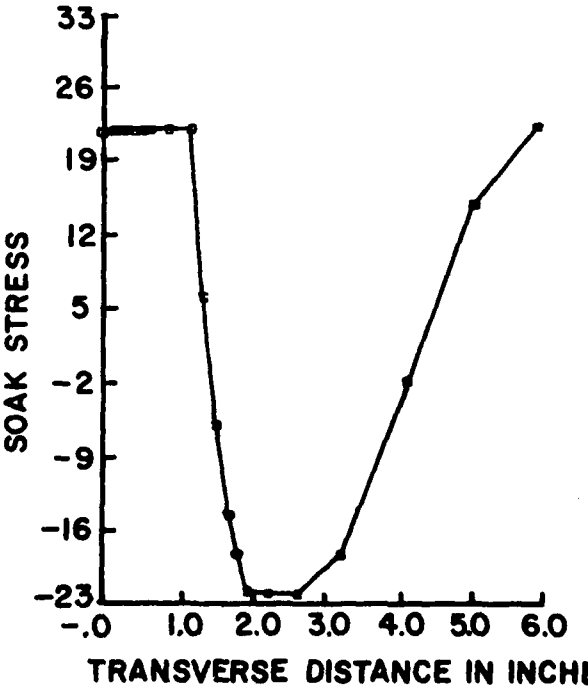

FIGURE 5.5 Transverse distribution of longitudinal stresses during soaking

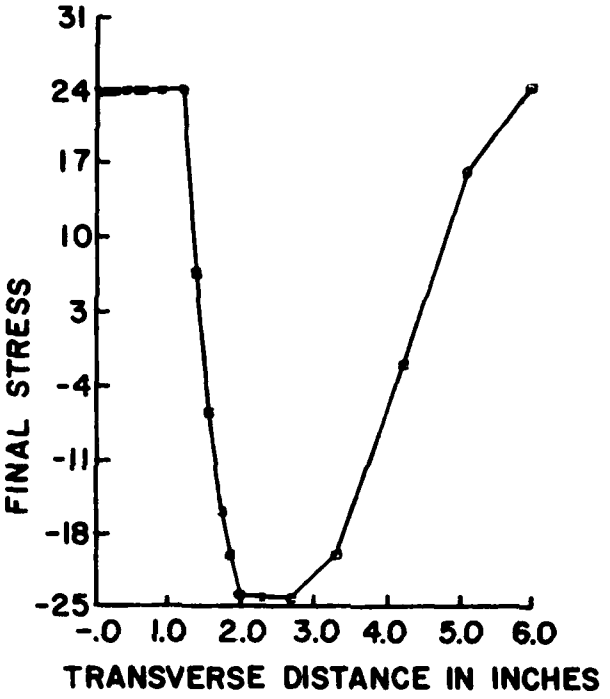

FIGURE 5.6 Transverse distribution of longitudinal residual stresses *after heat treating*

5.4 Experimental Program

As previously mentioned, extensive creep data for HY-130 steel could not be located in the published literature. As a consequence, it was decided that a series of experiments be performed using stainless steel 304 plates in order to test the validity of the one-dimensional model predictions.

The following three series of experiments are currently under way on 304 stainless steel specimens, each measuring 22 in x 6 in x 3/8 in:

A. (1+α) specimens to be welded, and then cut to determine the residual stress distribution in the as-welded condition.

B. (1+α) specimens to be welded, stress relieved at 500°F, and cut to determine the residual stress distribution.

C. (1+α) specimens to be welded, stress relieved at 900°F, and cut to determine the residual stress distribution.

In the above α is 0 or 1 so that reasonable confidence on the data obtained will be assured.

All specimens will be edge welded to ensure one-dimensionality. Transient strains and temperatures will be measured during both the welding and stress relieving operations using electric resistance strain gages and thermocouples respectively. Figure 5.7 shows the location of these strain gages and thermocouples.

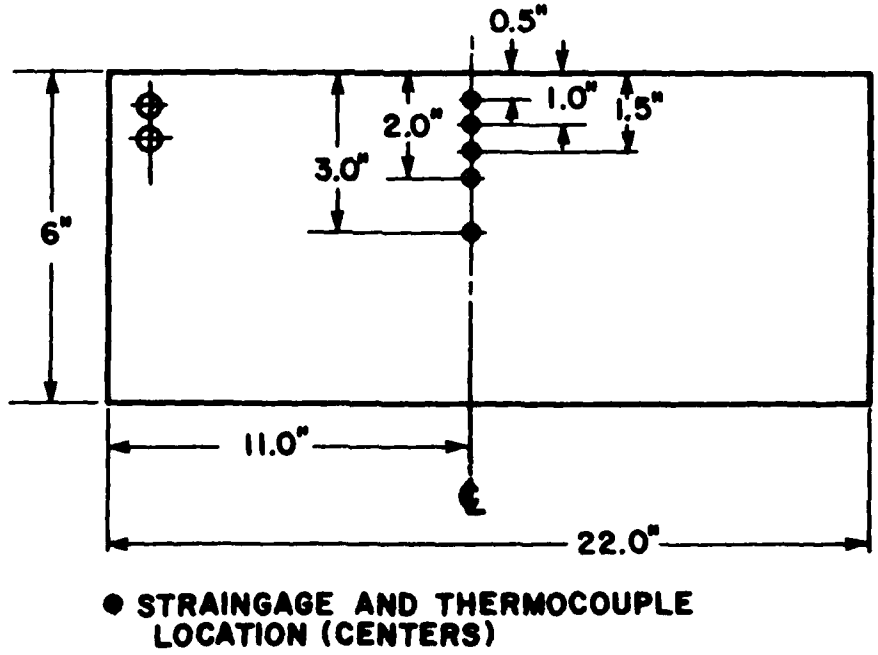

FIGURE 5.7 Configuration of specimens for thermal stress relieving experiments

The specimens that will be stress relieved at 900°F will have strain gages installed on one side only. After stress relieving they will be reinstrumented for measuring residual stresses because the previously installed strain gages, being effective only up to 600°F, will have been destroyed.

The degree of stress relief attained will be judged from the difference in residual stresses before and after the heat treatment. Since the residual stress measurement technique to be used is destructive (it is based on the principle of stress relaxation), the comparison will be based on the assumption that the effect of welding will be the same on all three experimental series (A, B, and C). This fact will be confirmed by comparing the measured transient thermal strains obtained during all welding experiments.

A similar series of experiments will be later performed on 1/2 in thick HY-130 steel plate specimens. These specimens will be sent to us by representatives of the Portsmouth Naval Shipyard.

Finally, it should also be noted that considerable effort is currently being devoted in upgrading the M.I.T. experimental data acquisition system. A sophisticated microcomputer (MINC-23 manufactured by the Digital Equipment Corp.) has been purchased for this purpose using funds not related to this research project. Dedicated signal conditioning equipment for strain gages and thermocouples has also been purchased and is being interfaced with the microcomputer through an advanced data acquisition controller. Delays in the delivery of these equipments, which are currently underoing final testing, have caused part of the delay in performing the aforementioned experiments.

6. PROGRESS OF TASK 5 - IMPROVED COMPUTER PROGRAMS
(December 1, 1980 to November 30, 1981)

6.1 General Status

The objective of Task 5 of the current research program is to develop manuals of improved computer programs for analyzing (1) heat flow, (2) transient thermal stresses and metal movement, and (3) residual stresses and distortion of weldments. Manuals are also to be developed for programs on thermal stress relieving developed under Task 4. Although Task 5 includes some efforts at improving existing computer programs, it does not include major improvements of old computer programs or development of new ones.

A unique feature of Task 5 is the revision of the programs in such a way that they can become more useful to practicing engineers. Moreover, a series of examples to aid engineers in understanding their use, capabilities, and limitations are also to be included.

Two subtasks to be performed under Task 5 have been identified in the proposal to O.N.R. dated November 1980, as follows:

Task 5.1: Development of Improved Manuals of Independent Welding Programs

Task 5.2: Development of Manuals of Programs which are Compatible with the ADINA Program

Progress has been made towards developing the manuals included under both subtasks. It is expected that by the end of the research program all work will have been completed.

Details of the work done are included in the next two sections. Note that all manuals will be published separately from the current third technical progress report.

6.2 Manuals of Independent Welding Programs

During the past decade M.I.T. researchers under the direction of Professor K. Masubuchi have developed a series of computer programs for analyzing various problems related to heat flow, transient thermal strains, residual stresses, and distortion in weldments. On some computer programs manuals have already been prepared, some of which were included in the monograph prepared under Task 1 of a previous O.N.R.-sponsored research program.[36] Since then large amounts of experimental data have been obtained and compared with analytical predictions. Considerable efforts have been made at the same time to improve these programs.

Among these programs, the one-dimensional one was proven to be very useful for the case of welding thin plates and T-shaped built-up beams. As a consequence it was decided that a new manual for this program needs to be written. This new manual is published separately:

Imakita, A., Papazoglou, V.J., and Masubuchi, K., "Consolidated Manual of One-Dimensional Computer Programs for Analyzing Heat Flow, Transient Thermal Strains, Residual Stresses, and Distortion in Weldments", prepared under Contract N00014-75-C-0469 (M.I.T. OSP # 82558) for the Office of Naval Research, M.I.T.. December 1981.

In what follows a summary of the modifications made in these programs is described. For more details one is referred to the aforementioned manual.

One-Dimensional Program. This computer program is capable of calculating the temperatures, thermal strains, and stresses developed in a thin plate during and after welding, assuming a one-dimensional state of stress. The following modifications as compared to the earlier version of the program were made prior to developing the revised manual:

(1) The numerical integration method was modified,

---

[36] This research program, entitled "Development of Analytical and Empirical Systems for Parametric Studies of Design and Fabrication of Welded Structures", was in progress from December 1974 through November 1977. A final report was issued on November 30, 1977.

(2) The number of integration points was increased to improve accuracy,

(3) The temperature dependence of the surface heat loss coefficient was taken into account, and

(4) The output format was changed to facilitate easier handling of the results.

A detailed sample analysis accompanied by a number of comments is also included in the manual.

One-Dimensional Program for T-shaped Beams. This computer program is an extension of the previous one and is aimed at calculating temperatures, thermal strains, residual stresses, and longitudinal bending distortion during the welding fabrication of built-up T-beams. The following modifications were made in this program:

(1) The temperature dependence of material properties was used in conjunction with a parabolic interpolation instead of the linear one previously used,

(2) The heat flow between the web and the flange plates was taken into account,

(3) The strain calculation procedure was changed to confirm with the one used in the simple one-dimensional program,

(4) The program is now capable to also perform calculations for the case of edge welds, and

(5) The output data format was changed, while at the same time more results can be printed out.

The manual includes detailed sample analyses of both edge and T-beam welds.

Conclusions. No efforts have been or will be undertaken to develop manuals for the two-dimensional finite element programs that have been developed independently in the past by M.I.T. investigators. This decision was based on the availability of the much more sophisticated and efficient programs ADINAT and ADINA.

6.3 Manuals of Programs Compatible to ADINA

During the initial stages of the current research project it was decided that all computer programs developed should be compatible with a general purpose finite element computer program to facilitate easier integration with other kinds of numerical analyses, e.g., structural static and dynamic, fracture, etc. Upon consultation with representatives of the Office of Naval Research the general purpose finite element codes ADINAT and ADINA, capable of performing nonlinear heat transfer and thermal-elastic-plastic stress analyses respectively, were chosen. Both of these codes were developed by Professor K. J. Bathe and co-workers at the Department of Mechanical Engineering, M.I.T.

To make these programs capable of analyzing the welding problem, i.e., heat flow and stress calculations during welding, several modifications had to be made. Details of these modifications were presented in Sections 2.3 and 2.4 of this report. Efforts are currently being made to publish manuals that will explain in detail the programs developed and modified. These manuals will also contain directions for the more efficient use of the programs as well as some sample analyses.

More specifically, the following manuals are currently under preparation:

(1) A manual describing the programs developed to calculate schematic continuous cooling transformation (CCT) diagrams from isothermal data, i.e., from experimentally obtained time-temperature-transformation (TTT) diagrams.

(2) A manual describing the program developed to calculate the microstructure history of a material resulting from a given temperature history and based on an idealized CCT diagram of the material.

(3) A manual describing the subroutines developed for the numerical calculation of the phase transformation strains. The calculations are based on the microstructure history and the linear expansion/contraction characteristics of each allotropic phase. These transformation strains can then be added to the thermal strain component in any nonlinear finite element code. The manual will describe in detail how this has been worked out for the program ADINA.

It is also expected that manuals will be written outlining the procedures needed for the efficient use of the finite element programs ADINAT and ADINA in welding problems. These manuals will also be aimed at practicing engineers.

Finally, it should be pointed out that all the above mentioned manuals will be published separately during the first half of 1982.

7. PUBLICATIONS AND DEGREES GRANTED

7.1 Publications

Work done under the present contract from the Office of Naval Research has resulted in the following publications:

(1) Masubuchi, K., "Models of Stresses and Deformation due to Welding: A Review", presented at the Conference on Modeling of Casting and Welding Processes, Franklin Pierce College, Rindge, New Hampshire, August 4-8, 1980.

(2) Masubuchi, K., and Papazoglou, V.J., "Thermal Strains and Residual Stresses in Heavy HY-130 Butt Welds", Proceedings of 1980 Fall Meeting of SESA, Ft. Lauderdale, Florida, October 12-15, 1980.

(3) Papazoglou, V.J., and Masubuchi, K., "Analytical Methods for Determining Temperatures, Thermal Strains, and Residual Stresses due to Welding", presented at the 1980 ASM Materials and Processes Congress, Cleveland, Ohio, October 28-30, 1980.

(4) Papazoglou, V.J., and Masubuchi, K., "Analysis of Thermal Strains and Residual Stresses in High Strength Steel Weldments", presented at the 62nd Annual Meeting of AWS, Cleveland, Ohio, April 6-9, 1981; submitted for publication in the Welding Journal.

(5) Masubuchi, K., "Welding Stresses", presented at the 28th Sagamore Army Materials Research Conference on Residual Stresses and Stress Relaxation, Lake Placid, New York, July 13-17, 1981.

(6) Agapakis, J., and Masubuchi, K., "Analysis and Control of Residual Stress, Distortion and their Consequences in Welded Structures", Proceedings of Conference on Trends in Welding Research in the United States sponsored by ASM, New Orleans, Louisiana, November 16-18, 1981.

(7) Papazoglou, V.J., and Masubuchi, K., "Numerical Analysis of Thermal Stresses during Welding Including Phase Transformation Effects", submitted for presentation at the ASME PVP Division Meeting, Orlando, Florida, June 27-July 1, 1982.

It is expected that other publications will also be made after the completion of the current research program.

7.2 Degrees Granted

The following degrees in chronological order have been granted to students working on this project (note that some of these students were U.S. or allied countries' Navy Officers and so their services were furnished at no cost to the project):

Lipsey, M.D.: Ocean Engineer, and Master of Science in Naval Architecture and Marine Engineering.

Coneybear, G.W.: Master of Science in Naval Architecture and Marine Engineering.

Mylonas, G.A.: Master of Science in Naval Architecture and Marine Engineering, and Master of Science in Mechanical Engineering.

Rogalski, W.J.: Ocean Engineer, and Master of Science in Naval Architecture and Marine Engineering.

Mabry, J.P.: Ocean Engineer, and Master of Science in Naval Architecture and Marine Engineering.

Coumis, G.A.: Master of Science in Naval Architecture and Marine Engineering, and Master of Science in Mechanical Engineering.

Sousa Sá, P.A.: Ocean Engineer, and Master of Science in Mechanical Engineering.

Gonçalves, E.: Master of Science in Ocean Engineering, and Master of Science in Materials Science.

Suchy, A.F.: Ocean Engineer.

Papazoglou, V.J.: Ph.D. in Ocean Engineering.

Golçalves, E.: Ph.D. in Ocean Engineering.

McCord, R.S.: Ocean Engineer.

7.3 Theses Completed

The following theses detailing the work performed under this research program have been completed:

1. Lipsey, M.D., "Investigation of Welding Thermal Strains in High Strength Quenched and Tempered Steel", Ocean Engineer Thesis, M.I.T., June 1978.

2. Coneybear, G.W., "Analysis of Thermal Stresses and Metal Movement during Welding", S.M. Thesis, M.I.T., May 1978.

3. Mylonas, G.A., "Experimental Investigation of Residual Stress Distributions in Thick Welded Plates", S.M. Thesis, M.I.T., July 1979.

4. Rogalski, W.J., "An Economic and Technical Study on the Feasibility of Using Advanced Joining Techniques in Constructing Critical Naval Marine Structures", Ocean Engineer Thesis, M.I.T., May 1979.

5. Mabry, J.P., "Prediction and Control of Residual Stresses and Distortion in HY-130 Thick Pipe Weldments", Ocean Engineer Thesis, M.I.T., May 1979.

6. Coumis, G.A., "An Experimental Investigation of the Transient Thermal Strain Variation and the Triaxial Residual Stress Field Generated due to Electron Beam Welding of Thick HY-130 Plates", S.M. Thesis, M.I.T., June 1980.

7. Sousa Sá, P.A., "Investigation of Triaxial Residual Stress Distribution Remaining after GMA Welding of Thick HY-130 Steel Plates", Ocean Engineer Thesis, M.I.T., January 1981.

8. Gonçalves, E., "Investigation of Welding Heat Flow and Thermal Strain in Restraint Steel Plates", S.M. Thesis, M.I.T., May 1980.

9. Suchy, A.F., "Investigation of Temperature Distribution and Thermally Induced Thermal Strains in Highly Restrained, Thick, HY-130 Steel Plate Weldments", Ocean Engineer Thesis, M.I.T., June 1980.

10. Papazoglou, V.J., "Analytical Techniques for Determining Temperatures, Thermal Strains, and Residual Stresses during Welding", Ph.D. thesis, M.I.T., May 1981.

11. Gonçalves, E., "Fracture Analysis of Welded Structures", Ph.D. thesis, M.I.T., May 1981.

12. McCord, R.S., "An Investigation of Strain, Distortion, and Heat Distribution during Welding of Nickel-Aluminum Bronze", Ocean Engineer thesis, M.I.T., June 1981.